University Medical Center Ulm

Department of Otorhinolaryngology and Head & Neck Surgery

Director: Prof. Dr. med. Thomas K. Hoffmann

Exploring the Role of Marginal Zone B cells in Head and Neck Squamous Cell Carcinoma

Dissertation to obtain the doctoral degree in Medicine

of the Medical Faculty

of Ulm University

Submitted by

Jiantong Bao

Born in Jiangsu, P.R. China

2026

Dean of the Faculty of Medicine: Prof. Dr. Thomas Wirth

1st reviewer: Prof. Dr. Cornelia Brunner

2nd reviewer: Prof. Dr. Andrew Westhoff

Date of defense: 24. Sep. 2026

Information about previous publications

Parts of this dissertation have already been published in the following articles:

Bao J, Betzler AC, Hess J, Brunner C. Exploring the dual role of B cells in solid tumors: implications for head and neck squamous cell carcinoma. Front Immunol. 2023 Oct 5;14:1233085. DOI: 10.3389/fimmu.2023.1233085

Copyright © 2023 Bao, Betzler, Hess and Brunner. This is an open-access article distributed under the terms of the Creative Commons Attribution License (CC BY 4.0). The use, distribution or reproduction in other forums is permitted, provided the original author(s) and the copyright owner(s) are credited and that the original publication in this journal is cited, in accordance with accepted academic practice. No use, distribution or reproduction is permitted which does not comply with these terms. License URL: https://creativecommons.org/licenses/by/4.0/

Bao J, Hess J, Betzler AC, Zhang Z, Tsesmelis M, Schmid S, Berry G, Schuler PJ, Greve J, Laban S, Hoffmann TK, Mulaw M, Brunner C. Identification of marginal zone B cells in head and neck cancer with immunomodulatory characteristics. J Adv Res. 2025 Nov 29:S2090-1232(25)00966-X. DOI: 10.1016/j.jare.2025.11.070

Copyright © 2025 The Author(s). Published by Elsevier B.V. All rights reserved. This is an open-access article distributed under the terms of the Creative Commons Attribution License (CC BY 4.0). The use, distribution or reproduction in other forums is permitted, provided the original author(s) and the copyright owner(s) are credited and that the original publication in this journal is cited, in accordance with accepted academic practice. No use, distribution or reproduction is permitted which does not comply with these terms. License URL: https://creativecommons.org/licenses/by/4.0/

Table of Contents

List of Abbreviations V

1 Introduction 1

1.1 B cells with pro-tumorigenic activity 2

1.1.1 Immunosuppressive mechanisms employed by Bregs 4

1.2 B cells with anti-tumorigenic activity 8

1.2.1 TLS formation 8

1.2.2 Main effector tumor-infiltrating B cells 10

1.3 HNSCC diagnosis and staging 15

1.4 Treatment options for HNSCC 15

1.4.1 Surgical treatment and neck dissection 15

1.4.2 Radiotherapy 16

1.4.3 Radiochemotherapy 16

1.4.4 Targeted tumor therapy 16

1.4.5 Immunotherapy 17

1.5 Therapeutic modulation of tumor-infiltrating B cells 17

1.5.1 Strategies to promote effector B cell functions and TLS formation 21

1.5.2 Strategies to inhibit Bregs 22

1.6 Aim of this thesis 23

2 Materials and methods 24

2.1 Materials 24

2.1.1 Laboratory equipment 24

2.1.2 Consumable material 25

2.1.3 Chemicals and drugs 26

2.1.4 Commercial assays 27

2.1.5 Antibody list 27

2.1.6 Buffers and solutions 28

2.1.7 Software 29
2.2 Methods 31
2.2.1 Study Design 31
2.2.2 Study approval 31
2.2.3 Cohort characteristics 32
2.2.4 PBMC isolation 33
2.2.5 Tumor dissociation and TIL isolation 34
2.2.6 Flow cytometry 34
2.2.7 Single-cell transcriptome analysis 38
2.2.8 scRNA-seq downstream analysis 39
2.2.9 Survival analysis 40
2.2.10 ST analysis 40
2.2.11 Statistics, data analysis, and visualization 41
2.2.12 Data availability 41
3 Results 42
3.1 Landscape of TIB subsets in HNSCC patients 42
3.2 Single-cell transcriptomic profiling reveals TIB heterogeneity in HNSCC 50
3.3 Transcriptional remodeling of TIB subsets in HNSCC compared with HDs 54
3.4 Functional differentiation of MZB subsets in the HNSCC tumor microenvironment 59
3.5 MZB-2 exhibits enhanced immunomodulatory programs in HNSCC 67
3.6 Spatial proximity of MZB clusters to $CD4^+$ T cells suggests functional interaction 71
3.7 Immunoregulatory properties and prognostic relevance of MZB subsets in HNSCC 73
4 Discussion 76
4.1 Clinicopathological relevance of MZB, MZP, and GCB subsets in HNSCC 76

4.2 Comparative landscape of B cell composition and functions in HNSCC versus HDs 77

4.3 Distinctive features and functional divergence of MZB-1 and MZB-2 78

4.4 Antigen-presentation potential of MZB in the tumor microenvironment 79

4.5 Additional immunoregulatory communication pathways involving MZB-2 80

4.6 Conclusion 81

5 Summary 83

6 References 85

7 Acknowledegments 115

8 Curriculum Vitea 116

List of Abbreviations

95% CI	95% confidence interval
°C	Degrees Celsius (unit)
AcB	Activated B cell
ADCC	Antibody-dependent cellular cytotoxicity
ADCP	Antibody-dependent cellular phagocytosis
ADO	Adenosine
APC	Antigen-presenting cells
AID	Activation-induced deaminase
AJCC	American Joint Committee on Cancer
B10 Breg	IL-10 producing regulatory B cell
BCR	B-cell receptor
BP	Biological Processes
Breg	Regulatory B cell
BTK	Bruton's tyrosine kinase
C3	Complement component 3
CCL	CC-chemokine ligand
CITE-seq	Cellular indexing of transcriptomes and epitopes sequencing
CpG ODN	Cytosine-phosphate-guanine oligodeoxynucleotide
CR	Complement receptor
CT	Computed tomography
CTL	Cytotoxic T lymphocyte
CTLA-4	Cytotoxic T-lymphocyte associated protein 4
CXCL	CXC-chemokine ligand

DC	Dendritic cell
DEG	Differentially expressed gene
DN	Double negative B cell
EBV	Epstein-Barr virus
EGFR	Epidermal growth factor receptor
GC	Germinal center
GCB	Germinal center B cell
GDC	Genomic Data Commons
GES	Gene expression signature
GEO	Gene Expression Omnibus
GM-CSF	Granulocyte-macrophage colony-stimulating factor
GO	Gene Ontology
GrB	Granzyme B
GSEA	Gene Set Enrichment Analysis;
GSVA	Gene Set Variation Analysis
HPV	Human papillomavirus
HEV	High endothelial venule
HD	Healthy donor
HNSCC	Head and neck squamous cell carcinoma
HPCA	HumanPrimaryCellAtlasData
ICB	Immune checkpoint blockade
ICOS	Inducible T cell co-stimulator
IDO	Indoleamine 2,3-dioxygenase
IFN	Interferon
IHC	immunohistochemistry

IKK	inflammation-responsive IκB kinase
IL	Interleukin
IMRT	Intensity-modulated radiotherapy
Ig	Immunoglobulin
KEGG	Kyoto Encyclopedia of Genes and Genomes
LN	Lymph node
LTi	Lymphoid tissue inducer
LT	Lymphotoxin
L-R	ligand-receptor
MDSC	Myeloid-derived suppressor cell
MEK	Mitogen/extracellular signal-regulated kinase
MHC	Major histocompatibility complex
MRI	Magnetic resonance imaging
MSigDB	Molecular Signatures Database
MZ	Marginal zone
MZB	Marginal zone B cell
MZP	Marginal zone B cell precursor cells
NK cell	Natural killer cell
OSCC	Oral squamous cell carcinoma
ODN	Oligonucleotide
OPSCC	Oropharyngeal squamous cell carcinoma
PB	Plasma B cell
PC	Principal components
PCA	Principal components analysis
PD-1	Programmed cell death protein 1

PD-L1	Programmed cell death 1 ligand 1
PET-CT	Positron emission tomography-computed tomography
PanIN	Pancreatic intraepithelial neoplasia
PBMC	Peripheral blood mononuclear cells
R123	Rhodamine123
REC	Research ethics committee
scRNA-seq	Single-cell RNA sequencing
SHM	Somatic hypermutation
ST	Spatial transcriptomics
SEM	Standard error of mean
T2-MZP	Transitional 2-marginal zone precursor
TAA	Tumor-associated antigen
TAM	Tumor-associated macrophage
TAAB	Tumor-associated atypical B cell
T-bet	T cell-specific T box transcription factor
TCGA	The Cancer Genome Atlas
Tem	effector memory T cell
Tfh	Follicular helper T cell
Tfr	Follicular regulatory T cell
TGF	Transforming growth factor
Th	Helper T cell
Th1	$CD4^+$ T helper 1 cell
TIL	Tumor-infiltrating lymphocyte
TIB	Tumor-infiltrating B cell
TIME	Tumor immune microenvironment

TLM	Transoral laser microsurgery
TLR	Toll-like receptor
TLS	Tertiary lymphoid structure
Tn	Naive T cell
TNF	Tumor necrosis factor
TNM	Tumor–Node–Metastasis
TORS	Transoral robotic surgery
TRAIL	Tumor necrosis factor–related apoptosis-inducing ligand
Treg	Regulatory T cell
Trm	tissue-resident memory T cell
UICC	Union for International Cancer Control
VEGF	Vascular endothelial growth factor
VEGFR	Vascular endothelial growth factor receptor

1 Introduction

Head and neck squamous cell carcinoma (HNSCC) comprises a heterogeneous group of malignancies arising from the mucosal epithelium of the oral cavity, oropharynx, hypopharynx, and larynx. It represents a major global health burden, with over 870,000 new cases and 440,000 deaths reported annually [180]. Based on etiological and molecular characteristics, HNSCC is broadly categorized into human papillomavirus–positive (HPV^+) and HPV-negative (HPV^-) disease, which represent biologically and clinically distinct tumor entities [161].

HPV^+ HNSCC is predominantly associated with high-risk HPV subtypes, most notably HPV-16, and arises mainly in the oropharynx, including the palatine tonsils and base of tongue [63]. Viral oncogenes E6 and E7 drive malignant transformation through degradation of tumor suppressor proteins p53 and retinoblastoma, leading to genomic instability and uncontrolled cell proliferation [108]. As a consequence, HPV^+ tumors typically exhibit lower mutational burdens compared with HPV^- cancers but display distinct epigenetic and transcriptional profiles characterized by strong immune activation signatures.

In contrast, HPV^- HNSCC is largely driven by chronic exposure to tobacco smoke and alcohol consumption, which induce extensive DNA damage and accumulation of somatic mutations. These tumors frequently harbor alterations in TP53, CDKN2A, NOTCH1, and EGFR signaling pathways and demonstrate marked chromosomal instability. Clinically, HPV^- tumors are more often diagnosed at advanced stages, exhibit aggressive local invasion, and show limited responsiveness to therapy [104].

Importantly, HPV status represents one of the strongest prognostic determinants in HNSCC. Patients with HPV^+ tumors exhibit significantly improved overall survival and treatment responsiveness compared with their HPV^- counterparts, even after adjustment for stage and treatment modality [6]. This survival advantage has been attributed not only to intrinsic tumor biology but also to a more immunologically active tumor microenvironment characterized by increased infiltration of cytotoxic T cells, B cells, and tertiary lymphoid structures (TLSs).

Within the HNSCC tumor immune microenvironment (TIME), B cells form heterogeneous populations with distinct and sometimes opposing roles in cancer progression. Their function is shaped by a multitude of factors—hypoxic conditions, local cytokine profiles, interactions with tumor cells, and cross-talk with other tumor-infiltrating lymphocytes (TILs)—that collectively influence their polarization toward either pro- or anti-tumor activity.

1.1 B cells with pro-tumorigenic activity

Regulatory B cells (Bregs) constitute a diverse subset of B lymphocytes with prominent immunosuppressive functions across a range of malignancies, including HNSCC [85, 102, 218]. Initially studied in the context of autoimmune diseases such as systemic lupus erythematosus and collagen-induced arthritis, Bregs were found to attenuate inflammatory responses primarily via interleukin-10 (IL-10) secretion [26]. For instance, in murine models of arthritis, a specific subset of B cells known as transitional 2–marginal zone precursor (T2-MZP) cells exhibited IL-10–producing regulatory functions [48].

Subsequent studies extended these findings to solid tumors. In cancers such as breast and ovarian carcinoma, IL-10–secreting B cells, often referred to as B10 Bregs, hindered cytotoxic T cell activity and facilitated tumor growth [83]. Since then, additional Breg phenotypes have been discovered across various cancer types, distinguished by their surface markers and secretory profiles (**Figure 1**). Particularly, in HNSCC, a Breg subtype exhibiting a marginal zone B cell (MZB)-like phenotype and ectonucleotidases CD39 and CD73 expression, has been found to facilitate the conversion of extracellular adenosine triphosphate (ATP) into immunosuppressive adenosine (ADO) [85, 166].

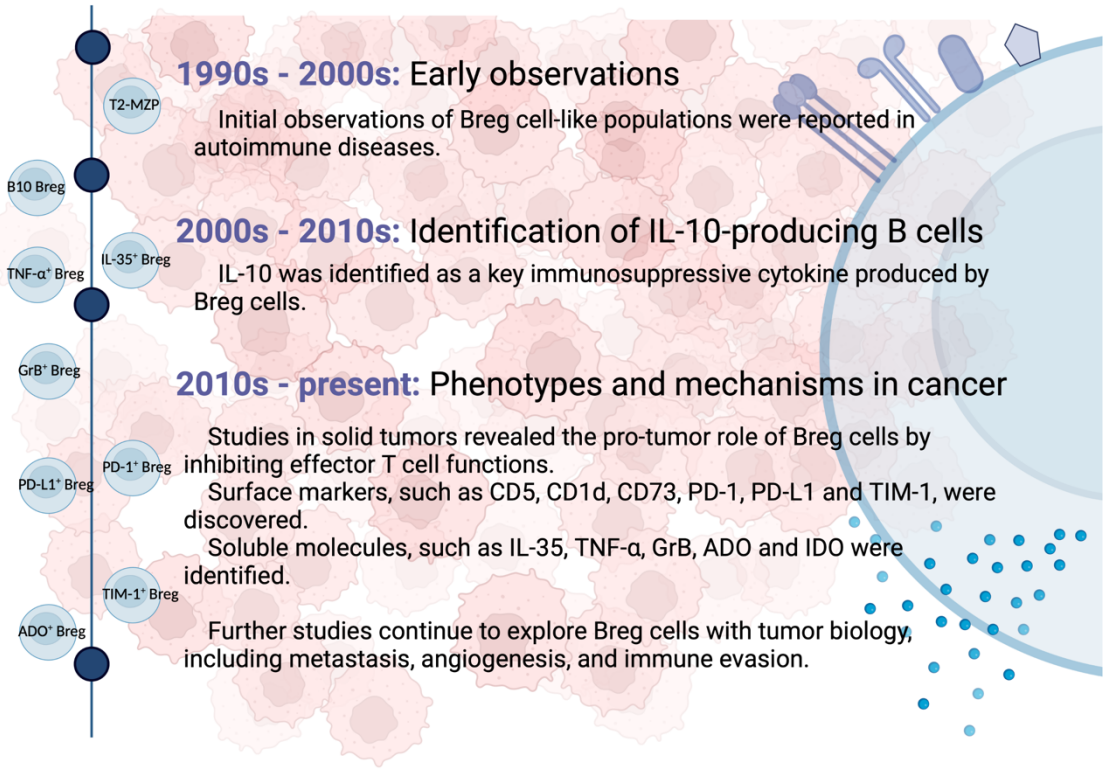

Figure 1. Historical milestones in Breg discovery.

Bregs were first identified in autoimmune diseases for their anti-inflammatory properties mediated by IL-10. They were later found in solid tumors, where they suppress anti-tumor immune responses. Multiple Breg phenotypes and secreted molecules have since been discovered. Ongoing studies investigate Breg characteristics within the tumor microenvironment. Figure by C. Brunner created with BioRender.com and reprinted as an author from J.Bao 2023 [11]. Licensed under CC BY 4.0, https://creativecommons.org/licenses/by/4.0/.

1.1.1 Immunosuppressive mechanisms employed by Bregs

Bregs facilitate tumor progression through soluble mediators and direct cellular interactions. Their immunosuppressive activity is mediated by the secretion of inhibitory cytokines, engagement of immune checkpoints, and modulation of effector immune cell responses. These mechanisms function through both autocrine and paracrine pathways, enabling Bregs to dampen antitumor immunity in a localized and systemic manner.

Autocrine and paracrine secretion of immunosuppressive factors

Bregs exert immunomodulatory effects in part by secreting immunosuppressive cytokines that shape the local immune landscape to favor tumor growth. Principal among these are IL-10, IL-35, and transforming growth factor-beta (TGF-β) (**Fig. 2**). In HNSCC, two IL-10-producing Breg subsets have been described: $CD19^{+}CD24^{hi}CD38^{hi}$ and $CD19^{+}CD25^{hi}$ cells [102]. These Bregs inhibit Th1 and Th17 differentiation by reducing IFN-γ and TNF-α production [83], impair dendritic cell (DC) function, and promote the M2 polarization of tumor-associated macrophages (TAMs) [102]. IL-10 also promotes regulatory T cells (Tregs) development and downregulates monocyte and NK cell activity [78, 82, 83, 121, 159, 215]. IL-35 fosters immune tolerance by converting conventional T cells into Tregs, inducing effector T cell exhaustion, and upregulating genes that support tumor proliferation [32, 47]. TGF-β, in turn, limits T cell activation and expansion while enhancing FoxP3 and CTLA-4 expression, both hallmarks of immunosuppression [1, 22, 88, 142]. Beyond canonical cytokines, unconventional Bregs secrete additional regulatory molecules such as granzyme B (GrB), indoleamine 2,3-dioxygenase (IDO), and ADO [85, 166].

Intercellular interactions and checkpoint engagement

In addition to soluble factors, Bregs modulate the immune response through direct cell-cell interactions involving costimulatory and checkpoint molecules, including CTLA-4–CD80/CD86 axis, CD40–CD40L signaling, PD-1–PD-L1 interactions, and Fas–FasL engagement.CD80/CD86 expressed on Bregs engage CTLA-4 on Tregs, promoting Treg expansion in the presence of TGF-β [88]. CD40–CD40L interaction between Bregs and $CD4^{+}$ T cells facilitates Th1/Th2 skewing and Treg induction [66, 142, 149, 191, 218]. IL-10–mediated activation of $PD\text{-}1^{hi}$ Bregs inhibits cytotoxic lymphocyte activity [206], while

PD-L1^{hi} Bregs suppress follicular helper T (Tfh) cell proliferation and differentiation, reducing memory B cell and plasma cell output [90]. The PD-1/PD-L1 axis is widely exploited by exhausted immune cells, including Bregs, to escape cytotoxic attack while maintaining an immunosuppressive cytokine profile [157, 190]. Dual blockade of PD-L1 and IL-10 pathways has been shown to restore cytotoxic T lymphocyte (CTL) function [190, 200]. On the other hand, FasL^{+} Bregs are capable of inducing apoptosis in Fas^{+} effector T cells, skewing the CD8^{+} T cell/Treg balance toward immune suppression [136, 184].

Furthermore, Bregs can amplify immunosuppression by modulating other suppressive cell types such as myeloid-derived suppressor cells (MDSCs). MDSCs induce Bregs in co-culture systems, demonstrating a reciprocal relationship between these two cell types [170].

Direct contribution to tumor progression

Beyond immunoregulation, Bregs directly contribute to tumorigenesis. In murine models of pancreatic intraepithelial neoplasia (PanIN), adoptive transfer of CD5^{+}CD1d^{hi} Bregs restored tumor growth in B cell-deficient hosts [152]. Similarly, T2-MZP B cells (B220^{+}CD23^{+}IgM^{hi}CD21^{hi}) accumulated in tumor-draining lymph nodes in melanoma models and promoted tumor expansion in an IL-10–independent manner [48, 58].

Despite advances in understanding their function, the developmental origin and phenotypic definition of Bregs remain ambiguous. Unlike other immune lineages, Bregs lack a unified set of lineage-defining transcription factors, and there is no consensus on their ontogeny or phenotypic trajectory [141]. Attempts to delineate Breg subsets using single-cell RNA sequencing (scRNA-seq) have often proven inconclusive, failing to consistently identify a discrete Breg cluster [77, 79].

It is increasingly proposed that B cells acquire regulatory properties contextually, rather than originating from a dedicated lineage [45, 141]. This functional plasticity appears to be shaped by a range of environmental stimuli. Local conditions such as hypoxia, acidic pH, tumor-derived lipid metabolites, and exosomes have all been implicated in promoting the acquisition of regulatory phenotypes by B cells [24, 128, 147, 155, 172, 174, 197, 211]. In addition, cytokines including IL-35, IL-21, IL-1β, and IL-6, as well as calcium signaling and surface receptor activation (e.g., Toll-like receptors (TLRs), CD40, and B cell receptors),

have been shown to contribute to Breg induction and function [39, 51, 127, 129, 153, 160, 189, 212].

A synthesized summary of Breg-mediated immunosuppressive and tumor-supportive functions is illustrated in **Figure 2**, highlighting the multifaceted ways through which Bregs influence cancer pathogenesis.

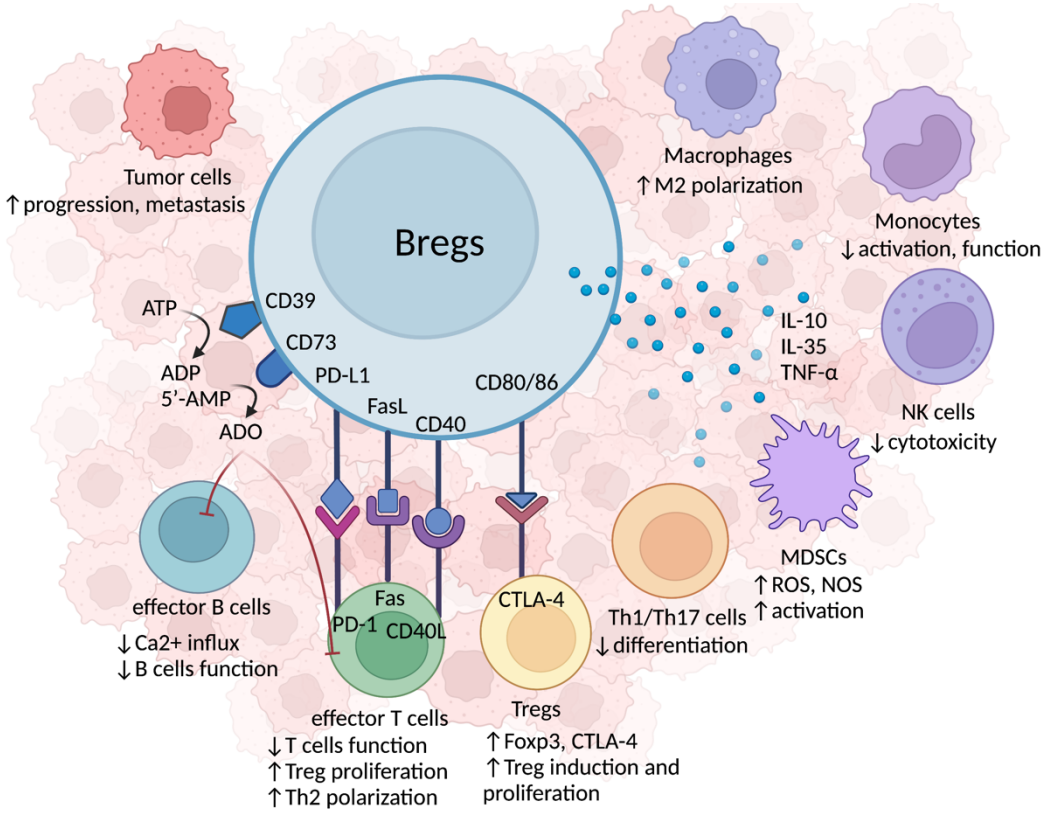

Figure 2. Immunosuppressive mechanisms of Bregs in HNSCC.

Bregs release IL-10, IL-35, and TNF-α to suppress effector immune cells, promote the expansion of regulatory TILs, and contribute to tumor progression and immune escape. Furthermore, co-expression of CD39 and CD73 allows these cells to catalyze ATP hydrolysis into ADO, which impairs calcium influx and disrupts T and B cell signaling. Bregs also form cell-cell contacts with other TILs. Bregs can induce anti-tumor T cell malfunction via PD-L1-PD-1 axis, or Fas/FasL binding. Bregs and effector T cells interact via CD40/CD40L to promote Th1/Th2 cell polarization and Treg proliferation. Bregs are also capable of forming cellular contacts with other immunosuppressive TILs, such as MDSCs and Tregs. The CD80/CD86 marker expressed on Bregs binds to CTLA-4 on Tregs, inducing Treg proliferation. Figure by C. Brunner created with BioRender.com and reprinted as an author from J.Bao 2023 [11]. Licensed under CC BY 4.0, https://creativecommons.org/licenses/by/4.0/.

Abbreviations: Breg, regulatory B cell; HNSCC, head and neck squamous cell carcinoma; TIL, tumor-infiltrating lymphocyte; IL, interleukin; TNF-α, tumor necrosis factor alpha; ATP, adenosine triphosphate; ADO, adenosine; PD-1, programmed death 1; PD-L1, programmed death ligand 1; FasL, Fas ligand; Th, T helper cell; Treg, regulatory T cell; MDSC, myeloid-derived suppressor cell; CTLA-4, cytotoxic T-lymphocyte–associated protein 4.

1.2 B cells with anti-tumorigenic activity

When tumor-infiltrating B cells (TIBs) are organized into TLSs, they often support anti-tumor responses. TLSs are non-encapsulated, immune-dense aggregates composed of lymphocytes and stromal elements that emerge in response to sustained inflammation or persistent antigenic stimulation [148, 165]. Mature TLSs contain $CD20^+$ B cell-rich areas including germinal-center B cells (GCBs), plasma cells, and memory B cells. These cells contribute to tumor clearance via antibody-mediated cytotoxicity, phagocytic mechanisms, and local complement activation.

1.2.1 TLS formation

TLSs arise via a process of lymphoid neogenesis, establishing localized sites for antigen recognition and immune priming [148] (**Fig. 3**). In HPV^+ HNSCC, higher frequencies of TLSs and germinal center (GC) maturation have been reported, likely due to persistent exposure to viral antigens such as episomal or integrated HPV DNA, which promotes early innate immune activation [34, 95, 96, 161].

Initiation of TLS formation involves the recruitment of lymphoid tissue inducer (LTi) cells. LTi cells interact with stromal cells through lymphotoxin (LT) $\alpha_1\beta_2$ and its receptor LTβR to induce VEGF-C production, which is essential for the development of high endothelial venules (HEVs) [36, 56]. HEVs function as conduits for lymphocyte entry into TLSs [125]. IL-17 secreted by LTi cells further promotes the expression of CXCL12, CXCL13, CCL19, and CCL21, reinforcing chemotactic gradients that facilitate TLS maturation [52, 115].

Fully matured TLSs include GCs marked by $CD23^+$ B cells. In contrast, immature TLSs lack these structures and consist of loosely arranged B cell clusters [94]. TLSs are commonly located at the invasive margins of HNSCC tumors, although they can also be found in stromal and intratumoral regions [42, 109, 164]. In oral squamous cell carcinoma (OSCC), intratumoral TLSs were present in 33.8% of samples, whereas peritumoral TLSs were more prevalent, appearing in 75.4% of cases [109].

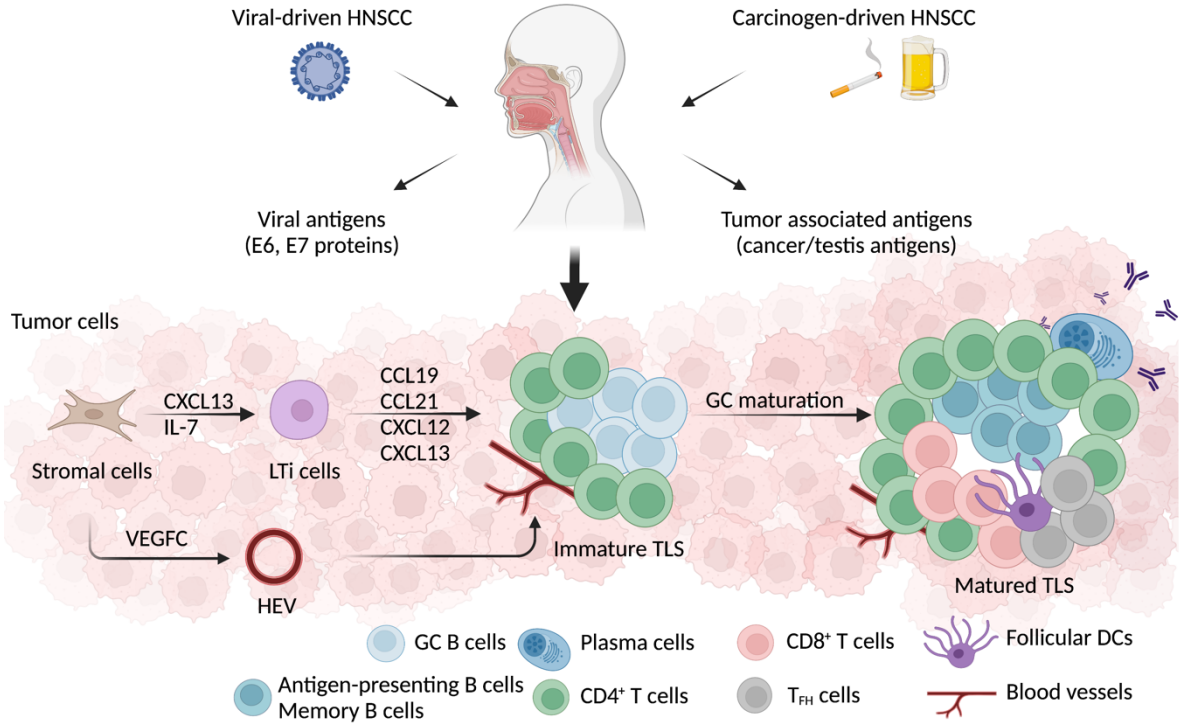

Figure 3. TLS formation in HNSCC.

HNSCC can be induced by either viral infection, or environmental carcinogens, such as smoking or excessive alcohol consumption. Besides tumor associated antigens, the HPV$^+$ HNSCC microenvironment also exposes E6 and E7 viral antigens. TLS, a crucial ectopic lymphoid cell formation, develops in the early stage of tumorigenesis. Local stromal cells that have been activated secret CXCL13 and attract LTi cells. LTi cells produce a series of chemokines, including CCL19, CCL21, CXCL12, and CXCL13, which aid in the recruitment of LTi cells and lymphocytes. Additionally, stromal cells secrete VEGF-C, which promotes HEV development in the vicinity of TLSs. After GC maturation, a well-defined TLSs is formed with a CD3$^+$ T cell zone composed of CD4$^+$, CD8$^+$, and Tfh cells, and a CD20$^+$ B cell zone comprising GCBs, memory B cells, and plasma cells. Besides lymphocytes, follicular DCs, fibroblasts, and neovascular cells are also involved in the process of TLS formation. Figure by C. Brunner created with BioRender.com and reprinted as an author from J.Bao 2023 [11]. Licensed under CC BY 4.0, https://creativecommons.org/licenses/by/4.0/.

Abbreviations: TLS, tertiary lymphoid structure; HNSCC, head and neck squamous cell carcinoma; HPV, human papillomavirus; LTi, lymphoid tissue inducer cell; GC, germinal center; GCB, germinal center B cell; Tfh, follicular helper T cell; HEV, high endothelial venule; VEGF-C, vascular endothelial growth factor C; FDC, follicular dendritic cell.

1.2.2 Main effector tumor-infiltrating B cells

GCBs

Increased levels of TIBs are particularly prominent in HPV^+ HNSCC as compared to HPV^- HNSCC [53, 102]. Instead of uncovering a T-cell-driven TIL signature that separates HPV^+ from HPV^- HNSCC, adjusting the number of TILs revealed a distinct set of B-cell associated genes which are highly expressed in HPV^+ HNSCC, such as *BCL2, ADAM28, CD200, ICOSLG,* and *SPIB*, the latter two being linked to activated B cells within GCs [53, 112, 179].

GCs are central to the functional maturation of B cells, enabling clonal expansion, somatic hypermutation (SHM), and selection of high-affinity clones that differentiate into memory B cells or plasma cells [62]. The GC architecture comprises a dark zone (for proliferation and SHM) and a light zone (for selection and maturation via interaction with Tfh cells) [60]. In HPV^+ HNSCC, gene expression patterns of GCBs mirror those seen in secondary lymphoid tissues, supporting the existence of functional GCs in situ [131, 161]. Comparing TLS^+ and TLS^- tumor tissues elucidated a B cell-related gene signature ranging from naïve B cells to terminally differentiated plasma cells, which further supports the concept of in situ B cell maturation within the TLSs [131].

GCBs in HNSCC express several key markers including *SEMA4A, AID,* and *BCL6*, all indicative of active GC processes and TLS maturation [41, 62, 114, 138, 161, 188]. A fully developed TLS includes $CD3^+$ and $CD20^+$ lymphocyte zones, follicular DCs, fibroblasts, and neovessels, creating a supportive environment for sustained anti-tumor responses [20].

MZBs

Under homeostatic conditions, MZBs are predominantly located in the splenic marginal zone (MZ), a specialized anatomical niche responsible for continuous blood filtration and early immune surveillance against circulating antigens [124]. Owing to their expression of pattern-recognition receptors, including TLRs, together with a polyreactive BCR repertoire, MZBs are uniquely equipped to sense blood-borne pathogens. Upon activation, they rapidly secrete large amounts of immunoglobulin M (IgM) in a manner largely independent of T-cell help, positioning them within the innate-like arm of the humoral immune system.

Following antigen uptake, MZBs can actively shuttle from the MZ into B-cell follicles, where they transport immune-complexed antigens to follicular dendritic cells (FDCs) [43, 49]. This process plays a critical role in GC initiation and the subsequent development of adaptive humoral immunity. In addition, MZBs are capable of migrating into T-cell areas within lymphoid follicles, where they contribute to $CD4^+$ T-cell activation [10, 35, 144]. thereby linking innate and T-cell-dependent immune responses.

In parallel with these immune-activating functions, MZBs and their transitional precursors also display immunoregulatory properties. Both MZBs and T2-MZP B cells have been reported to produce the anti-inflammatory cytokine IL-10, contributing to immune homeostatis [27, 48, 81]. Furthermore, ADO-expressing MZB populations with ectonucleotidases CD39 and CD73 were also discovered [85, 166, 175].

Functionally, T2-MZP B cells isolated from tumor-draining lymph nodes of B16-F10 melanoma–bearing mice were shown to exert tumor-promoting effects when transferred into B-cell-deficient hosts [58]. In line with these findings, our recent work in a murine HNSCC model revealed a substantial accumulation of MZBs within the TIME [175]. However, whether these MZBs predominantly mediate antitumor immunity or instead support immunosuppression and tumor progression remains unresolved.

At the level of cellular heterogeneity, two distinct MZB subsets—MZB-1 and MZB-2—have been described in humans, exhibiting divergent transcriptional programs and developmental trajectories [84]. Similarly, murine studies have identified two functionally discrete MZB populations based on differential CD80 expression, which vary in autoreactivity, radiosensitivity, and immunological function [106]. To date, the presence and functional relevance of these MZB subpopulations within human solid tumors have not yet been systematically characterized.

Memory B cells

Memory B cells are capable of memorizing antigens and sustaining a lasting immune response. Generated from naive B cells, they constitute the majority of TIL-B cells. In the TIME, atypical memory B cells with with antigen-presenting or direct cytotoxic functions have been identified [23, 73, 138, 145, 167, 171, 199, 201, 208].

Studies in ovarian, liver, and lung cancer demonstrate that memory B cells co-localizing with $CD8^+$ T cells enhance antigen presentation and correlate with favorable outcomes [18, 138, 201, 221]. Notably, HPV^+ OPSCC patients show a positive correlation between $CD20^+$ TIBs and HPV-specific $CD8^+$ clones, reinforcing the cooperative role of B and T cells [75]. Memory B cells with direct tumoricidal function have been identified in hepatocellular carcinoma, expressing effector molecules like IFN-γ, IL-12p40, GrB, and tumor necrosis factor–related apoptosis-inducing ligand (TRAIL) [171].

Plasma cells

Plasma cells play a pivotal role in anti-tumor immunity by producing antibodies against tumor-associated antigens (TAAs). They are found either within TLSs or scattered in stromal clusters [62, 68, 92, 99]. Following their terminal maturation in TLSs, IgG^+ and IgA^+ plasma cells are guided through the tumor tissue by $CXCL12^+$ fibroblasts [131].

The abundance of plasma cells has been positively correlated with enhanced CTL activity [99]. CXCL13-producing PD-$1^{hi}CD8^+$ T cells and bystander $CD8^+$ T cells adjacent to TLS-associated $CD20^+$ B cell zones recognize a broad range of viral epitopes, including HPV, EBV, CMV, and influenza antigens [173, 186]. These bystander $CD8^+$ T cells arise following humoral responses against viral antigens, as evidenced by heightened cytolytic activity in virally infected tumors [158]. Serological assays have detected viral antigen-specific antibodies in nearly all HPV^+ HNSCC patients [17], and therapeutic vaccination against HPV E6 and E7 proteins has been shown to drive TLS formation and T cell activation in cervical neoplasia [123]. Notably, meta-analyses indicate that the co-presence of TIBs or plasma cells with T cells is associated with superior clinical outcomes [201]. In contrast, HPV^- HNSCCs exhibit more heterogeneous humoral responses [8, 214]. In advanced-stage or HPV^- HNSCC patients, TAAs elicit more frequent antibody responses [103].

Other isotypes including IgM, IgE, and IgD have been sporadically detected in tumors. While IgM and IgD are rare and often linked to Bregs [58, 111, 202], elevated IgE or IgD levels in melanoma patients have been associated with poor prognosis [15, 62, 202].

A comprehensive summary of TIB phenotypes and functions is presented in Table 1.

Table 1 Phenotypes and functions of major TIB subtypes.

TIBs	Phenotype	Functions
GCB	$CD19^+CD20^+CD27^+CD38^+CD10^+IgD^-$; BCL6, AID, SEMA4A, and Ki67 expression	Undergo clonal expansion and somatic hypermutation within TLS, generating high-affinity tumor-reactive B-cell receptors. Support affinity maturation and determine differentiation into memory B cells or plasma cells.
MZB	$CD19^+CD27^+CD21^+CD23^-CD1c^+IgM^+$ [4, 84, 168, 187, 198]	Exhibit strong antigen-presenting capacity and rapidly secrete natural IgM under homeostatic conditions. Precise functional contribution in the tumor microenvironment remains unclear.
Memory B cell	$CD19^+CD20^+CD24^+CD27^+CD38^{low}$ (atypical $CD27^-$ phenotype)	Sustain long-term immune response.
antigen-presenting phenotype	MHC-mediated; CD40/CD80/CD86 expression	Present antigens to T cells, and stimulate the activation and effector functions of cytotoxic $CD8^+$ T cell.
direct tumor killing phenotype	IFN-γ, IL-12p40, GrB and TRAIL expression	Direct tumor cell killing effect.
Plasma cell	$CD19^{low}CD20^{low}CD24^-CD27^{hi}CD38^{hi}$, IgG or IgA expression	Produce antibodies which recognize the tumor-associated antigens, cause ADCC and ADCP, activate the complement system, and augment antigen presentation by DCs.
Breg	Multiple phenotypes	Produce immunosuppressive cytokines, such as IL-10, IL-35, and TGF-β; induce effector T and B cell malfunction; promote the proliferation of Tregs and MDSCs; promote tumor progression and metastasis.

Abbreviations continued on next page.

Table 1 (continued).

Abbreviations: TLS, tertiary lymphoid structure; TIL-B cells, tumor-infiltrating B cells; GCB, germinal center B cell; MZB, marginal zone B cell; MHC, major histocompatibility complex; AID, activation-induced deaminase; GrB, granzyme B; TRAIL, tumor necrosis factor–related apoptosis-inducing ligand; ADCC, antibody-dependent cellular cytotoxic; ADCP, antibody-dependent cellular phagocytosis; Treg cell, regulatory T cell; MDSC, myeloid-derived suppressor cell; hi: high; dim, medium.

1.3 HNSCC diagnosis and staging

The diagnosis of HNSCC is established through a combination of clinical examination, radiological imaging, and endoscopic assessment, histopathological confirmation [120]. Imaging modalities including contrast-enhanced computed tomography (CT), magnetic resonance imaging (MRI), and positron emission tomography combined with CT (PET-CT) play a central role in determining local tumor extent, lymph node (LN) involvement, and distant metastasis. Suspicious lesions are typically evaluated by endoscopy with biopsy, allowing for precise anatomical localization and pathological classification [54].

Tumor staging follows the Tumor–Node–Metastasis (TNM) classification system established by the Union for International Cancer Control (UICC) and the American Joint Committee on Cancer (AJCC) [117]. The TNM framework defines the anatomical extent of disease according to the size and local invasion of the primary tumor (T), the presence and extent of regional lymph node involvement (N), and the presence or absence of distant metastasis (M). The eighth edition introduced major revisions by incorporating HPV status as an independent staging criterion for oropharyngeal carcinoma, with HPV^+ and HPV^- oropharyngeal cancers staged using distinct classification criteria [80].

1.4 Treatment options for HNSCC

The management of HNSCC requires a multidisciplinary approach. Treatment strategies depend on tumor location, stage, HPV status, patient comorbidities, and functional considerations.

1.4.1 Surgical treatment and neck dissection

Surgery remains a cornerstone of therapy for early-stage HNSCC and plays a central role in locally advanced disease. Advances in surgical techniques, including transoral laser microsurgery (TLM) and transoral robotic surgery (TORS), have enabled improved oncologic control while preserving speech and swallowing function [55]. Neck dissection is performed to address regional LN metastases. Depending on disease extent, selective, modified radical, or radical neck dissection may be employed. Pathological assessment of

surgical specimens provides essential information on margin status, extranodal extension, and lymphovascular invasion, guiding the need for adjuvant therapy.

1.4.2 Radiotherapy

Radiotherapy is used as a definitive modality in early-stage disease, as adjuvant treatment following surgery, or as part of combined-modality therapy for advanced tumors. Modern techniques such as intensity-modulated radiotherapy (IMRT) allow highly conformal dose delivery while minimizing toxicity to surrounding normal tissues. Despite technical advances, radiotherapy is associated with significant acute and long-term side effects, including mucositis, xerostomia, dysphagia, and fibrosis, which substantially affect quality of life [2].

1.4.3 Radiochemotherapy

Adjuvant radiochemotherapy constitutes the standard of care for unresectable locally advanced HNSCC and for patients with high-risk pathological features after surgery [54]. Cisplatin-based regimens remain the most widely used radiosensitizing chemotherapy. Radiochemotherapy improves locoregional control and overall survival but is associated with considerable toxicity, limiting its applicability in elderly or comorbid patients. HPV^{+} tumors generally show enhanced sensitivity to radiochemotherapy, which has prompted ongoing clinical trials investigating treatment de-escalation strategies.

1.4.4 Targeted tumor therapy

Molecularly targeted therapies have expanded treatment options in recurrent or metastatic HNSCC. Epidermal growth factor receptor (EGFR) is overexpressed in the majority of tumors, making it a rational therapeutic target. Cetuximab, a monoclonal antibody against EGFR, was the first targeted agent approved for HNSCC and has demonstrated clinical benefit when combined with radiotherapy or chemotherapy [16]. However, resistance mechanisms and limited predictive biomarkers have constrained the overall efficacy of targeted approaches.

1.4.5 Immunotherapy

The advent of immune checkpoint inhibition has transformed the therapeutic landscape of HNSCC. Antibodies targeting the programmed cell death protein-1 (PD-1) and its ligand PD-L1, such as nivolumab and pembrolizumab, have shown significant survival benefit in recurrent or metastatic disease [21, 50]. Immunotherapy is particularly effective in tumors with pre-existing immune infiltration, including HPV^+ cancers, although durable responses are observed only in a subset of patients [46, 50, 204]. Ongoing research aims to identify predictive biomarkers and rational combination strategies involving chemotherapy, radiotherapy, and immune modulation.

1.5 Therapeutic modulation of tumor-infiltrating B cells

Current cancer immunotherapies are largely dominated by immune checkpoint blockade (ICB), primarily targeting the reactivation of CTL. However, the efficacy of this approach remains limited in HNSCC, with only approximately 20% of patients showing initial responsiveness to PD-1 blockade therapies [46, 50, 204]. Furthermore, even among initial responders, the emergence of acquired resistance poses a significant challenge.

To overcome the limitations of monotherapy, targeting TIBs represents a promising strategy for enhancing immune responsiveness. Given the dual roles of B cells in promoting or suppressing anti-tumor immunity, novel approaches that manipulate TIB populations may complement existing T cell–based immunotherapies.

In HNSCC, patients harboring viral antigens (e.g., HPV-derived E6/E7) or a high tumor mutation burden tend to respond more favorably to ICB, likely due to increased neoantigen availability [70, 139]. Interestingly, PD-L1—classically associated with tumor and DCs—has also been identified on subsets of Bregs, implicating B cells directly in immune checkpoint regulation [170, 202].

Although direct B cell–targeted therapies in solid tumors are still emerging, several immunotherapeutic agents have shown potential in modulating TIB behavior and TLS formation. These include agents that:

- induce TLS neogenesis or maturation
- promote differentiation of B cells into effector subsets
- enhance B cell–mediated antigen presentation and cooperation with T cells
- suppress immunosuppressive Bregs

A concise overview of therapeutic strategies aimed at modulating TIB function is summarized in Table 2.

Table 2 Immunotherapeutic strategies targeting TIBs.

Agent	Phase	Description	Related functions
GVAX	Neoadjuvant clinical trial (NCT02451982 and NCT02648282)	Therapeutic cancer vaccine	Induce GM-CSF secretion, promote TLS formation, facilitate TIL infiltration, foster effector T cell activation and cellular communications [116, 216].
Anti-VEGFR	Preclinical	Angiogenesis modulator	Used as an adjuvant to enhance ICB therapy, induce HEV formation, improve anti-PD-L1 treatment, promote TIL infiltration [3].
GSK3359609	Phase II/III clinical trial (NCT04128696 and NCT04428333)	ICOS agonist	Promote memory and effector T cell development, induce specific humoral immune responses [5].
Engineered DCs	Preclinical Phase I clinical trial (NCT01574222)	Targeted cytokine/chemokine delivery system	Targeted expression of ideal cytokines or chemokines, initiate TLS resemble, enhance Th1 cell skewing, promote $CD8^+$ CTL infiltration [29, 105, 195].
CXCL13-coupled CpG-ODN	Preclinical	Therapeutic cancer vaccine	Targeted delivering of stimulatory CpG-ODN to effector B cells, activate effector TIL-B cells while block the generation of Breg cells, promote GrB-expressing CTLs [14].
Nanoengineered synthetic immune niches	Preclinical	Synthetic scaffolds with modified TILs and TAA-pulsed DCs	Artificial-designed "TLSs" for reprogramming immunosuppressive TIME [146, 194, 219].
Tirabrutinib	Preclinical	BTK inhibitor	Suppress Breg cell accumulation, reduce IL-10 and IL-35 secretion, foster $CD8^+$ CTL accumulation [40].

Table 2 (continued).

Agent	Phase	Description	Related functions
Cobimetinib	Preclinical	MEK inhibitor	Reduce Breg cell infiltration, interrupt chronic BCR signaling, spare anti-tumor humoral immunity [210].
Resveratrol	Preclinical	STAT3 inhibitor	Hamper Breg cell generation, downregulate TGF-β secretion, impair the conversion of $FoxP3^+$ Treg cells [9, 107]
Lipoxin A4	Preclinical	Lipid mediator	Suppress Breg cell induction, reduce Treg cell proliferation, relieve CTL activities [192].
IL-35 neutralizing antibody	Preclinical	IL-35 antidote	Reduce $PD\text{-}L1^+$ Breg cells, increase $CD8^+CXCR3^+CCR5^+$ T cells, improve anti-PD-1 treatment, enhance IgG- and IgA- expressing plasma cell differentiation [132, 133, 181].

Abbreviations: TIL-B cell, tumor-infiltrating B cell; GM-CSF: granulocyte-macrophage colony-stimulating factor; VEGFR, vascular endothelial growth factor receptor; ICB, immune checkpoint blockage; TAA, tumor-associated antigen; ICOS, inducible T cell costimulator; DC, dendritic cell; TLS, tertiary lymphoid structure; IL-10, interleukin-10; GrB, granzyme B; MEK, mitogen/extracellular signal-regulated kinase; BCR, B cell receptor; BTK, Bruton's tyrosine kinase; ODN, oligonucleotide.

1.5.1 Strategies to promote effector B cell functions and TLS formation

Elevated densities of TIBs and TLSs are associated with improved responses to ICB therapies [23, 25, 73, 91, 145, 158]. In HPV^+ HNSCC, patients treated with radiotherapy and PD-1 inhibitors exhibited enhanced GC formation, increased effector B cell differentiation, and elevated IgG/IgM antibody levels [91].

Several therapeutic cancer vaccines have shown promise in inducing TLSs. GVAX, a GM-CSF–secreting tumor vaccine, elicited robust TLS development in pancreatic cancer patients, correlating with improved clinical prognosis (NCT00727441) [116, 216]. CpG oligodeoxynucleotides (CpG ODNs), as nanoparticle-based vaccine adjuvants, penetrated B cells and plasmacytoid DCs to trigger potent immune activation. When coupled with CXCL13, CpG ODNs promoted $CXCR5^+$ effector TIBs and GrB-expressing CTLs without stimulating $CD20^{low}$ Bregs [14, 30].

Combination therapies involving ICBs and targeted agents have enhanced TLS induction. Co-administration of ICBs with vascular-targeting peptides or anti-VEGFR2 antibodies promoted de novo TLS and HEV formation, cytolysis, and immune activation in previously immune-excluded tumors [3, 87].

Stimulation of co-stimulatory pathways represents another viable approach. The inducible T-cell co-stimulator (ICOS), expressed on activated T cells, contributes to T cell signaling, cytotoxic differentiation, and Treg modulation. In HPV^+ HNSCC, its ligand ICOSL is upregulated on activated TIBs within GCs [53]. Combined therapy with ICOS agonist GSK3359609 and pembrolizumab demonstrated improved objective response and disease control in the INDUCE-1 trial compared to GSK3359609 monotherapy [156].

Cell-based cytokine delivery is another emerging frontier. IL-36γ, expressed by endothelial cells, maintains follicular B cell function [196]. Engineered DCs expressing IL-36γ and T-bet promoted Th1 polarization and TLS formation in sarcoma models [29, 195]. Similarly, CCL21-expressing DCs, evaluated in a phase I trial for advanced lung cancer (NCT01574222), triggered systemic anti-tumor responses and enhanced $CD8^+$ TIL recruitment [105].

Synthetic scaffolds have been developed to mimic lymphoid niches, incorporating LN-derived stromal cells and tumor antigen–pulsed DCs into biocompatible matrices [146, 194, 219, 220]. Integration of a 12-chemokine GES enables the design of tumor-specific, ectopic TLSs [37, 130, 150, 165, 207].

1.5.2 Strategies to inhibit Bregs

Given their immunosuppressive and tumor-promoting properties, Bregs have emerged as promising targets in cancer immunotherapy. One such candidate is CD200, a type I membrane glycoprotein implicated in immunoregulatory signaling and found on Bregs in HPV^+ HNSCC [53]. However, the clinical application of anti-CD200 therapy, such as samalizumab, has thus far yielded unsatisfactory results in both hematological and solid malignancies, with reports of various adverse effects including rash, arthralgia, headache, and hematologic toxicity [122, 169]. These outcomes may be attributed to the widespread expression of CD200 across hematopoietic and non-hematopoietic cells, underscoring the need for caution in selecting depletion targets [113].

Rather than direct depletion, targeting pathways involved in Breg differentiation and function may offer more selective immunomodulation. Small molecule inhibitors of BTK, mitogen-activated protein kinase kinase (MEK), and signal transducer and activator of transcription 3 (STAT3) have shown efficacy in reducing Breg-mediated suppression. Tirabrutinib, a BTK inhibitor, was shown to decrease the abundance of $CD5^+CD1d^{hi}$ Bregs, lower IL-10 and IL-35 secretion, enhance $CD8^+IFN\text{-}\gamma^+$ CTL responses, and limit tumor growth in PanIN-bearing mice [40]. Likewise, cobimetinib, a MEK inhibitor, diminished populations of T2-MZP, B10, and $TIM1^+$ Bregs in colorectal cancer models, while preserving the anti-tumor functions of conventional B cells [210]. Resveratrol, a natural antioxidant that inhibits STAT3, reduced the generation of TGF-β-secreting Bregs and suppressed Breg-driven Treg differentiation in breast cancer models [9, 107].

Therapeutic strategies aimed at modulating Breg phenotypes are also being explored. Lipoxin A4, a bioactive lipid with anti-inflammatory effects, selectively inhibited B10 Breg development while preserving effector B cell function and reducing Tregs within tumors and lymph nodes [192]. In pancreatic cancer models, blockade of IL-35 diminished $PD\text{-}L1^+$

Bregs but promoted $CXCR3^+CCR5^+$ $CD8^+$ T cell infiltration and restored responsiveness to PD-1 blockade [132, 181]. Furthermore, conditional deletion of IL-35 in B cells enhanced plasma cell differentiation and elevated anti-tumor antibody production [133].

Collectively, these findings underscore the potential of integrating TLS-promoting therapies with Breg-targeted strategies to improve immunotherapy outcomes in solid malignancies such as HNSCC. Ongoing research is essential to further elucidate the mechanisms governing TLS assembly and Breg plasticity, thereby facilitating the rational design of TIB-centered therapeutic interventions.

1.6 Aim of this thesis

Once considered peripheral in tumor immunology, TIBs are now increasingly recognized as integral components of the TIME, capable of exerting both pro- and anti-tumor functions depending on their differentiation state, spatial organization, and local cytokine milieu. Among the diverse TIB subsets, MZBs remain largely uncharacterized within the tumor context. Despite their well-established roles in antimicrobial defense and immune regulation under homeostatic conditions, the contribution of MZBs to tumor development, immune evasion, or tumor control remains poorly understood, and their relevance in human solid malignancies has not been systematically explored.

In recent work, we observed high numbers of MZB-like cells infiltrating murine HNSCC, where they exhibited immunosuppressive potential within the TIME [175]. Building on our previous findings, the present study aimed to validate the presence of MZBs in human HNSCC and to comprehensively investigate their cellular characteristics, immunoregulatory functions, spatial distribution, and potential prognostic significance.

2 Materials and methods

2.1 Materials

2.1.1 Laboratory equipment

Table 3: List of laboratory equipment.

Equipment	Manufacturer
-80 °C HERH Freeze HFUB Series Freezer	Thermo Fisher Scientific, USA
-20 °C Premium No Frost Freezer	Liebherr, Switzerland
4 °C Refrigerator	Liebherr, Switzerland
Automated Cell Counter	Bio-Rad Laboratories, USA
Bead Bath Mini M720 Water Bath	Sheldon Manufacturing Inc., USA
Bench Centrifuge 5810 R	Eppendorf AG, Germany
Bench Centrifuge 5424R	Eppendorf AG, Germany
Fume Cupboard	Wesemann GmbH, Germany
Gallios 3L10C Flow Cytometer	Beckman Coulter, USA
gentleMACS Octo Dissociator with Heaters	Miltenyi Biotec GmbH, Germany
Heracell CO_2 Incubator	Thermo Fisher Scientific, USA
Herasafe laminar Flow Hood	Thermo Fisher Scientific, USA
Ice Flaker AF 80	Scotsman, UK
Liquid Nitrogen Tank	MTI IndustrieGase AG, Germany
MACS MultiStand magnetic bead separator	Miltenyi Biotec GmbH, Germany
Microscope CK30	Olympus Corporation, Japan
Mini G Centrifuge	IKA, Germany
Perfusion Tubing Pump	Ismatec, Germany
pH Meter, pH50+	XS instruments, Italy
Pocket Balance CM 150-1 N	KERN & SOHN GmbH, Germany
Polymax 2040 Platform Shaker	Heidolph Instruments GmbH, Germany
QBD1 Heating System	Grant Instruments, UK

Table 3 (continued).

Equipment	Manufacturer
Transferpette® S Pipettes (10 µl, 20 µl, 100 µl, 1000 µl)	Brand GmbH, Germany
Tube Roller	NeoLab Migge GmbH, Germany
TissueLyser® II	Qiagen GmbH, Germany
VORTEX-GENIE® 2 Mixer	Scientific Industries Inc., USA

2.1.2 Consumable material

Table 4: List of consumable materials.

Consumable Material	Manufacturer
MACS SmartStrainer	Miltenyi Biotec GmbH, Germany
15 cm Tissue Culture Dish	Thermo Fisher Scientific, USA
Cryogenic Vials (2 ml)	Falcon, USA
Cover Slips	VWR chemicals, France
Glass Pipettes (5 ml, 10 ml, 25 ml)	Brand GmbH, Wertheim, Germany
Microscope Slides / Glass Slides	Marienfeld-Superior GmbH, Germany
Multi-well Plates (24-well, 96-well)	Greiner Bio-One GmbH, Germany
Nitril Gloves	Shield Scientific BV, Netherlands
Pipette Tips (0.1 - 1000 µl)	Sarstedt AG & Co. KG, Germany
Serological Transfer Pipettes (2 ml)	BD Falcon, USA
Serological Transfer Pipettes (5 ml, 10ml, 25 ml)	Sarstedt, Germany
Sterile Surgical Blades	B Braun Melsungen AG, Germany
SUPRA Cannula	Ehrhardt-Soehne GmbH, Germany
Syringe Filters (0.22 µm)	VWR chemicals, France
Syringe Needles (20 G/22 G/26 G)	B.Braun, Germany
Syringes (1 ml/5 ml/10 ml)	B.Braun, Germany
Tissue Culture Dishes (3.5cm, 6cm, 10cm)	BD Falcon, USA
Tissue Culture Flasks (25 cm^2/75 cm^2)	BD Falcon, USA

Table 4 (continued).

Consumable Material	Manufacturer
Microcentrifuge Tubes (0.5 ml, 1.5 ml, 2.0 ml)	Eppendorf AG, Germany
Conical Tubes (15 ml, 50 ml)	Falcon, USA
Vacuum Filtration Unit Filtropur 0.22 µm	Sarstedt, Germany

2.1.3 Chemicals and drugs

Table 5: List of Chemicals and drugs.

Material	Manufacturer
Ammonium Chloride (NH_4Cl)	Carl Roth GmbH, Germany
Bovine Serum Albumin Fraction V (BSA)	AppliChem GmbH, Germany
CryoStor® CS10 Cryopreservation Medium	STEMCELL Technologies, Canada
DAPI (4',6-Diamidino-2-phenylindol)	AppliChem GmbH, Germany
Dimethyl sulfoxide (DMSO)	AppliChem GmbH, Darmstadt, Germany
DNase I solution	Bioline, USA
Donkey serum (Blocking Reagent)	Sigma Aldrich, USA
Dulbecco's Phosphate-Buffered Saline (DPBS, 1×)	Thermo Fisher Scientific, USA
EDTA-Na_2 (Ethylenediaminetetraacetic Acid Disodium Salt)	AppliChem GmbH, Germany
Ethylene Glycol	Carl Roth GmbH, Germany
Erythrocyte Lysis Buffer	Thermo Fisher Scientific, USA
Fetal Bovine Serum (FBS), Heat-inactivated	Gibco, USA
Ficoll-Paque PLUS	Cytvia, USA
Glycerol	AppliChem GmbH, Germany
Hydrogen Carbonate (Sodium Bicarbonate, $NaHCO_3$)	Carl Roth GmbH, Germany
MACS Buffer (0.5% BSA, 2 mM EDTA in PBS)	Miltenyi Biotec GmbH, Germany
Paraformaldehyde (PFA), 4% Solution	AppliChem GmbH, Germany
Phosphate-Buffered Saline (PBS)	AppliChem GmbH, Germany
Triton X-100	AppliChem GmbH, Germany

Table 5 (continued).

Material	Manufacturer
Trypan Blue Solution (0.4%)	Sigma Aldrich, USA

2.1.4 Commercial assays

Table 6: Critical commercial assays.

Kit	Source	Catalogue No.	RRID
Tumor Dissociation Kit	Miltenyi Biotec	130-095-929	SCR_020276
CD45 (TIL) MicroBeads, Human	Miltenyi Biotec	130-118-780	SCR_021158
Versacomp Antibody Capture Bead Kit	Beckman Coulter	B22804	SCR_022159
EasySep B cell Isolation Kit	STEMCELL	17954	AB_2783451
B cell Expansion kit, Human	Miltenyi Biotec	130-124-195	AB_273699

2.1.5 Antibody list

Table 7: List of antibodies.

Antibody	Source	Application	Catalogue No.	RRID
anti-human CD39 PE/Cy7	Invitrogen	IF	25-0399-42	AB_1582280
anti-human CD39 APC	BD Biosciences	IF	560239	AB_1645459
anti-human CD39 PerCy7	Biolegend	IF	328212	AB_2099950
anti-human CD1c PE	Biolegend	IF	331506	AB_1088999
anti-human CD19 APC/Fire750	Biolegend	IF	302258	AB_2629691
anti-human CD24 PE/AF610	Invitrogen	IF	MHCD2422	AB_10375871
anti-human CD24 PE/Dazzle594	Biolegend	IF	311134	AB_2566349
anti-human CD73 eFluor450	Invitrogen	IF	48-0739-42	AB_11041811
anti-human CD73 PE/Dazzle594	Biolegend	IF	344020	AB_2565301
anti-human IgD AF700	Biolegend	IF	348230	AB_2563335

Table 7 (continued).

Antibody	Source	Application	Catalogue No.	RRID
anti-human IgM BV421	Biolegend	IF	314516	AB_2561443
anti-human CD38 PerCP	Biolegend	IF	303520	AB_893313
anti-human CD38 FITC	Biolegend	IF	303504	AB_314356
anti-human CD10 PE/Cy7	Biolegend	IF	312214	AB_2146548
anti-human CD23 APC	Invitrogen	IF	17-0238-42	AB_2016666
anti-human CD45RB PE	Biolegend	IF	310204	AB_314807
anti-human CD45 AmCyan	BD Biosciences	IF	339192	AB_647361
anti-human CD27 APC	Invitrogen	IF	17-0279-42	AB_10671130
anti-human CD27 PE/Cy5	Invitrogen	IF	15-0279-42	AB_10717249
anti-human CD21 FITC	Invitrogen	IF	11-0219-42	AB_2572442
anti-human ABCB1 (CD243) FITC	Invitrogen	IF	11-2439-42	AB_11220266
anti- CD3 (SP7)	abcam	IF	ab16669	AB_443425
anti- CD20 (SP32)	abcam	IF	ab64088	AB_1139386
anti- CD39 (EPR20627)	abcam	IF	ab223842	AB_2889212
anti- BCL6	abcam	IF	ab272859	AB_470983
CD169 monoclonal antibody (Hsn 7D2)	Invitrogen	IF	MA1-16891	AB_568734
CD1d polyclonal antibody	Invitrogen	IF	PA5-102477	AB_2851879

2.1.6 Buffers and solutions

Table 8: List of buffers or solutions for immunofluorescence staining.

Buffer or solution	Ingredients	Amount
Cryoprotectant Solution (100 ml)	PBS 1X	50 ml
	Ethylene Glycol	20 ml
	Glycerol	30 ml

Table 8 (continued).

Buffer or solution	Ingredients	Amount
Cryoprotectant Solution (100 ml)	PBS 1X	50 ml
	Ethylene Glycol	20 ml
	Glycerol	30 ml
10% BSA (100 ml)	Albumin Bovine Fract V	10 g
	PBS 1X	fill up to 100 ml
10% Triton Solution (50 ml)	Triton-X-100	5 ml
	PBS 1X	45 ml
Erythrocyte Lysis Buffe (pH 7.2 – 7.4)	NH_4CI	150 mM
	$NaHCO_3$	10 mM
	EDTA-Na_2	100 mM
Blocking Solution for Immunofluorescence (10 ml)	10% BSA	3000 µl
	10% Triton solution	300 µl
	PBS 1X	6700 µl

2.1.7 Software

Table 9: List of software used in this thesis.

Software	Manufacturer	RRID
Kaluza	Beckman Coulter Life Sciences	SCR_018638
FlowJo 10	BD Biosciences	SCR_008520
Zotero 6.0.37	George Mason University	SCR_013619
Graphpad Prism 10.0	Graphpad Software	SCR_002798
Adobe Illustrator 2021	Adobe Systems	SCR_010279
R version 4.0.3	The R Foundation	SCR_001905
R version 4.2.0	The R Foundation	SCR_001905
MS Office 2019	Microsoft	SCR_016137
Photoshop 2021	Adobe Systems	SCR_014199
BioRender	BioRender	SCR_018361

Besides the above-mentioned softwares, ChatGPT (version 5.2; OpenAI) was used solely for language editing and improvement of English clarity in the thesis.

2.2 Methods

2.2.1 Study Design

To explore the functional relevance of MZBs in HNSCC, we employed an integrative approach combining flow cytometry, scRNA-seq, and spatial transcriptomics (ST). The study aimed to delineate discrete MZB and GCB subsets, examine their spatial and cellular interactions with other TILs, compare their functional profiles between malignant and non-malignant tissues, evaluate their immunomodulatory properties, and assess their potential prognostic impact (**Fig. 4**).

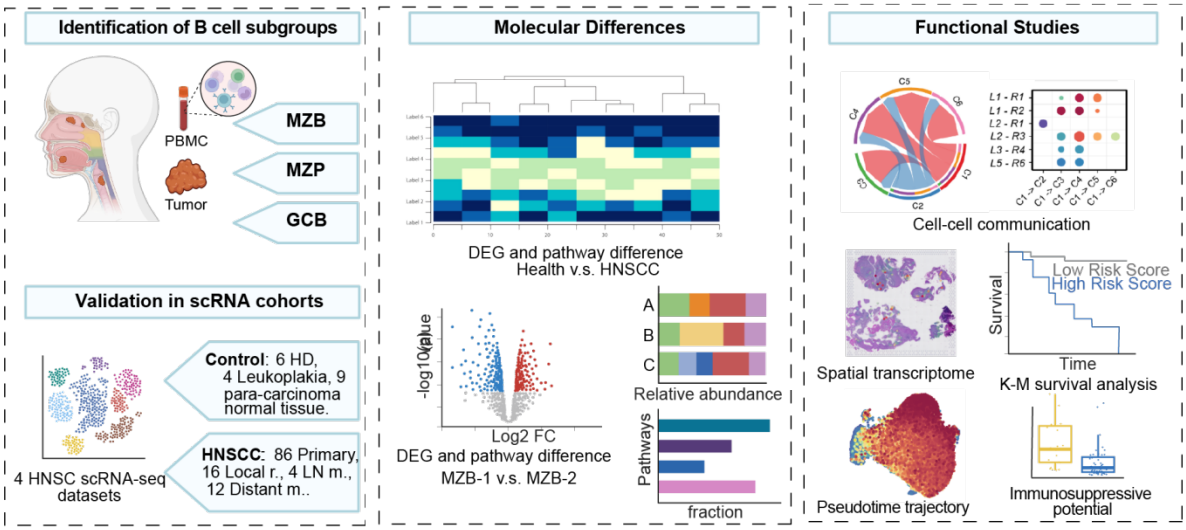

Figure 4. Schematic research flow chart.

Reprinted as an author from J.Bao 2025 [12], CC BY 4.0, https://creativecommons.org/licenses/by/4.0/.

2.2.2 Study approval

Human tumor tissue was obtained during surgery from HNSCC patients with research ethics committee approval (REC; reference number: 90/15) and written informed consent from the patient. Blood samples were obtained from patients with HNSCC and healthy volunteers (non-tumor patients) with written informed consent and REC approval (reference number: 90/15).

2.2.3 Cohort characteristics

The study cohort included both HNSCC patients and healthy donors (HD), irrespective of gender. Biological sex was not considered a variable in the study design. Tumor tissue specimens were collected intraoperatively, while peripheral blood samples were obtained from both patient and control groups. The HPV status of tumor biopsies was evaluated using p16 immunohistochemistry (IHC) and PCR-based HPV DNA detection.

The MZB cohort consisted of 81 peripheral blood mononuclear cell (PBMC) samples and 24 TIL samples from HNSCC patients, as well as 20 PBMC samples from HDs. Clinical characteristics are summarized in **Table 10**.

Table 10: Clinicpathologcial charateristics of the MZB cohort.

Characteristic	HNSCC Patients (PBMCs, n=81)	Healthy Volunteers (PBMCs, n=20)	HNSCC Patients (TILs, n=24)
Age, median (range)	66 (40–90)	57.28 (43–85)	54.46 (40–76)
Male, n (%)	63 (77.78%)	16 (80%)	20 (83.33%)
Female, n (%)	18 (22.22%)	4 (20%)	4 (16.67%)
Tobacco use, n (%)	57 (70.37%)	12 (60%)	18 (75%)
Alcohol use, n (%)	53 (65.43%)	16 (80%)	13 (54.17%)
HPV+, n (%)	24 (29.63%)	-	5 (20.83%)
HPV−, n (%)	20 (24.69%)	-	8 (33.33%)
HPV undetermined, n (%)	37 (45.68%)	-	11 (45.83%)
Tumor site: Oral cavity	10 (12.34%)	-	14 (58.33%)
Tumor site: Larynx/Hypopharynx	20 (48.78%)	-	3 (12.50%)
Tumor site: Nasopharynx/Oropharynx	44 (54.32%)	-	14 (58.33%)
Tumor stage I–II	11 (13.58%)	-	5 (20.83%)
Tumor stage III-IV	70 (86.41%)		19 (79.17%)
Recurrence, n (%)	16 (19.75%)	-	-
Death, n (%)	11 (13.58%)	-	-

The T2-MZP cohort included 38 PBMC and 20 TIL samples from HNSCC patients and 10 PBMC samples from HDs (**Table 11**).

Table 11: Clinicpathologcial charateristics of the MZP cohort.

Characteristic	HNSCC Patients (PBMCs, n=38)	Healthy Volunteers (PBMCs, n=10)	HNSCC Patients (TILs, n=20)
Age, median (range)	59.85 (45–82)	48.75 (43–60)	62.6 (49–73)
Male, n (%)	29 (76.32%)	8 (80%)	16 (80%)
Female, n (%)	18 (47.37%)	2 (20%)	4 (20%)
Tobacco use, n (%)	28 (73.68%)	6 (60%)	12 (60%)
Alcohol use, n (%)	25 (65.79%)	8 (80%)	19 (95%)
HPV+, n (%)	11 (28.94%)	-	5 (25%)
HPV−, n (%)	12 (31.58%)	-	6 (30%)
HPV undetermined, n (%)	15 (39.47%)	-	9 (45%)

Table 11 (continued).

Characteristic	HNSCC Patients (PBMCs, n=38)	Healthy Volunteers (PBMCs, n=10)	HNSCC Patients (TILs, n=20)
Tumor site: Oral cavity	7 (18.42%)	-	3 (15%)
Tumor site: Larynx/Hypopharynx	7 (18.42%)	-	7 (35%)
Tumor site: Nasopharynx/Oropharynx	20 (52.63%)	-	10 (50%)
Tumor stage I–II	7 (18.42%)	-	5 (25%)
Tumor stage III–IV	31 (81.58%)		15 (75%)
Recurrence, n (%)	16 (19.75%)	-	-
Death, n (%)	11 (13.58%)	-	-

The GCB cohort consisted of 42 PBMC and 16 TIL samples from HNSCC patients, and 15 PBMC samples from HDs (**Table 12**).

Table 12: Clinicpathologcial charateristics of the T2-MZP cohort.

Characteristic	HNSCC Patients (PBMCs, n=42)	Healthy Volunteers (PBMCs, n=15)	HNSCC Patients (TILs, n=16)
Age, median (range)	64.43 (45–85)	53.27 (43–72)	58 (40–72)
Male, n (%)	32 (76.19%)	12 (80%)	12 (75%)
Female, n (%)	11 (26.19%)	3 (20%)	4 (25%)
Tobacco use, n (%)	32 (76.19%)	7 (46.67%)	13 (81.25%)
Alcohol use, n (%)	31 (73.81%)	11 (73.33%)	14 (87.5%)
HPV+, n (%)	12 (28.57%)	-	7 (43.75%)
HPV−, n (%)	13 (30.95%)	-	9 (56.25%)
HPV undetermined, n (%)	17 (40.48%)	-	-
Tumor site: Oral cavity	6 (14.29%)	-	6 (37.5%)
Tumor site: Larynx/Hypopharynx	10 (23.81%)	-	4 (25%)
Tumor site: Nasopharynx/Oropharynx	22 (52.38%)	-	6 (37.5%)
Tumor stage I–II	8 (19.05%)	-	4 (26.67%)
Tumor stage III–IV	34 (80.95%)	-	11 (73.33%)
Recurrence, n (%)	12 (28.57%)	-	-
Death, n (%)	2 (4.76%)	-	-

2.2.4 PBMC isolation

PBMCs were isolated from whole blood samples collected at the ENT Clinic of Ulm University Hospital. Following standard density gradient centrifugation using Ficoll-Paque™, mononuclear cells were harvested, washed with PBS, and resuspended in freezing medium (10% DMSO and 90% FBS). Samples were initially frozen in a controlled-rate freezer and subsequently stored in liquid nitrogen. Upon use, cryopreserved cells were rapidly thawed in a 37°C water bath and washed to remove residual DMSO. All handling was conducted under aseptic conditions to preserve cell viability.

2.2.5 Tumor dissociation and TIL isolation

Tumor specimens were processed immediately after surgical resection. Following removal of excess adipose tissue, samples were weighed and transferred into sterile tubes. Enzymatic digestion was performed using the Tumor Dissociation Kit (Miltenyi Biotec), and mechanical disruption was applied via the gentleMACS Dissociator according to the manufacturer's optimized protocol. Upon completion, the dissociated tissue suspension was filtered through a 70 µm cell strainer to remove debris and residual tissue fragments.

The resulting cell suspension was centrifuged at 300 × g for 7 minutes, and the supernatant was discarded. The pellet was treated with 1 ml erythrocyte lysis buffer diluted in 9 ml Ampuwa Pyrogen-Free Water and incubated for 10 minutes at room temperature to eliminate residual red blood cells. After a second centrifugation at 300 × g, the supernatant was removed, and the cell pellet was resuspended in 2 ml of RPMI medium. Cell viability and concentration were subsequently determined by using standard cell counting procedures.

To isolate $CD45^+$ TILs, magnetic separation was performed using CD45 (TIL) MicroBeads (Miltenyi Biotec). MicroBeads were added to the cell suspension and incubated as per the manufacturer’s instructions. After magnetic enrichment, $CD45^+$ TILs were collected and processed directly for downstream flow cytometric analysis.

2.2.6 Flow cytometry

Single-cell suspensions from PBMCs and CD45+ TILs were subjected to flow cytometry using standardized staining protocols. A 1 ml aliquot of cell suspension was centrifuged at 400 × g for 7 minutes, followed by removal of the supernatant. The cell pellet was resuspended in pre-prepared antibody cocktails specific to each cohort as depicted in **Table 13 – 15**.

Samples were incubated for 30 minutes at 4°C to allow antibody binding. For the MZP cohort, an additional step was included: cells were pre-stained with R123 for 10 minutes at room temperature, followed by a 3-hour chase period prior to antibody staining. All staining steps were performed under light-protected and aseptic conditions to ensure sample integrity and reproducibility.

Table 13. MZB FACS panel.

Wave Band	Channel	Antibody	Dose
488 nm	FL1	CD21 FITC	3ul
	FL2	CD1c PE	5ul
	FL3	CD73 PE/Dazzle594	4ul
	FL4	CD27 PE/Cy5	5ul
	FL5	CD39 Pe/Cy7	4ul
633 nm	FL6	CD23 APC	4ul
	FL7	IgD AF700	4ul
	FL8	CD19 APC/Fire750	3ul
405 nm	FL9	IgM BV421	3ul
	FL10	CD45 AmCyan	3ul

Table 14. MZP FACS panel.

Wave Band	Channel	Antibody	Dose
488 nm	FL1	ABCB1 FITC	5ul
	FL2	CD45RB PE	5ul
	FL3	CD73 eFluor450	4ul
	FL4	CD27 PE/Cy5	5ul
	FL5	CD10 PE/Cy7	5ul
633 nm	FL6	CD39 APC	4ul
	FL7	IgD AF700	4ul
	FL8	CD19 APC/Fire750	3ul
405 nm	FL9	IgM BV421	3ul
	FL10	CD45 AmCyan	3ul

Table 15. GCB FACS panel.

Wave Band	Channel	Antibody	Dose
488 nm	FL1	CD38 FITC	5ul
	FL3	CD73 PE/Dazzle594	4ul
	FL4	CD27 PE/Cy5	5ul
	FL5	CD10 PE/Cy7	5ul

Table 15 (continued).

Wave Band	Channel	Antibody	Dose
633 nm	FL6	CD39 APC	4ul
	FL7	IgD AF700	4ul
	FL8	CD19 APC/Fire750	3ul
405 nm	FL9	IgM BV421	3ul
	FL10	CD45 AmCyan	3ul

Following antibody incubation, cells were washed with 2 ml of FACS buffer (PBS containing 0.05% BSA) and centrifuged at 400 × g for 7 minutes. The supernatant was discarded, and the cell pellet was resuspended in 300 µl of FACS buffer. Samples were subsequently acquired using the Gallios flow cytometer (Beckman Coulter). Instrument settings and gating strategies were applied as detailed in **Figures 5 – 7** to ensure consistent and accurate analysis across all cohorts.

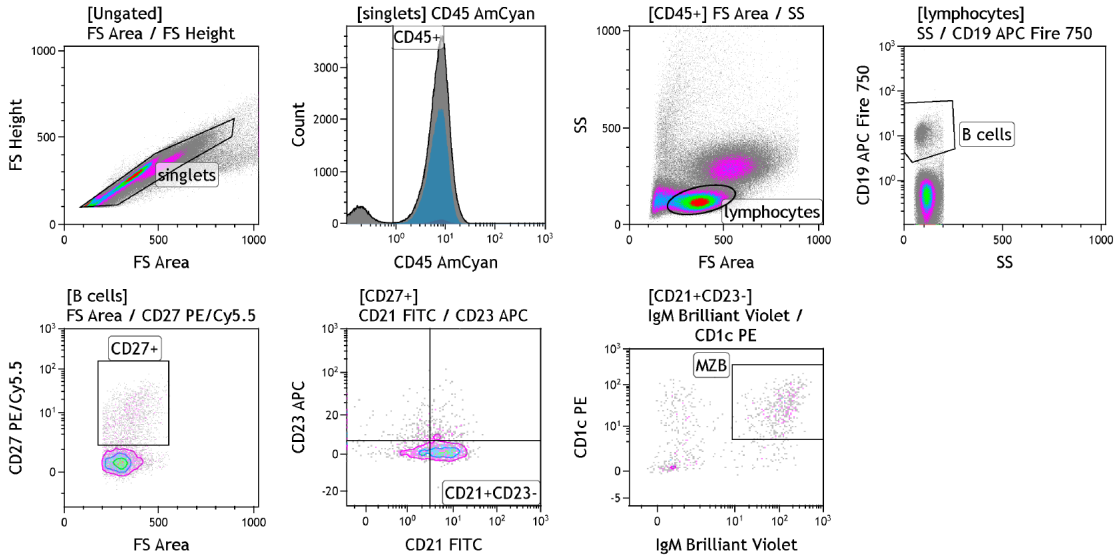

Figure 5. MZB gating strategy.

Representative flow cytometry plots showing the sequential gating strategy used to define marginal zone B cells (MZBs). Singlets were first selected based on FS-A and FS-H, followed by gating of $CD45^+$ leukocytes and lymphocytes according to FS-A and SS characteristics. $CD19^+$ B cells were then identified, and $CD27^+$ B cells were further gated. Within the $CD27^+$ compartment, $CD21^+CD23^-$ cells were selected, and MZBs were subsequently defined as $CD1c^+IgM^+$ cells.

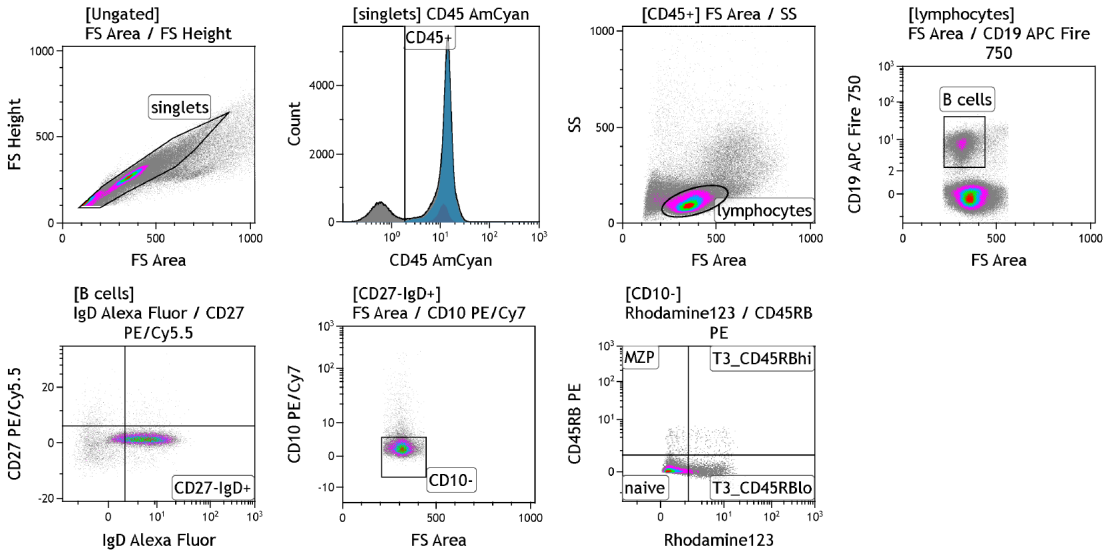

Figure 6. MZP gating strategy.

Representative flow cytometry plots showing the sequential gating strategy used to identify marginal zone precursor B cells (MZPs). Singlets were first selected based on FS-A and FS-H, followed by gating of $CD45^+$ leukocytes and lymphocytes according to FS-A and SS characteristics. $CD19^+$ B cells were then identified within the lymphocyte gate. Among B cells, $CD27^-IgD^+$ cells were selected, followed by exclusion of $CD10^+$ cells. MZPs were subsequently defined within the $CD10^-$ population based on high CD45RB expression and rhodamine 123 staining.

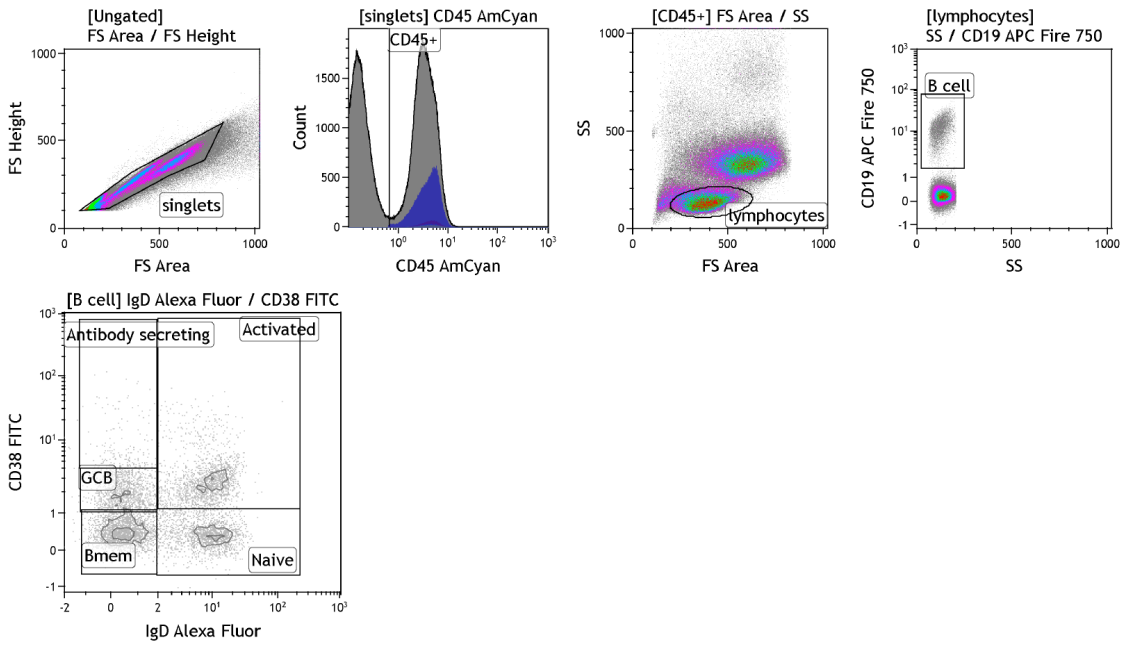

Figure 7. GCB gating strategy.

Representative flow cytometry plots showing the sequential gating strategy used to identify germinal center B cells (GCBs). Singlets were first selected based on FS-A and FS-H, followed by gating of $CD45^+$ leukocytes and lymphocytes according to FS-A and SS characteristics. $CD19^+$ B cells were then identified within the lymphocyte gate. GCBs were subsequently defined within the B cell population based on IgD and CD38 expression.

Compensation was performed using the Versacomp antibody capture bead kit. Single-stained and unstained PBMCs were used to generate compensation matrices and correct for spectral spillover. Data were analyzed using Kaluza 2.1 (Beckman Coulter), with further processing in Microsoft Excel (2019) and GraphPad Prism 10.0.

2.2.7 Single-cell transcriptome analysis

Four publicly available scRNA-seq datasets (GSE139324, GSE164690, GSE181919, GSE234933) comprising 118 HNSCC patients and controls were integrated. Overall, 118 HNSCC patients (with samples from 86 primary HNSCC, 16 local recurrence, 4 LN metastasis, 12 distant metastasis), 9 normal para-carcinoma tissue, 6 tonsil samples of HD, and 4 samples of leukoplakia were accumulated. After filtering for quality (excluding cells with >15% mitochondrial transcripts, <500 genes, or >20,000 transcripts), normalization and batch correction were performed using *SCTransform* and *Harmony* (with sample ID as vector covariant) [33, 97].

Clustering was conducted using principal components analysis (PCA) (top 15 PCs) followed by *Seurat::FindClusters* (resolution = 0.1). B cells were extracted and reclustered (30 PCs, resolution = 1.3) to define subpopulations.

B cell subclusters were annotated using a combined approach of reference mapping, marker gene validation, and gene signature scoring. SingleR (v1.10.0) was first applied for automated annotation using GSE193868 (a CITE-seq dataset with defined MZB clusters) as the primary reference, along with HPCA and BlueprintEncodeData for cross-validation [7, 84]. Predicted labels were confirmed by evaluating top differentially expressed genes (DEGs) for canonical B cell subtype markers [101, 135]. Additionally, gene signatures relevant to MZB and GCB development from MSigDB C5 were used to calculate enrichment scores, supporting the final assignment of cluster identities. Clusters were labeled based on consistent predictions and expression of canonical MZB and GCB markers.

DEGs were identified using the Wilcoxon rank sum test with $|\log FC| > 0.25$ and ≥10% expression threshold (*Seurat::FindMarkers*).

2.2.8 scRNA-seq downstream analysis

Downstream analyses included Gene Ontology (GO), Gene Set Variation Analysis (GSVA), Gene Set Enrichment Analysis (GSEA), and cell-cell communication inference. GO enrichment was performed using the clusterProfiler package (v4.4.4) on DEGs ($\log2FC > 0.15$, adjusted $p < 0.05$), to elucidate biological processes distinguishing B cell subclusters in HNSCC versus healthy controls [213]. The compareCluster function was used with a significance threshold of $p < 0.05$.

GSVA was applied to quantify pathway activity at the subcluster level using the GSVA package (v1.46.0) with default parameters, referencing the Reactome database [71].

Cell-cell communication was inferred using CellChat (v1.6.1) and the CellChatDB.human ligand-receptor (L-R) database [86]. Subcluster annotations were refined across all $CD45^+$ TILs using a clustering resolution of 0.8. Annotations were guided by HPCA references and original labels from the GSE139324, GSE164690, GSE181919, and GSE234933 datasets. Lymphocyte subsets—including T cells, monocytes, DCs, and macrophages—were identified and merged with B cell annotations to generate a comprehensive immune atlas.

CellChat was then used to model signaling interactions, with a focus on MZB-1 and MZB-2.

GSEA was performed to compare signaling pathway enrichment between MZB-1 and MZB-2 clusters, using GO, KEGG, and MSigDB C7 (immunologic signature) gene sets [203]. Particular attention was given to NOTCH-related signatures within MSigDB C7 to assess differential pathway activity in primary HNSCC samples.

2.2.9 Survival analysis

To assess the prognostic relevance of MZB-1, MZB-2, and GCB cell infiltration in HNSCC, we analyzed the Cancer Genome Atlas (TCGA) HNSC dataset. Cell type proportions were inferred using CIBERSORTx, a deconvolution algorithm that estimates cellular composition from bulk RNA-seq data [137]. The signature matrix was derived from our integrated scRNA-seq dataset with annotated TIL subtypes, while TCGA HNSC served as the query dataset. HPV status was reannotated based on oncoviral genotyping [19].

Kaplan–Meier survival curves were generated, and statistical significance was assessed using the Mantel–Cox log-rank test. The maxstat algorithm was employed to define optimal thresholds for dichotomizing patients based on MZB-1 and MZB-2 abundance, enabling robust survival group stratification.

2.2.10 ST analysis

To investigate the spatial localization of MZB clusters, we analyzed the publicly available ST dataset GSE220978. Spots with fewer than 200 detected features were excluded, and the data were normalized using the SCTransform method [69]. Dimensionality reduction was performed via PCA, followed by unsupervised clustering using Seurat's FindNeighbors and FindClusters functions based on the top 30 principal components. Clusters were visualized using UMAP and SpatialDimPlot.

For cell type deconvolution, the GSE181919 scRNA-seq dataset was selected as the reference. After normalization and clustering via the Louvain algorithm, existing annotations from the reference dataset were used to infer cell identities in the Visium spots. Seurat's Label Transfer workflow [178] was applied, identifying anchors with FindTransferAnchors and assigning cell types using TransferData, based on the highest classification probability

per spot. Annotations were validated against the original publication's pathologist-assigned labels and multiplex immunofluorescence data [217].

To improve the resolution of MZB cluster assignment, we repeated the Label Transfer procedure using our own extensively annotated scRNA-seq dataset as the reference and GSE220978 as the query. This ensured consistent and high-confidence spatial mapping of MZB subpopulations within the tumor tissue.

2.2.11 Statistics, data analysis, and visualization

All statistical analyses and data visualizations were performed using GraphPad Prism (v10.0) and R (v4.0.3 and 4.2.0). Circos plots were generated using the circlize package [65], volcano plots with EnhancedVolcano [89], and heatmaps with ComplexHeatmap [64]. Single-cell visualizations were created using Seurat (v3.2.2), ggplot2, and ggpubr [72].

Data normality was assessed with Shapiro-Wilk's test, and variance homogeneity with Levene's test. Residuals meeting criteria ($p > 0.05$) were considered valid; extreme outliers ($\geq 3 \times$ interquartile range) were excluded. Mann-Whitney U test was used for non-parametric comparisons, and unpaired t-tests with Welch's correction for parametric comparisons. Multiple group comparisons used one-way ANOVA followed by Bonferroni post hoc tests.

Results are presented as mean ± SEM or box plots showing median, quartiles, and range (Tukey style). Statistical significance was defined as: *$p < 0.05$; **$p < 0.01$; ***$p < 0.001$; ***$p < 0.0001$.

2.2.12 Data availability

The scRNA-seq datasets GSE139324, GSE164690, GSE181919, and GSE234933, as well as the ST dataset GSE220978, are publicly available from the Gene Expression Omnibus (GEO; https://www.ncbi.nlm.nih.gov/geo/) [222]. Bulk RNA-seq data of the TCGA-HNSC cohort were retrieved from the Genomic Data Commons (GDC) portal (https://portal.gdc.cancer.gov/) [223]. All analysis scripts and reproducible code are available at https://github.com/immMLab/Marginal-Zone-B-cells-in-HNSCC.

3 Results

3.1 Landscape of TIB subsets in HNSCC patients

Building upon our prior murine studies, which demonstrated an accumulation of immunosuppressive MZBs during tumor progression, we sought to determine whether similar B cell subpopulations are present and functionally relevant in human HNSCC [175]. To this end, comprehensive immunophenotyping was performed in both tumor tissues and peripheral blood of HNSCC patients, focusing on B cell subsets with potential pro- or anti-tumorigenic roles.

Three dedicated flow cytometry panels were established to identify MZB, MZP, and GCB subsets. Using these panels, we confirmed the presence of all three populations—MZB, MZP, and GCB—within both the TIME and circulation, marking the first documentation of MZB and MZP in human squamous epithelial tumors of the head and neck.

MZBs were identified as $CD19^{+}CD27^{+}CD21^{+}CD23^{-}CD1c^{+}IgM^{+}$ [4, 84, 168, 187, 198] (**Fig. 8a**). Notably, MZBs were enriched in HPV^{+} patients relative to HPV^{-} patients in both tumor tissues (**Fig. 8b**) and peripheral blood (**Fig. 8c**). The MZB proportion did not vary significantly by tumor site (**Fig. 8b, d**). However, circulating MZB levels were higher in patients with T2 tumors (**Fig. 8e**), and overall MZB frequencies positively correlated with tumor progression (AJCC 8th Edition), in both PBMCs and tumors (**Fig. 8b, f**).

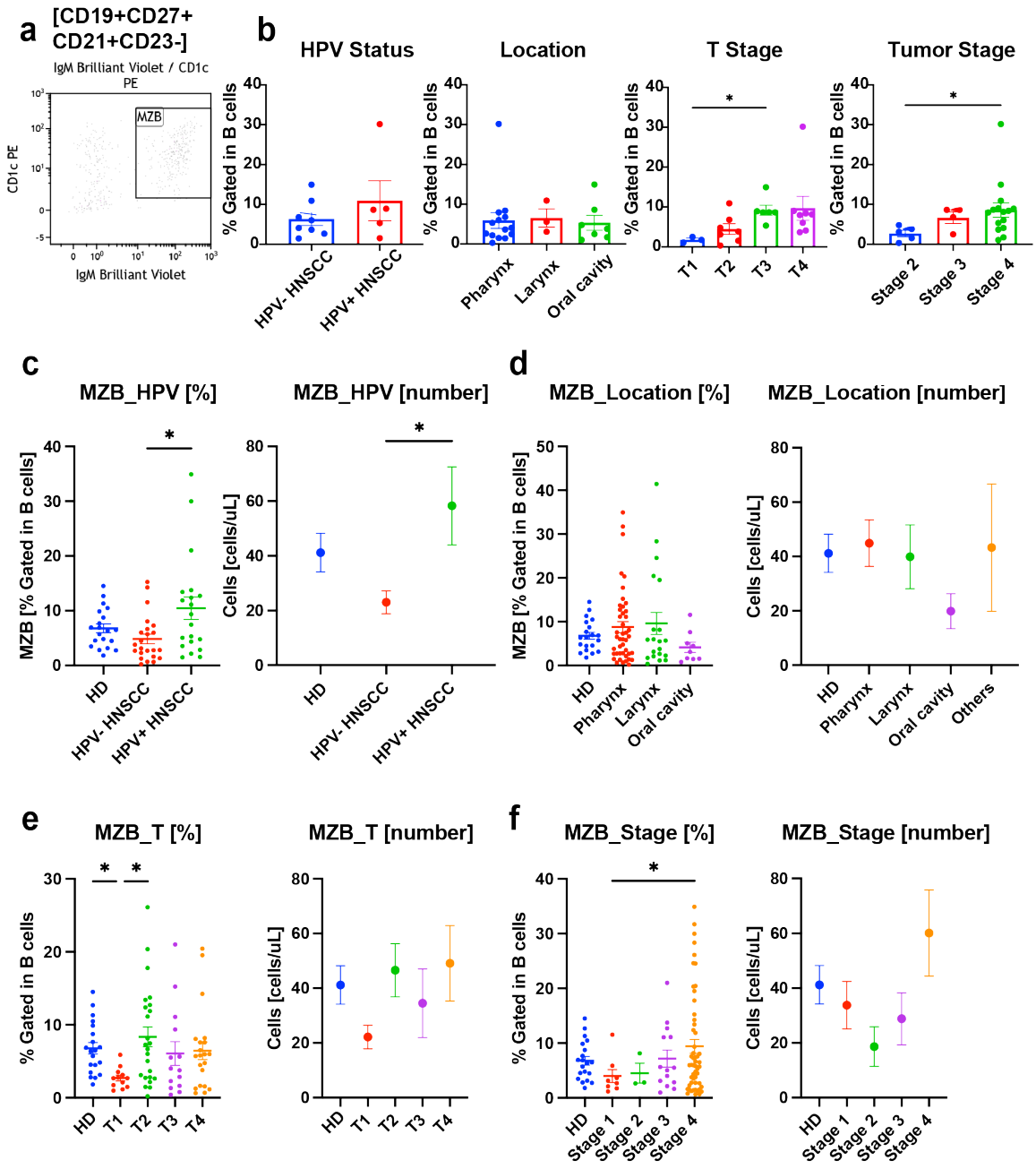

Figure 8. Flow cytometric analysis of MZBs in HNSCC.

(a) MZB gating strategy.

(b) MZB distribution in tumor tissues (n = 24) stratified by HPV status, tumor location, AJCC T stage, and clinical stage.

(c-f) MZB distribution in PBMCs from HDs (n = 20) and patients with HNSCC (n = 81) stratified by HPV status (c), primary tumor location (d), AJCC T stage (e), and clinical stage (f).

Cell proportions were tested using unpaired t-test with Welch's correction or one-way ANOVA with Bonferroni post-hoc analysis. Legend continued on next page.

Figure 8 (continued).

Modified as an author from J.Bao 2025 [12], CC BY 4.0, https://creativecommons.org/licenses/by/4.0/.

Abbreviations: MZB, marginal zone B cell; HNSCC, head and neck squamous cell carcinoma; PBMC, peripheral blood mononuclear cell; HD, healthy donor; HPV, human papillomavirus; AJCC, American Joint Committee on Cancer.

MZP were gated as $CD19^{+}CD27^{-}IgD^{+}CD10^{-}R123^{-}CD45RB^{+}IgM^{+}$ [177, 187] (**Fig. 9a**). A mild enrichment of MZPs was seen in HPV^{+} tumors (**Fig. 9b**), but not in peripheral blood (**Fig. 9c**). MZP frequencies were unaffected by tumor site (**Fig. 9b, d**). In PBMCs, MZPs declined progressively with increasing T stage (**Fig. 9e**) and clinical stage (**Fig. 9f**), when adjusted for leukocyte counts. No consistent pattern was observed in tumor-resident MZPs (**Fig. 9b**).

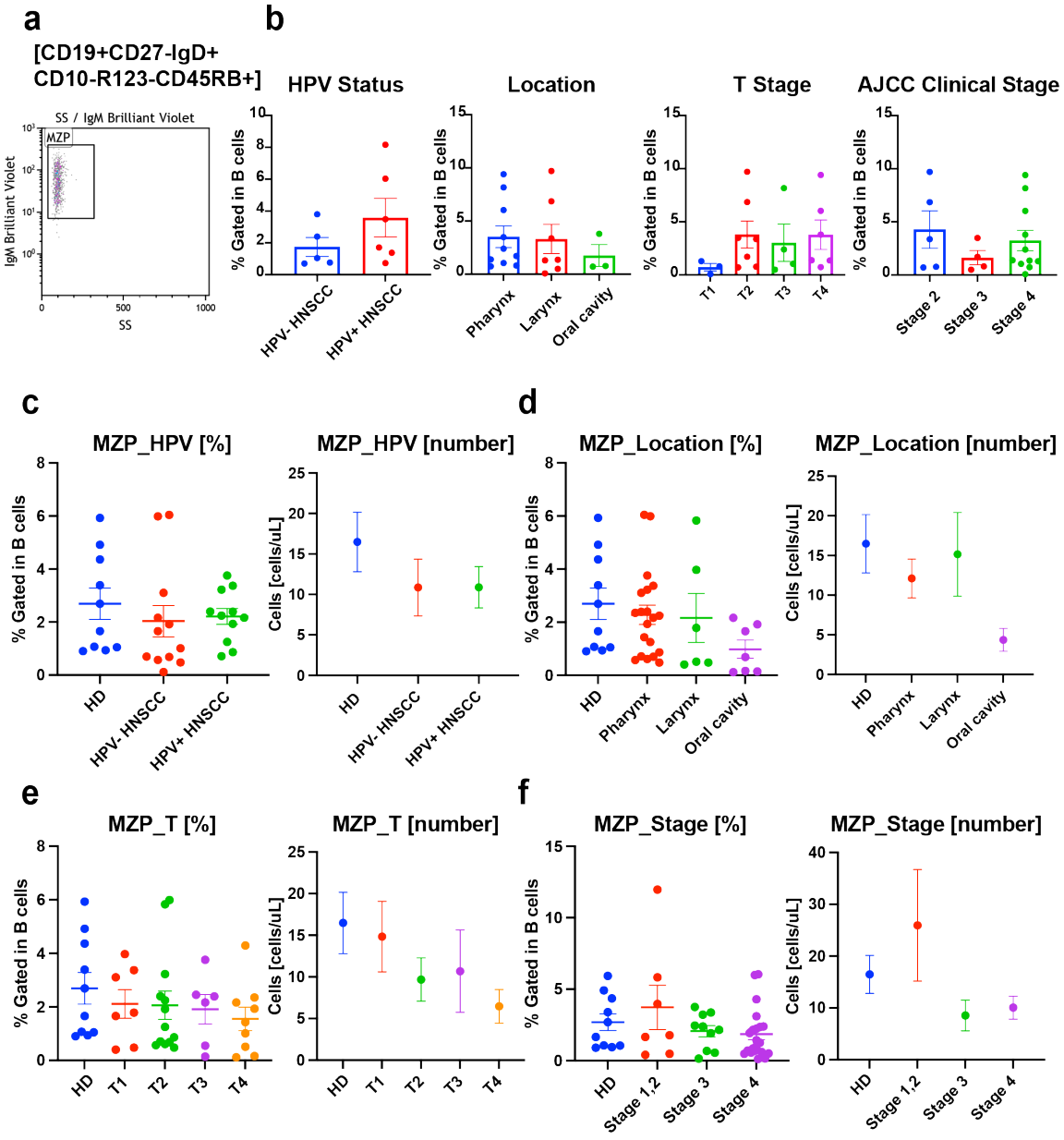

Figure 9. Flow cytometric analysis of MZP in HNSCC.

(a) MZP gating strategy.

(b) MZP distribution in tumor tissues (n = 20) stratified by HPV status, tumor location, AJCC T stage, and clinical stage.

(c-f) MZP distribution in PBMCs from HDs (n = 10) and patients with HNSCC (n = 38) stratified by HPV status (c), primary tumor location (d), AJCC T stage (e), and clinical stage (f).

Cell proportions were tested using unpaired t-test with Welch's correction or one-way ANOVA with Bonferroni post-hoc analysis. Legend continued on next page.

Figure 9 (continued).

Modified as an author from J.Bao 2025 [12], CC BY 4.0, https://creativecommons.org/licenses/by/4.0/.

Abbreviations: MZP, marginal zone precursor B cell; HNSCC, head and neck squamous cell carcinoma; PBMC, peripheral blood mononuclear cell; HD, healthy donor; HPV, human papillomavirus; AJCC, American Joint Committee on Cancer.

GCB were defined as $CD38^{+}IgD^{-}$ [161] (**Fig. 10a**). GCBs were more prevalent in the tumor tissues of HPV^{+} patients compared to HPV^{-} patients (**Fig. 10b**), a difference that was less pronounced in circulation (**Fig. 10c**). Within tumors, GCBs were most enriched in pharyngeal tumors, followed by laryngeal and oral cavity tumors, although not statistically significant (**Fig. 10b**). GCB frequencies in tumors declined with advancing T and clinical stages (**Fig. 10b**), a trend not observed in PBMCs (**Fig. 10d–f**).

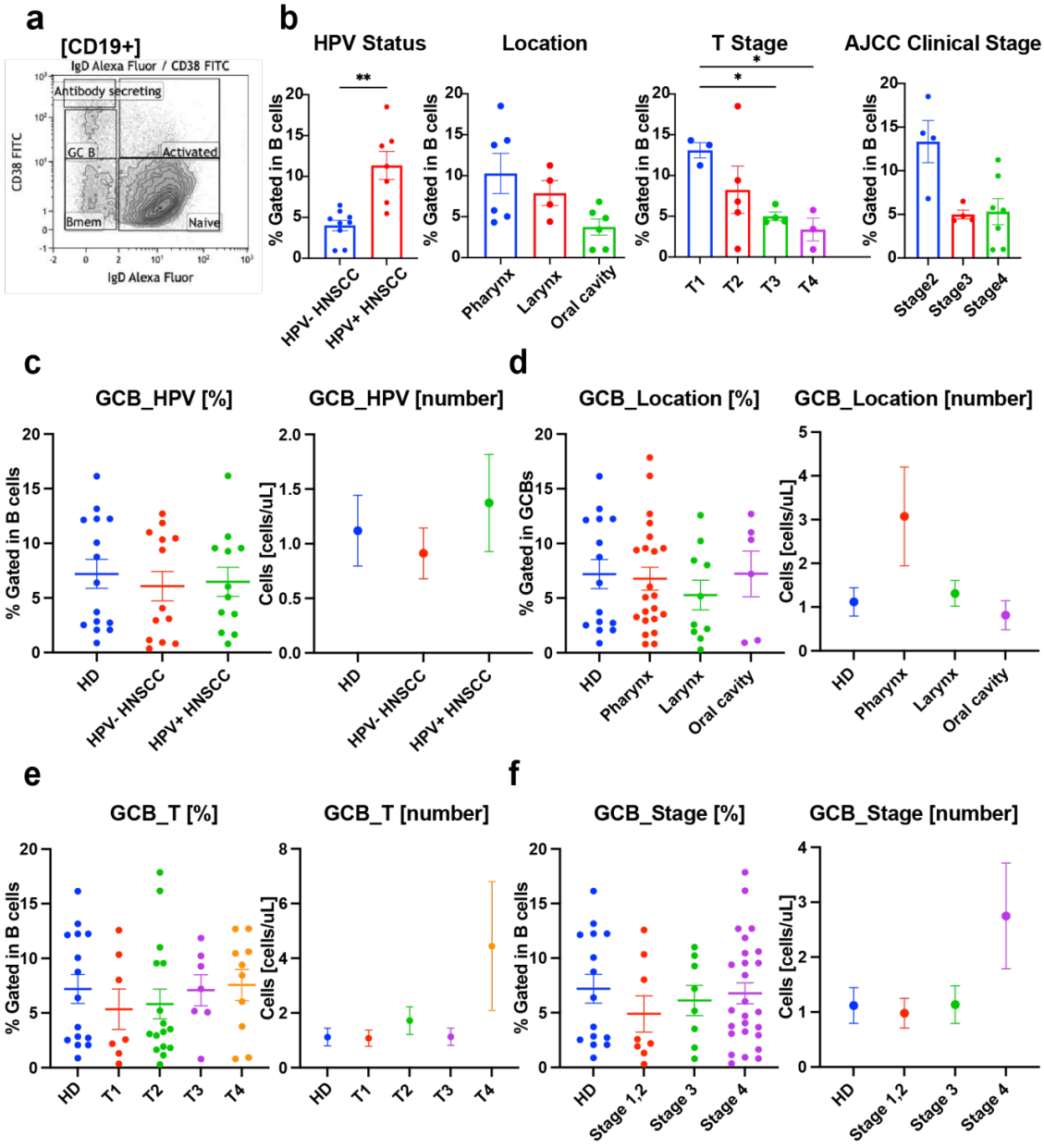

Figure 10. Flow cytometric analysis of GCB in HNSCC.

(a) GCB gating strategy.

(b) GCB distribution in tumor tissues (n = 16) stratified by HPV status, tumor location, AJCC T stage, and clinical stage.

(c-f) GCB distribution in PBMCs from HDs (n = 15) and patients with HNSCC (n = 42) stratified by HPV status (c), primary tumor location (d), AJCC T stage (e), and clinical stage (f).

Cell proportions were tested using unpaired t-test with Welch's correction or one-way ANOVA with Bonferroni post-hoc analysis. Legend continued on next page.

Figure 10 (continued).

Modified as an author from J.Bao 2025 [12], CC BY 4.0, https://creativecommons.org/licenses/by/4.0/.

Abbreviations: GCB, germinal center B cell; HNSCC, head and neck squamous cell carcinoma; PBMC, peripheral blood mononuclear cell; HD, healthy donor; HPV, human papillomavirus; AJCC, American Joint Committee on Cancer.

Additionally, analysis of other B cell subsets revealed key distinctions between HPV^+ and HPV^- HNSCC. $CD38^{hi}$ antibody-secreting cells and $CD38^-IgD^-$ memory B cells were slightly elevated in HPV^- tumors. Conversely, HPV^+ tumors exhibited a higher frequency of $CD27^-CD21^{lo}$ tissue-like memory B cells and $CD27^+CD21^{+/-}$ resting/activated memory B cells, suggesting a more activated or diverse memory B cell repertoire in HPV^+ TIME (**Fig. 11**).

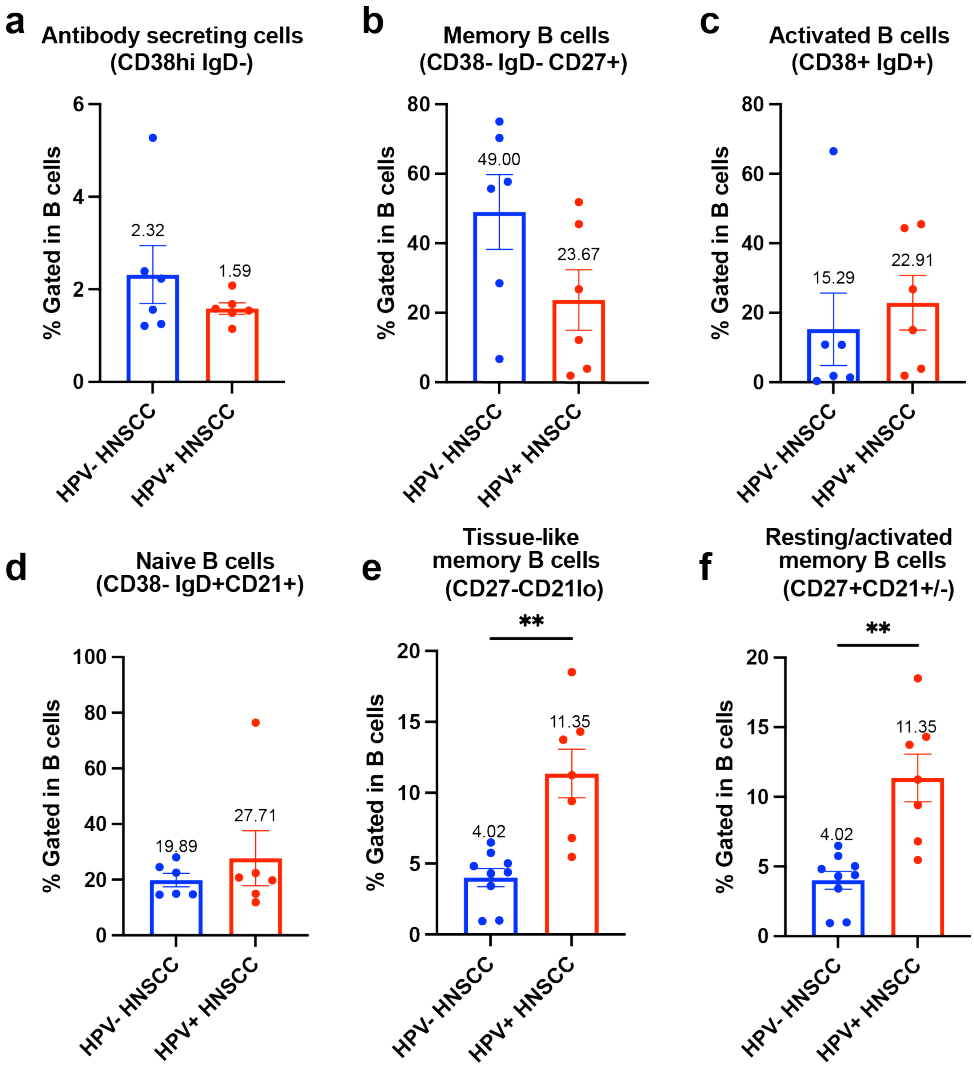

Figure 11. B Cell Population Differences Between HPV+ and HPV− Patients.

(a–f) Comparative frequencies of antibody-secreting cells, memory B cells, and naïve/activated subsets in dissected tumor tissues (n = 16) from HPV$^+$ and HPV$^-$ patients.

Abbreviations: HPV, human papillomavirus; HNSCC, head and neck squamous cell carcinoma.

In summary, we identified and characterized MZB, MZP, and GCB subpopulations in both peripheral blood and TIME of HNSCC patients. MZBs increased and GCBs decreased with advancing tumor stage, particularly the T stage, suggesting dynamic reprogramming of the B cell compartment. Furthermore, HPV$^+$ tumors demonstrated greater abundance and heterogeneity in B cell subsets, indicating a distinct immunological landscape compared to HPV$^-$ HNSCC.

3.2 Single-cell transcriptomic profiling reveals TIB heterogeneity in HNSCC

To validate and extend the flow cytometry findings, scRNA-seq analysis were performed on four publicly available datasets comprising 118 HNSCC patients and 6 HDs [13, 31, 34, 100]. After integration and quality control of $CD45^+$ cells across all datasets, a total of 288,638 high-quality cells were retained. The integrated dataset displayed substantial inter-patient and inter-tissue heterogeneity, as visualized by UMAP plots (**Fig. 12a–c**).

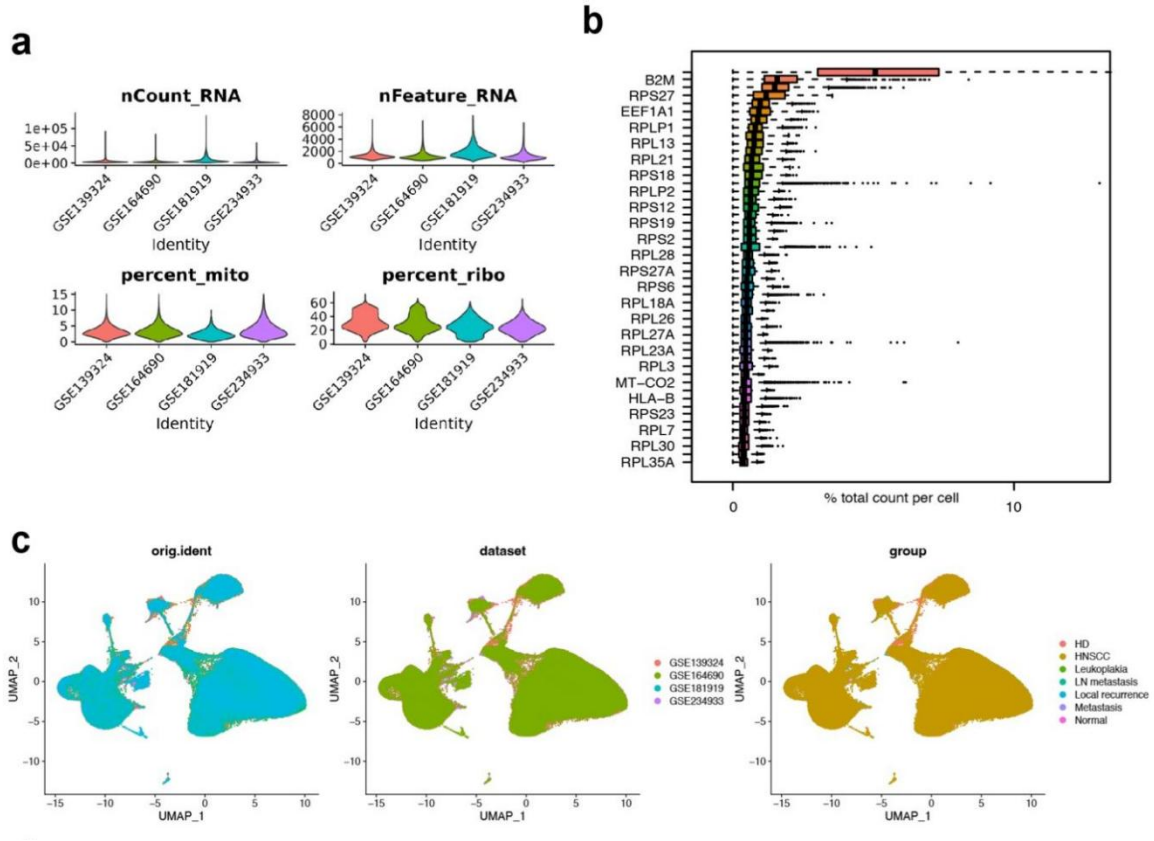

Figure 12. scRNA-seq Quality Control and Normalization.

(a-b) Quality control metrics across the four integrated scRNA-seq datasets.

(c) UMAP plots showing the distribution of cells labeled by donor, datasets, and tissue origin.

Abbreviations: scRNA-seq, single-cell RNA sequencing; UMAP, uniform manifold approximation and projection.

In the initial clustering, major immune and stromal compartments were annotated, including T cells, B cells, monocytes, macrophages, DCs, epithelial cells, mast cells, and pericytes (**Fig. 13a**). The B cell compartment was extracted for secondary clustering and refined

annotation using a composite approach involving the reference CITE-seq dataset GSE193868, MSigDB signatures, and canonical B cell markers (see Methods).

Thirteen transcriptionally distinct B cell subclusters were resolved (**Fig. 13a–b**). Two MZB clusters (MZB-1 and MZB-2), characterized by high expression of *CD27, CR2 (CD21), IGHM, IGHD, CD1C,* and *PLD4*, were revealed. The transcriptomic signatures of these clusters differed from those of HDs, particularly in MZB-2, which displayed enhanced activation marker expression and increased interaction potential as described in the below chapters.

Three activated B cell (AcB) subsets 1–3 were defined based on differential expression of *CD86, FCER2, MALAT1,* and *BCL7A*. AcB1 was enriched for interferon-responsive genes (e.g., *IFI6, IFIT1, MX1*); AcB2 showed enrichment for BCR activation genes (e.g., *JUN, FOS*); and AcB3 expressed heat shock protein genes linked to stress and tumor responses. A distinct $CD27^{-}IgD^{-}$ double-negative (DN) B cell population was also identified (**Fig. 13b**).

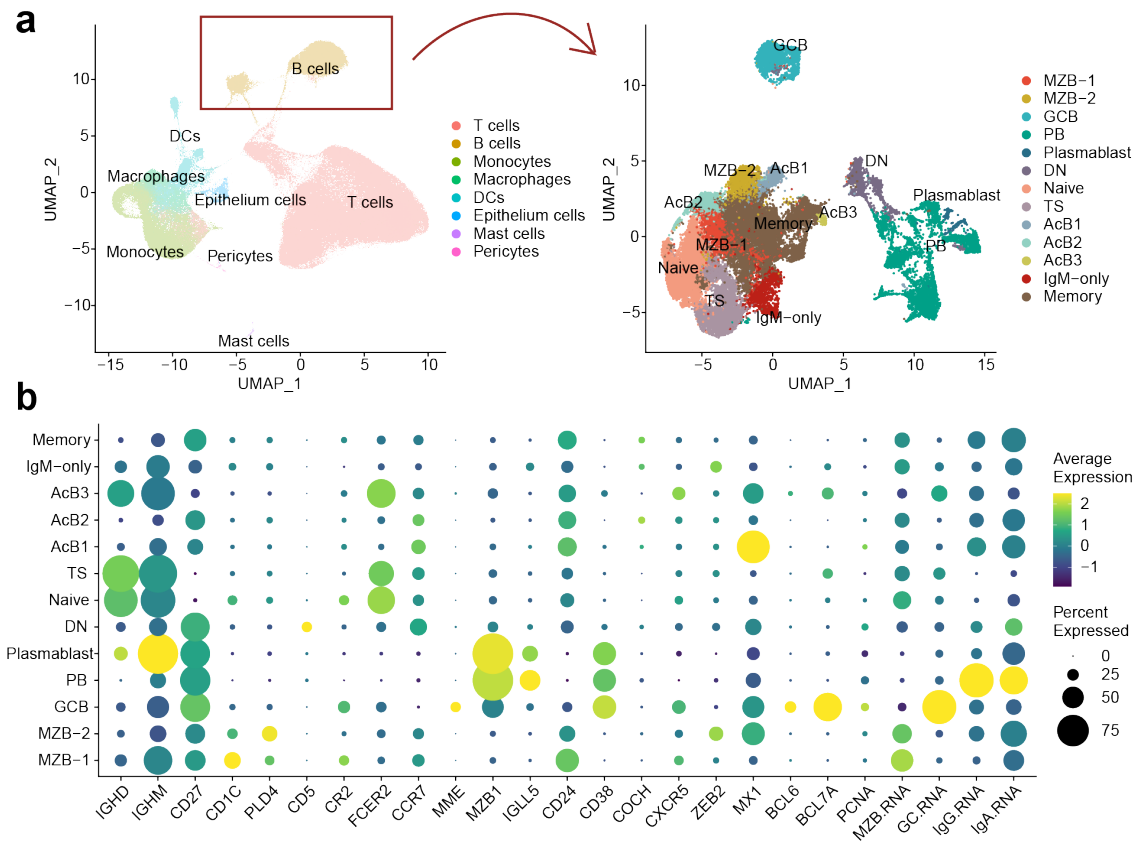

Figure 13. scRNA-seq analysis of CD45⁺ TILs and B cell subtypes.

(a) UMAP showing cell clusters of CD45⁺ TILs and isolated B cell subclusters.

(b) Dot plot summarizing expression of marker genes for key B cell subtypes, including MZB, GCB, and antibody isotypes. The following gene groups were used: MZB.RNA (*CD1C, PLD4, CDH17, DOCK11, PTK2B, DLL1, LFNG, MFNG, NOTCH2, DOCK10,* and *BCL3*); GC.RNA (*MME, PCNA, BCL6,* and *BCL7A*); IgG.RNA (*IGHG1, IGHG2, IGHG3, IGHG4*); IgA.RNA (*IGHA1* and *IGHA2*).

Reprinted as an author from J.Bao 2025 [12], CC BY 4.0, https://creativecommons.org/licenses/by/4.0/.

Abbreviations: scRNA-seq, single-cell RNA sequencing; TIL, tumor-infiltrating lymphocyte; UMAP, uniform manifold approximation and projection; MZB, marginal zone B cell; GCB, germinal center B cell; GC, germinal center; IgG, immunoglobulin G; IgA, immunoglobulin A.

The distribution of B cell subsets varied substantially between PBMCs and tumor tissues, as well as across disease conditions and anatomical sites (**Fig. 14a**). MZBs and GCBs were enriched in tumor tissues, particularly in HPV⁺ samples, whereas AcBs were mostly confined to primary tumors and absent from circulation and normal tissue. MZBs were absent from leukoplakia and adjacent normal tissues.

Across tumor T stages, MZBs and GCBs were enriched in early-stage (T1–T2) tumors and declined in T3–T4. MZB-2 frequency was further reduced in tumors with extensive nodal involvement (N stage). GCBs were most abundant in oropharyngeal tumors, while MZB frequencies did not significantly vary by tumor site (**Fig. 14b**). Tumors enriched for GCBs also showed elevated naive and memory B cell proportions, but not plasma cells (**Fig. 14c**).

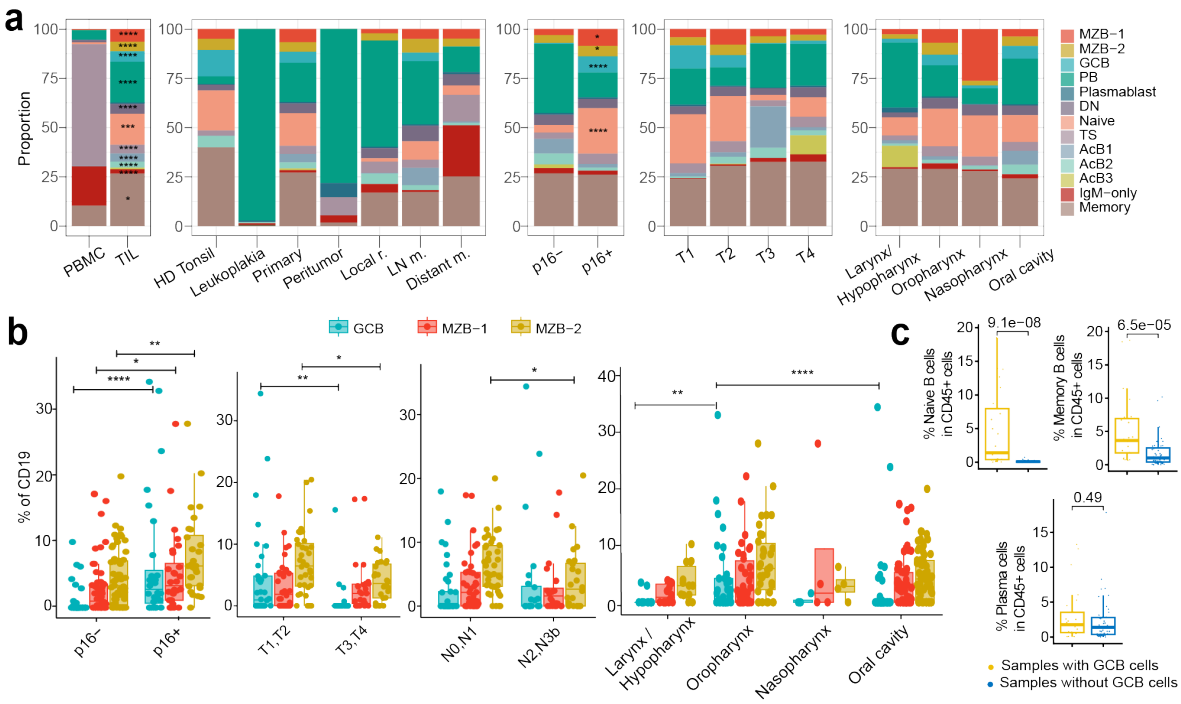

Figure 14. scRNA-seq analysis of TIB subsets.

(a) Stacked bar plots of B cell subset proportions across different sample origins and clinical conditions.

(b) Proportional differences in GCB, MZB-1, and MZB-2 based on HPV status, T and N stages, and tumor location.

(c) Boxplots comparing naive B cells, memory B cells, and plasma cells between GCB^{+} and GCB^{-} tumors. Statistical tests: unpaired t-test (Welch's correction) or one-way ANOVA with Bonferroni post hoc.

Reprinted as an author from J.Bao 2025 [12], CC BY 4.0, https://creativecommons.org/licenses/by/4.0/.

Abbreviations: scRNA-seq, single-cell RNA sequencing; TIB, tumor-infiltrating B cell; GCB, germinal center B cell; MZB, marginal zone B cell; HPV, human papillomavirus; T stage, primary tumor stage; N stage, lymph node stage. r., recurrence; m., metastasis.

3.3 Transcriptional remodeling of TIB subsets in HNSCC compared with HDs

To delineate molecular distinctions in B cell populations between HDs and HNSCC patients, we compared both the abundance and transcriptomic signatures of B cell subsets in HD tonsillar tissues and primary HNSCC tumors. Regardless of anatomical tumor origin (tonsillar or non-tonsillar), HNSCC tumors harbored a higher frequency of plasma B cells (PBs) compared to HDs. In contrast, GCB and naive B cells were more prominent in HDs than in HNSCC tissues (**Fig. 15a-b**).

Despite substantial overlaps, transcriptomic comparison of B cell subclusters revealed several distinct gene expression alterations between HNSCC tumors and HD tonsils. Among the top DEGs (adjusted $p < 0.01$), several were implicated in mitochondrial ATP synthesis, including *ATP5MC2, ATP5F1E, ATP5MG, ATP5E, ATP5L,* and *ATP5J*. Elevated expression of apoptosis-associated genes (*MTRNR2L8, MTRNR2L12*) and immunoglobulin gene segments (*IGKV1-5, IGKV3-15, IGLV3-1*) were also observed, reflecting enhanced immunoglobulin rearrangement and stress responses (**Fig. 15c**).

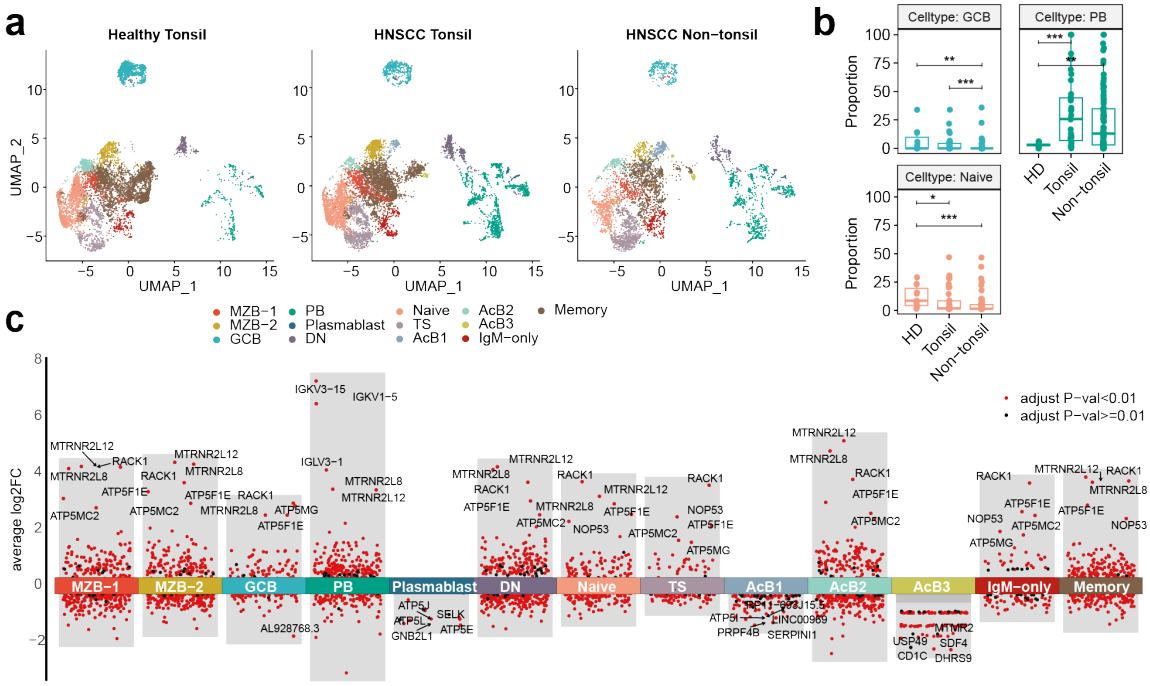

Figure 15. Comparative analysis of B cell subsets in HNSCC and HDs.

(a-b) B cell population proportions in HD tonsils, primary tonsillar HNSCC, and non-tonsillar HNSCC tissues. One-way ANOVA with Bonferroni correction was applied.

(c) Top five DEGs per B cell cluster. Genes with adjusted $p < 0.01$ shown in red; $0.01 < p < 0.05$ in black.

Reprinted as an author from J.Bao 2025 [12], CC BY 4.0, https://creativecommons.org/licenses/by/4.0/.

Abbreviations: HNSCC, head and neck squamous cell carcinoma; HD, healthy donor; DEG, differentially expressed gene.

GO Biological Process (BP) enrichment analysis further identified key pathways elevated in TIBs, particularly those involved in mitochondrial metabolism (e.g., oxidative phosphorylation, ATP biosynthesis, aerobic respiration), hypoxia responses, and oxidative stress detoxification (**Fig. 16**). These metabolic shifts align with hallmark features among various tumors [61, 151]. Additionally, a pronounced activation of viral-related pathways was identified in HNSCC patients compared to HDs, encompassing defense responses to viruses, viral genome replication, regulation of viral processes, and viral entry into host cells. This may be attributable to the viral etiology of HPV^{+} oropharyngeal squamous cell carcinoma.

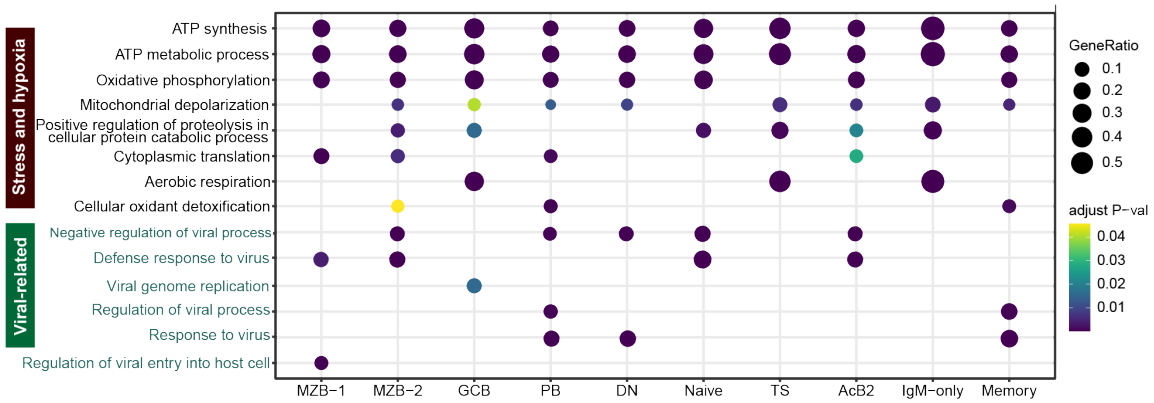

Figure 16. GO BP enrichment in B cells from HNSCC patients versus HDs.

Highlighted GO BP pathways include stress and hypoxia responses, and antiviral immune responses, compared HNSCC patients to HDs.

Reprinted as an author from J.Bao 2025 [12], CC BY 4.0, https://creativecommons.org/licenses/by/4.0/.

Abbreviations: GO, Gene Ontology; BP, biological process; HNSCC, head and neck squamous cell carcinoma; HD, healthy donor.

To dissect the viral signature further, ReactomePA-based pathway enrichment was performed on HPV^+ versus HPV^- HNSCC cases. HPV^+ B cell clusters demonstrated elevated enrichment in viral translation, antigen-activated BCR signaling, and MHC-II-mediated antigen presentation pathways (**Fig. 17**).



Figure 17. Pathway Enrichment Analysis.

Comparison of enriched pathways between HPV+ and HPV- HNSCC patients, annotated by ReactomePA database.

Abbreviations: HPV, human papillomavirus; HNSCC, head and neck squamous cell carcinoma; ReactomePA, Reactome Pathway Analysis.

Collectively, these findings highlight that B cell subsets in HNSCC patients display altered abundance and transcriptomic activity compared to HDs, particularly in antiviral and metabolic pathways. Transcriptomic profiling of TIBs showed remarkable expression in genes related to ATP synthesis, apoptosis, and immunoglobulin gene rearrangement, compared to B cells from HDs. GOBP analysis highlighted stress and hypoxia pathways, and viral response pathways as the most significantly enriched in TIBs from HNSCC patients compared to those from HDs. Enrichment of PBs in tumor tissues, coupled with metabolic and immune activation signatures, suggest a tumor-adaptive or virus-induced reprogramming of B cell function.

3.4 Functional differentiation of MZB subsets in the HNSCC tumor microenvironment

To assess functional pathways enriched in B cell clusters, we applied GSVA. MZB-1, PBs, and DN B cells were enriched in cell–cell communication-related pathways, whereas AcB1–3 and MZB-2 showed pronounced activation of interferon (IFN) signaling and Eph/ephrin-mediated responses. Notably, MZB-2 and DN B cells upregulated genes involved in MHC-I-mediated antigen presentation. MZB-1 exhibited modest activation of NOTCH-1 signaling, though no notable differences were observed in NOTCH-2 signaling between MZB-1 and MZB-2 (**Fig. 18**).

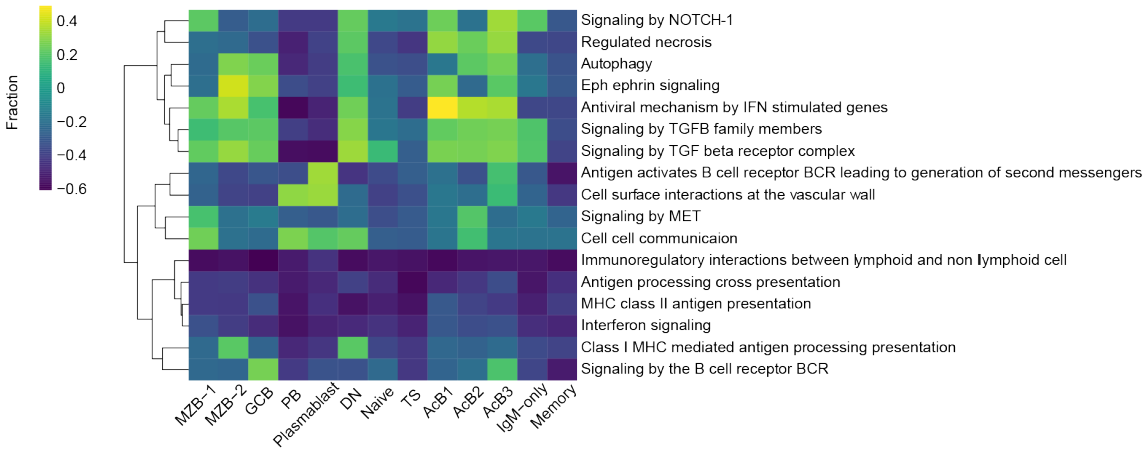

Figure 18. GSVA pathway analysis of B cell subclusters.

Top 20 enriched pathways per cluster (Reactome database), shown as standardized GSVA scores.
Reprinted as an author from J.Bao 2025 [12], CC BY 4.0, https://creativecommons.org/licenses/by/4.0/.
Abbreviations: GSVA, gene set variation analysis; Reactome, Reactome Pathway Database.

Given the involvement of MZB-1 in intercellular signaling, we conducted cell–cell communication analysis using CellChat. We annotated 32 immune and non-immune clusters, including naive, effector memory, tissue-resident memory, follicular helper, regulatory, and γδ T cells; cDC1, cDC2, pDC, DC3 subsets; $CD14^+$ and $CD16^+$ monocytes; as well as macrophages, NK cells, mast cells, epithelial cells, and pericytes (**Fig. 19**).

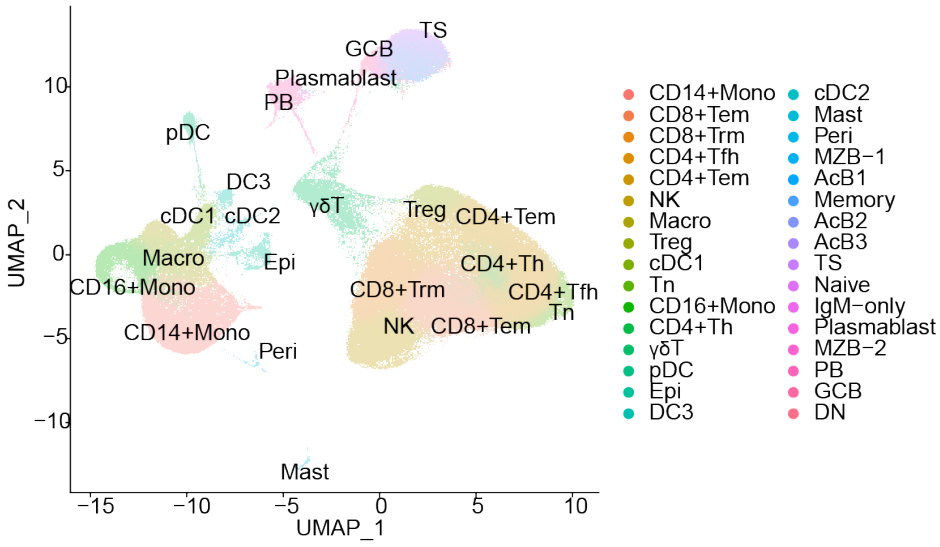

Figure 19. UMAP representation of CD45$^+$ TIL composition.

UMAP visualization of CD45$^+$ TIL composition in the scRNA-seq cohort colored by cell subsets, annotated on the basis of Seurat unsupervised clusters with main T cell subpopulations: Tn, CD8$^+$ Trm, CD4$^+$ and CD8$^+$ Tem, CD4$^+$ Tfh, Treg, and γδ T cells; four DC populations (cDC1, cDC2, pDC, and DC3); two monocyte populations (CD14$^+$ and CD16$^+$), and mast cells, macrophages, and NK cells. Two small clusters -- epithelial cells and pericytes -- were also detected.

Reprinted as an author from J.Bao 2025 [12], CC BY 4.0, https://creativecommons.org/licenses/by/4.0/.

Abbreviations: scRNA-seq, single-cell RNA sequencing; TIL, tumor-infiltrating leukocyte; UMAP, uniform manifold approximation and projection; Tn, naïve T cell; Trm, tissue-resident memory T cell; Tem, effector memory T cell; Tfh, follicular helper T cell; Treg, regulatory T cell; DC, dendritic cell; cDC, conventional dendritic cell; pDC, plasmacytoid dendritic cell; NK, natural killer cell.

MZB-1 and MZB-2 both engaged extensively in MHC-I and MHC-II interactions with CD4$^+$ and CD8$^+$ T cells (**Fig. 20a**). Key L-R pairs included *HLA-A/B/C–CD8A/B* for MHC-I, and *HLA-DRA/DRB1/DPA1/DPB1–CD4* for MHC-II (**Fig. 20b**).

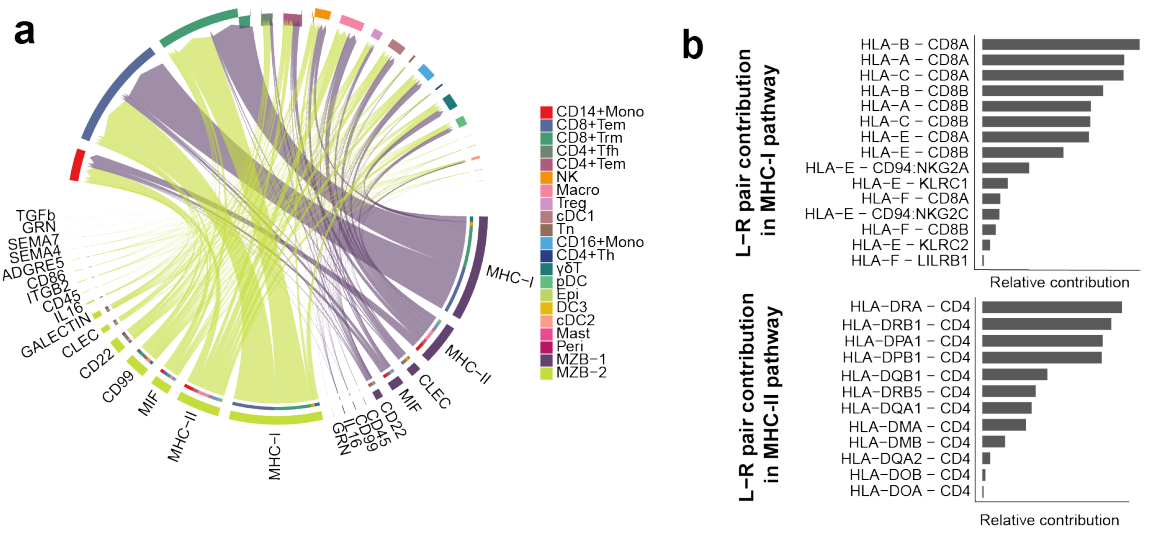

Figure 20. Main cell–cell interaction of MZB subsets.

(a) Circos plots showing the main cell communication pathways of MZB-1 cluster (purple) and MZB-2 cluster (light green). Interactions are visualized by lines, with the influenced cell type situated in the terminal point.
(b) Key L-R pairs involved in MHC I/II pathways.
Reprinted as an author from J.Bao 2025 [12], CC BY 4.0, https://creativecommons.org/licenses/by/4.0/.
Abbreviations: MZB, marginal zone B cell; L–R, ligand–receptor; MHC, major histocompatibility complex.

Further analysis showed that, compared to MZB-1, MZB-2 exhibited enhanced communication potential with T cells, placing it among the highest within TIBs (**Fig. 21a**). Specifically, MZB-2 harbored more coinhibitory and adhension L-R pairs with $CD4^+$ Tfh and $CD4^+$ Tem cells, showing increased engagement of ligands such as *CD74–MIF*, *CD99–CD99*, and *LGALS9–CD44/PTPRC* (**Fig. 21b**).

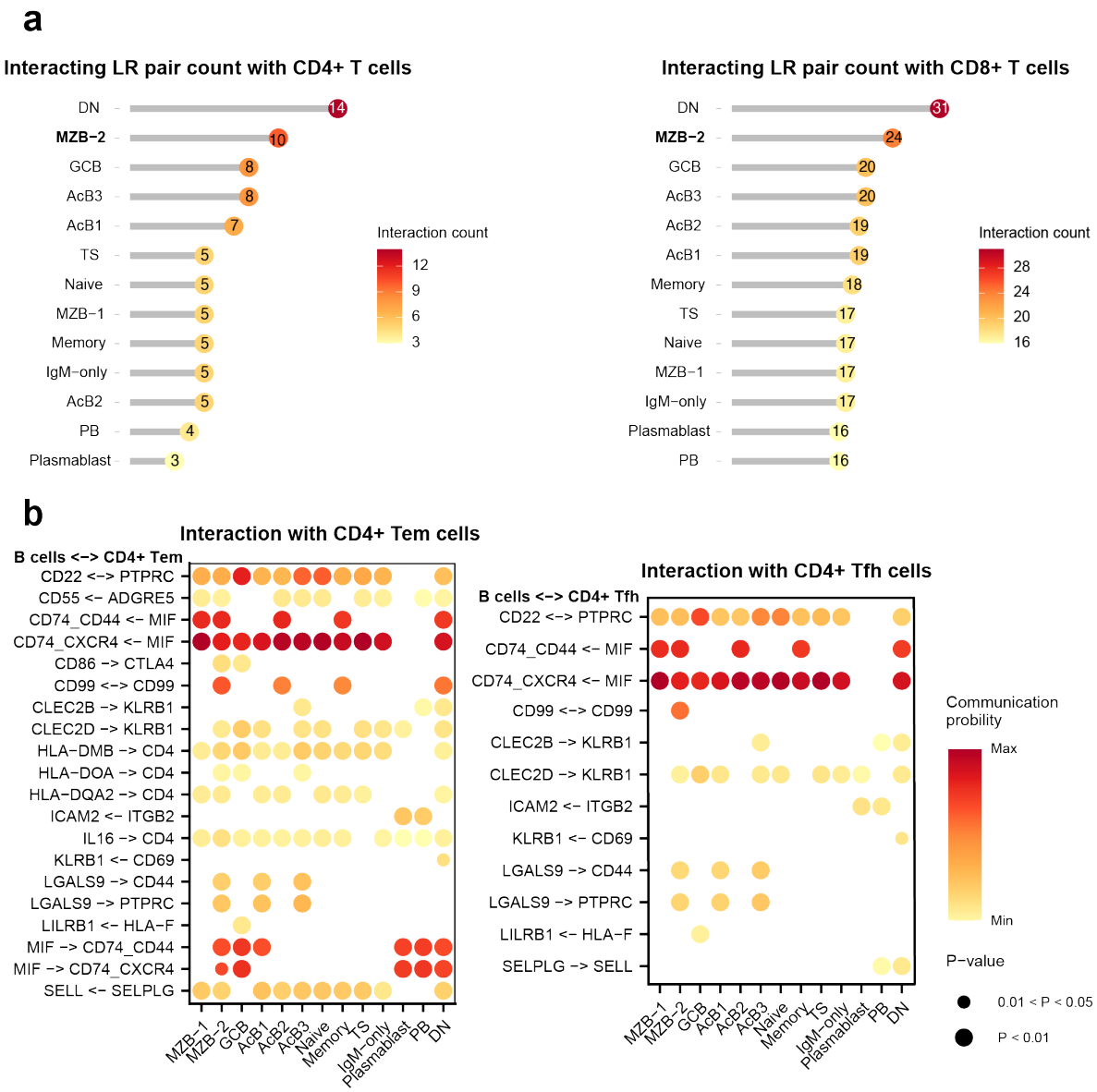

Figure 21. Enhanced T cell interaction by MZB-2.

(a) CellChat-predicted number of significant L–R pairs between T cell and B cell subsets.

(b) Key L-R interactions involving B cell subsets and CD4$^+$ Tfh/Tem cells.

Modified as an author from J.Bao 2025 [12], CC BY 4.0, https://creativecommons.org/licenses/by/4.0/.

Abbreviations: MZB, marginal zone B cell; L–R, ligand–receptor; Tfh, follicular helper T cell; Tem, effector memory T cell.

Beyond T cell interactions, MZB-2 also communicated with APCs such as CD14$^+$ monocytes, cDC1, and macrophages through costimulatory and adhesion molecule-mediated pathways (e.g., *ADGRE5–CD55*, *ICAM1/2–ITGAL*) (**Figs. 22**). The strong interaction potential between MZB-2 and APCs supports the hypothesis that tumor-resident

MZB-2 may acquire DC-like properties within TIME, consistent with its functional plasticity observed in physiological contexts [168].

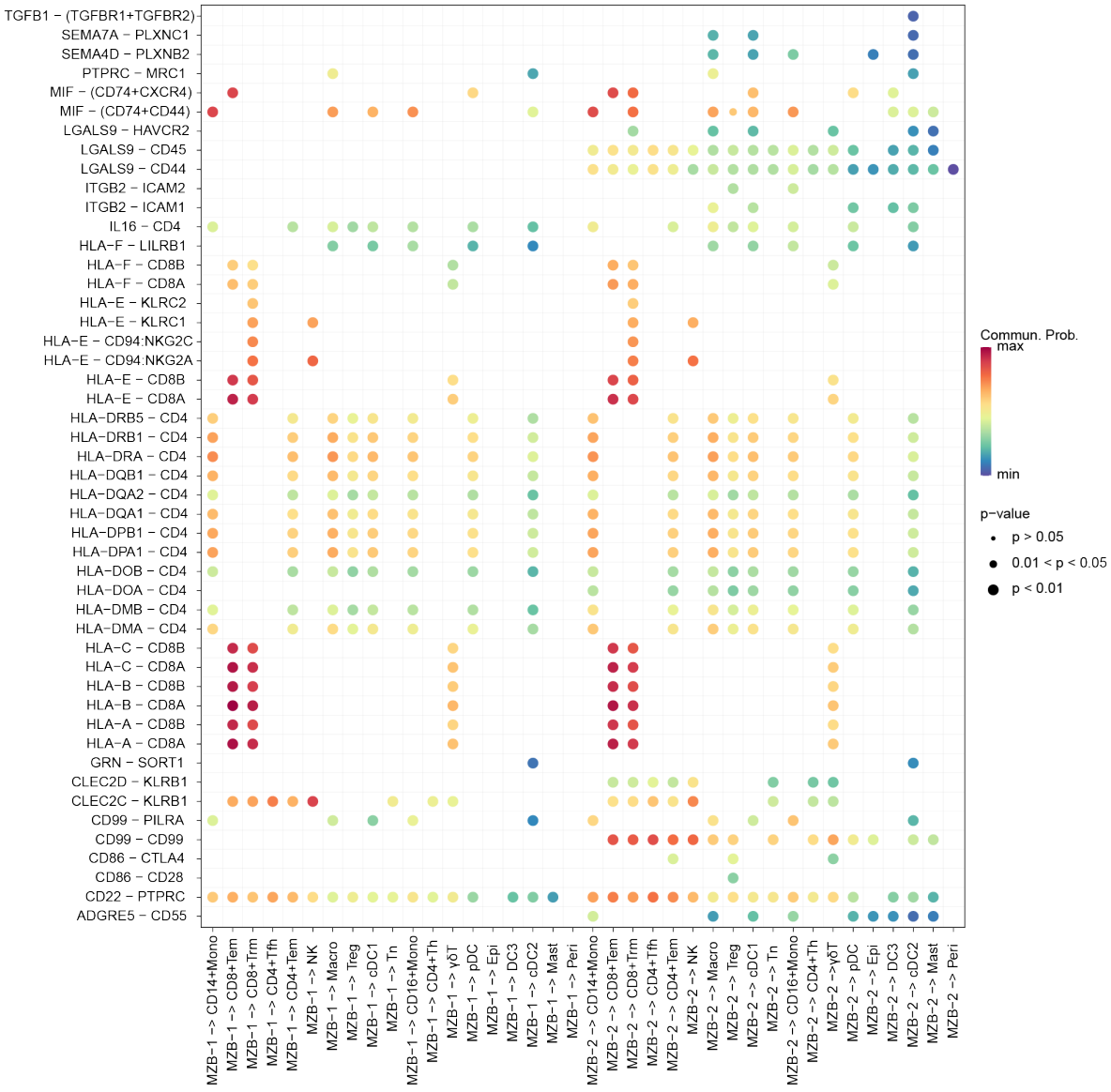

Figure 22. Broad interaction network of MZB subsets.

Dot plot showing L–R interaction intensity between MZB-1/MZB-2 and other TIL subsets in primary HNSCC patients.

Abbreviations: MZB, marginal zone B cell; L–R, ligand–receptor; TIL, tumor-infiltrating lymphocyte; HNSCC, head and neck squamous cell carcinoma.

To assess whether these interactions were tumor-specific, we compared MZB signaling in HNSCC and HD tonsil tissues. In HDs, both MZB-1 and MZB-2 clusters retained activation of MHC-I and MHC-II pathways (**Fig. 23a**). Notably, however, the MZB-2–$CD4^+$ Tem interaction demonstrated divergent L–R usage: the CD86–CTLA-4 coinhibitory pair was detected exclusively in HNSCC, whereas the CD86–CD28 costimulatory pair was restricted to HDs (**Fig. 23b**). Pathway intensity analysis further revealed that in HDs, the CD40 costimulatory pathway was significantly enriched, while in HNSCC patients, multiple immunosuppressive pathways—including PD-L1 and IFN-II signaling—were preferentially expressed (**Fig. 23c**). While both HNSCC tumors and HD tonsils shared MHC-I and MHC-II pathways, MHC-I signaling was significantly more intense in the tumor context, suggesting a more pronounced MHC-I-mediated antigen presentation and recognition in the tumor milieu [205] (**Fig. 23c**).

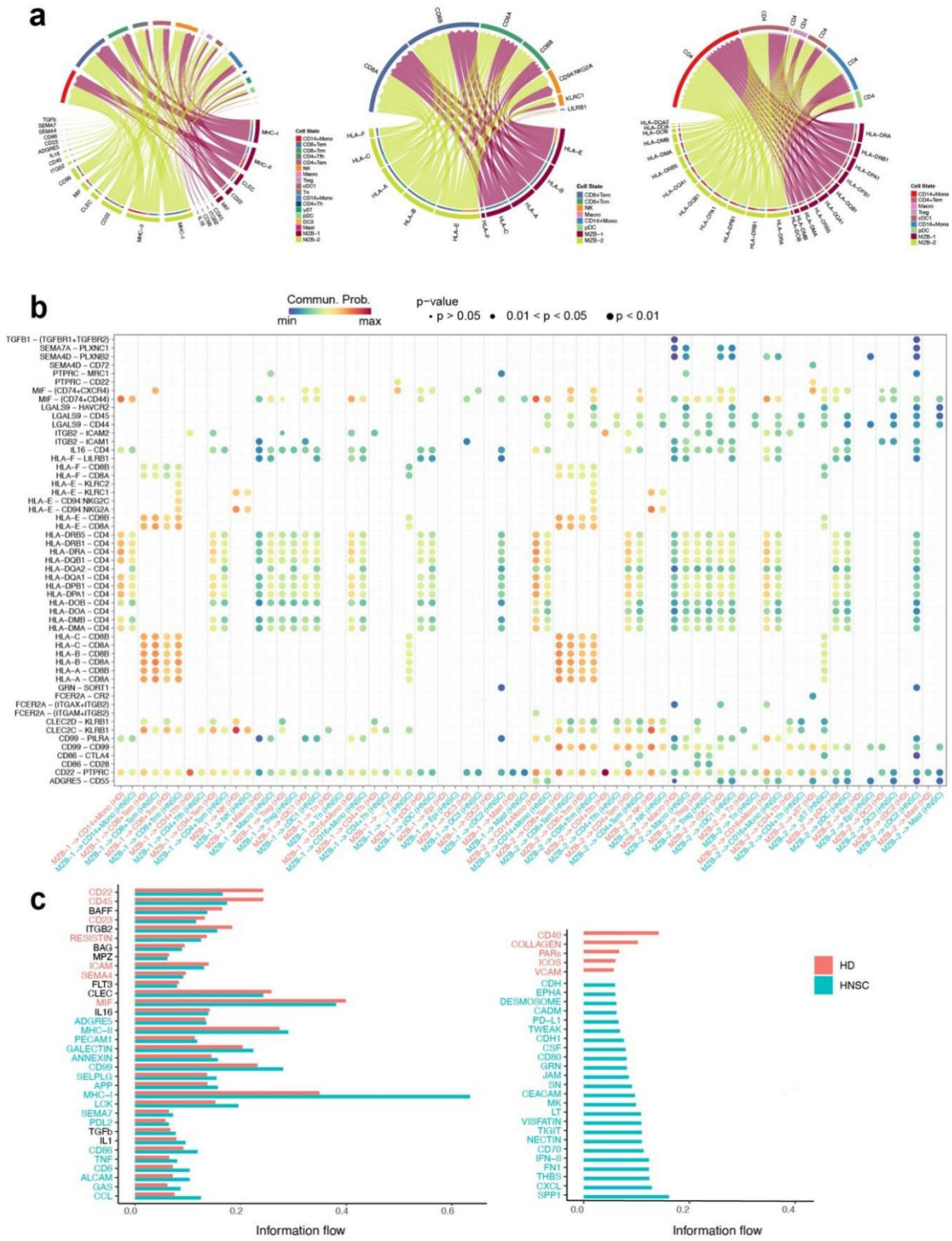

Figure 23. Comparative cell–cell signaling between HDs and HNSCC.

Legend continued on next page.

Figure 23 (continued).

(a) Circos plots showing the main cellchat pathways of MZB-1 cluster (purple) and MZB-2 cluster (light green) in HDs. Interactions are visualized by lines, with the influenced cell type situated in the terminal point.

(b) Dot plot showing the L-R intensity between MZB-1/2 clusters and other immune cells in HDs (red) and HNSCC patients (blue).

(c) Quantified pathway strength comparison between HDs and HNSCC patients.

Abbreviations: HD, healthy donor; HNSCC, head and neck squamous cell carcinoma; MZB, marginal zone B cell; L–R, ligand–receptor.

In conclusion, MZB clusters in HNSCC exhibited broad immune communication capabilities, particularly through MHC-mediated interactions with T cells. Compared to MZB-1, MZB-2 showed a more extensive signaling with $CD4^+$ T cells and APCs, indicating its potential for antigen presentation and T cell modulation within the TIME. Although such cellular interactions were also observed in HDs, indicating they are not tumor-exclusive, HNSCC patients displayed greater reliance on MHC-I–mediated signaling and an enrichment of immunoregulatory interactions, reflected by the upregulation of immunosuppressive L-R pairs and the absence of stimulatory secondary signals.

3.5 MZB-2 exhibits enhanced immunomodulatory programs in HNSCC

To elucidate functional distinctions between MZB-1 and MZB-2 clusters, we performed differential gene expression analysis. MZB-1 was enriched for genes involved in chemotaxis and early lymphocyte activation, such as *CXCR4*, *CD69*, and *ZFP36L2*. In contrast, MZB-2 displayed upregulation of genes associated with B cell maturation (*TOX*, *RFTN1*, *HLA* alleles), myeloid lineage differentiation (*TESC*), and immune regulation (*SUB1*), the latter of which is known to promote genomic stability and suppress viral replication [98, 193](**Fig. 24**).

Additional markers elevated in MZB-2 included *ITGAX* and *CCR1*, implicated in monocyte adhesion and chemotaxis, as well as *CD86*, a canonical costimulatory molecule for T cell activation via CD28/CTLA-4 binding [154]. The expression of *TNFSF11* (RANKL) further suggested a role in apoptotic signaling and immunomodulation.

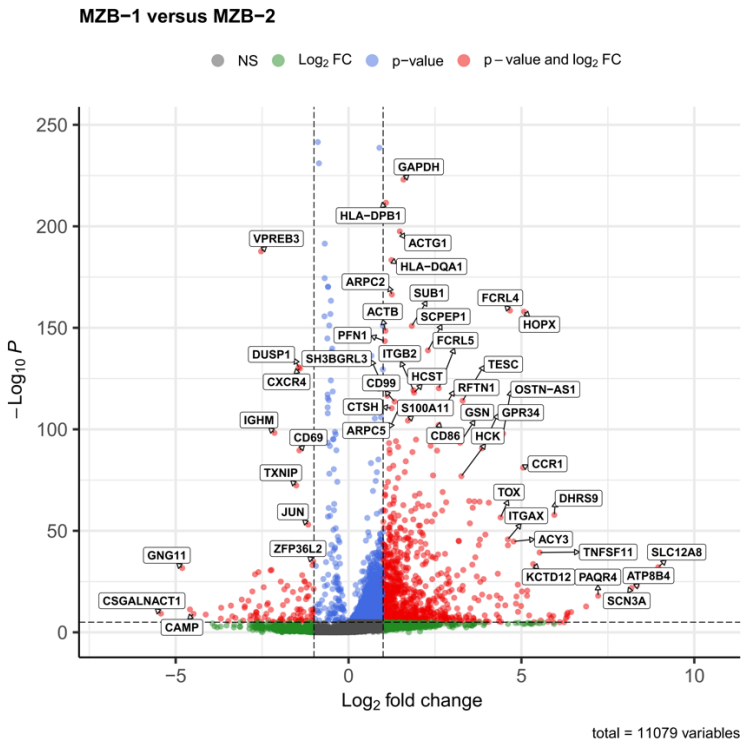

Figure 24. Volcano plot of DEGs between MZB-1 and MZB-2 clusters.

Expression profiles of key genes differentially expressed between MZB-1 and MZB-2 clusters. DEGs with a BH-adjusted p-value < 0.01 and |log2FC| > 1 are considered significantly differentially expressed and highlighted in red.

Reprinted as an author from J.Bao 2025 [12], CC BY 4.0, https://creativecommons.org/licenses/by/4.0/.

Abbreviations: DEG, differentially expressed gene; MZB, marginal zone B cell; BH, Benjamini–Hochberg; FC, fold change.

We next evaluated genes of particular immunological relevance. Compared to MZB-1, MZB-2 upregulated transcriptional features of an activated B cell state, which include B cell activation, transcriptional control, cytokine/chemokine signaling, and MHC-II-related pathways (**Fig. 25a**), consistent with an advanced activation state compared to MZB-1. Moreover, MZB-2 exhibited strong expression of *FCRL4* and *FCRL5*, atypical B cell markers recently linked to tumor-associated atypical B cells (TAABs) with functional interactions with $CD4^+$ T cells [209].

GSEA revealed that compared to MZB-1, MZB-2 was significantly enriched in pathways related to immune effector processes, leukocyte activation, intercellular adhesion, and was highly enriched in several immune regulation pathways, reinforcing its immunoactive

phenotype and its putative role in facilitating T cell modulation and local immune remodeling (**Fig. 25b**).

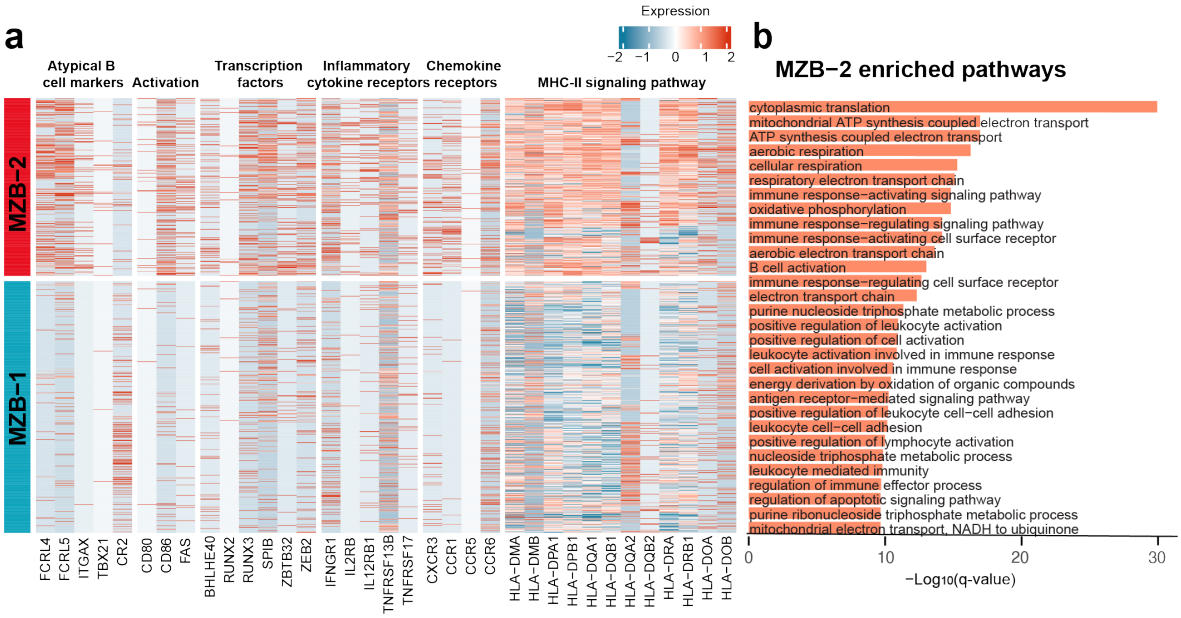

Figure 25. Functional divergence between MZB-1 and MZB-2 subsets.

(a) Expression levels of selected differentially expressed genes between MZB-1 and MZB-2 clusters within primary HNSCC tissues. Genes are involved in B cell activation, cytokine signaling, transcriptional regulation, and MHC-II antigen presentation (BH-adjusted p-value < 0.01, two-sided unpaired Wilcoxon test).

(b) GSEA pathway enrichment comparing MZB-2 to MZB-1 using GO Biological Processes. Pathways enriched in MZB-2 include leukocyte activation, cytokine-mediated signaling, and cell–cell adhesion.

Reprinted as an author from J.Bao 2025 [12], CC BY 4.0, https://creativecommons.org/licenses/by/4.0/.

Abbreviations: MZB, marginal zone B cell; HNSCC, head and neck squamous cell carcinoma; BH, Benjamini–Hochberg; MHC-II, major histocompatibility complex class II; GSEA, gene set enrichment analysis; GO, Gene Ontology.

We further explored the role of NOTCH signaling in MZB biology. Although *NOTCH-2* is considered critical for MZB lineage commitment [162], expression of *NOTCH-2* was low in both MZB-1 and MZB-2 clusters (0.066 and 0.027, respectively), with the highest levels observed in IgM-only B cells. While we observed substantial gene set overlap among MZB-1, IgM-only, and TS B cells (**Fig. 26a**), we detected no significant enrichment of *NOTCH-2* expression or pathway activity in MZB-2. Moreover, contrary to their conclusion that MZB-1 and MZB-2 are developmentally unrelated, our CytoTRACE-based pseudo-time analysis suggests a potential continuum between these two subsets, with MZB-1 potentially serving as a precursor to MZB-2 (**Fig. 26b**).

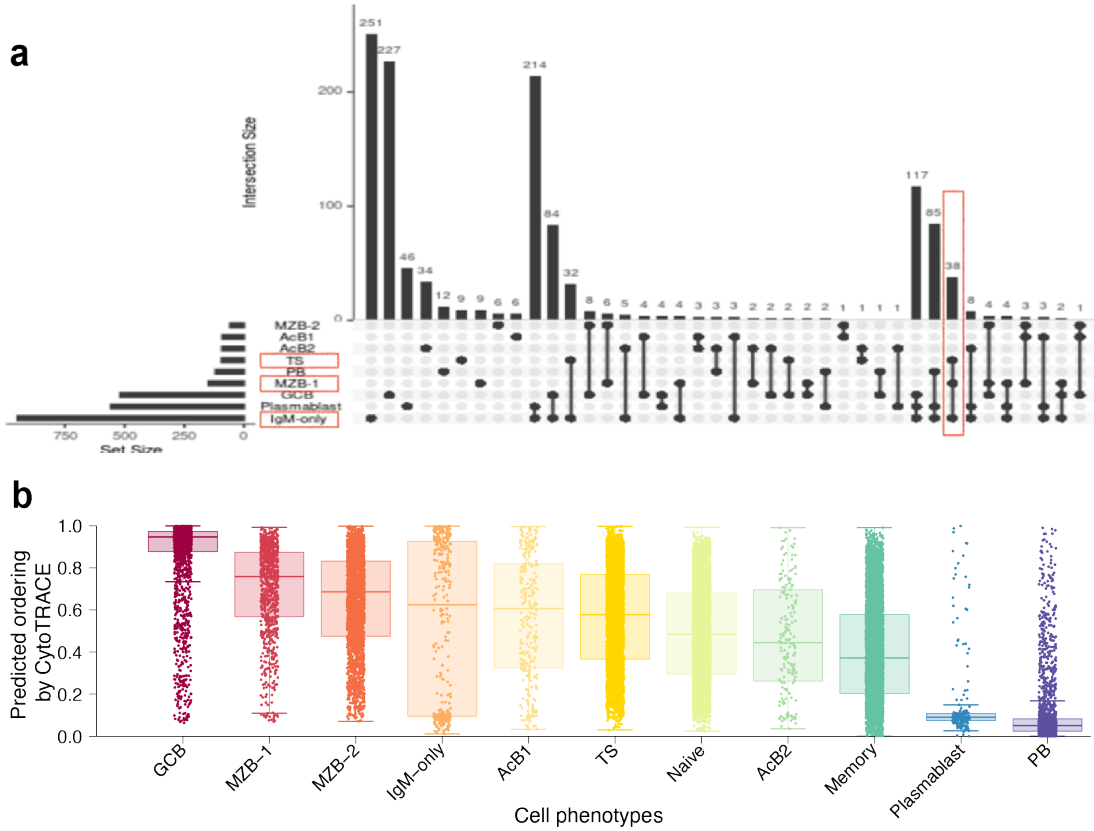

Figure 26. Transcriptional and developmental characteristics of MZB subsets in HNSCC.

(a) Gene set intersection analysis demonstrating overlapping transcriptomic profiles among MZB-1, IgM-only, and TS B cells in HNSCC.

(b) Pseudo-time trajectory analysis using CytoTRACE infers a differentiation continuum between MZB-1 and MZB-2 clusters.

Abbreviations: MZB, marginal zone B cell; HNSCC, head and neck squamous cell carcinoma; TS, tumor-associated stromal; IgM, immunoglobulin M.

In summary, MZB-2 exhibits a more advanced and immunoactive transcriptional profile than MZB-1, marked by elevated activation markers and enrichment in immune response pathways. It also expresses multiple transcription factors, cytokine, and chemokine receptors, highlighting its functional plasticity and potential role in immune regulation.

3.6 Spatial proximity of MZB clusters to CD4⁺ T cells suggests functional interaction

To investigate the spatial context of MZB clusters within the TIME, we analyzed ST data from the publicly available Visium dataset GSE220978, which includes paired tumor and adjacent normal tissues from four untreated HNSCC patients [217]. For cell type deconvolution, we used scRNA-seq data from GSE181919 as the reference, comprising nine major cell populations—including malignant epithelial cells, T cells, B/plasma cells, and DCs—visualized via UMAP embedding (**Fig. 27a**). The spatial distribution of inferred cell types, particularly tumor and immune cell populations, aligned well with histological annotations and multiplex immunofluorescence data from the original publication (**Fig. 27b**).

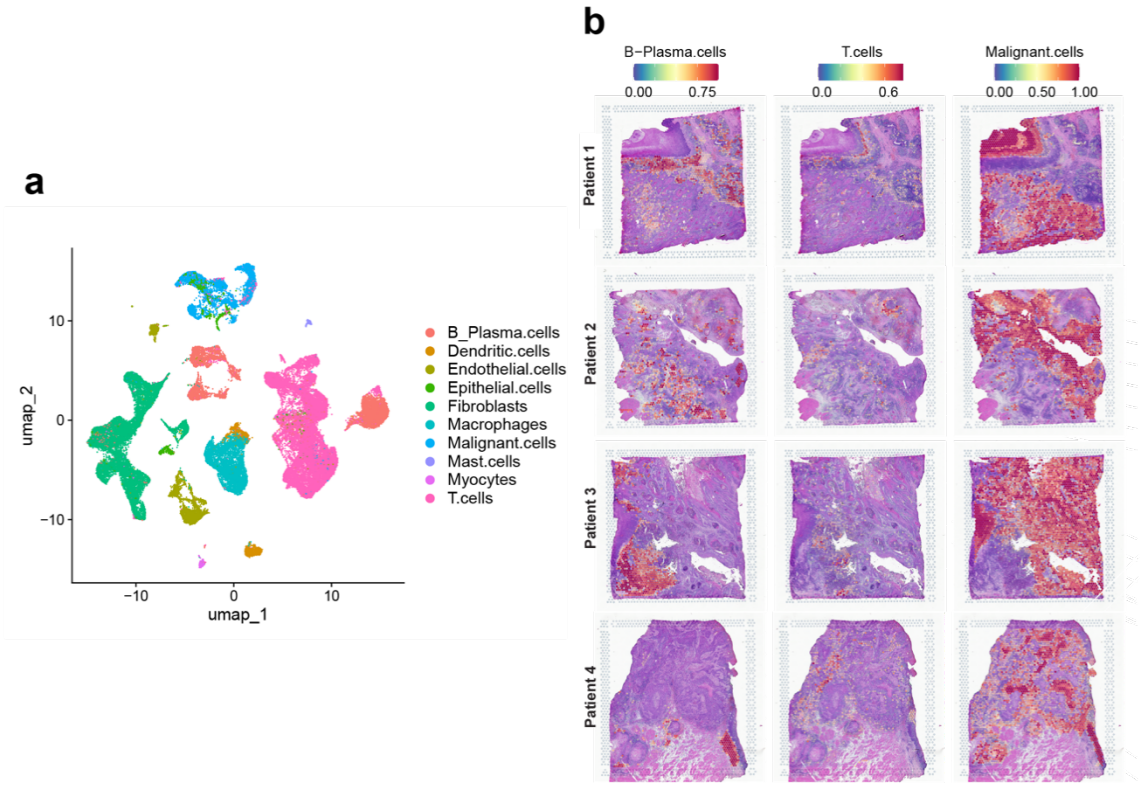

Figure 27. Spatial transcriptomic landscape of the HNSCC TIME.

(a) UMAP visualization of cell clusters in the reference scRNA-seq dataset (GSE181919).

(b) Spatial deconvolution of Visium dataset GSE220978, showing tumor cells and major immune cell populations.

Reprinted as an author from J.Bao 2025 [12], CC BY 4.0, https://creativecommons.org/licenses/by/4.0/.

Abbreviations: HNSCC, head and neck squamous cell carcinoma; TIME, tumor immune microenvironment; scRNA-seq, single-cell RNA sequencing; UMAP, uniform manifold approximation and projection.

To further resolve spatial interactions, we refined annotations of B and T cell subsets by applying Seurat's label transfer method using the reference scRNA-seq dataset. Within tumor regions enriched for MZB clusters, we observed a consistent spatial colocalization with CD4⁺ T cell subsets, particularly CD4⁺ Tfh and CD4⁺ Tem cells (**Fig. 28a**), suggesting potential cell–cell communication in situ.

Notably, in one patient sample (Patient 1), we identified a TLS characterized by the co-enrichment of MZB-1, GCB, and CD4⁺ Tfh cells within a confined region (**Fig. 28b**). This spatial arrangement supports the existence of an MZB–Tfh–GC axis, potentially contributing to local antigen presentation and adaptive immune modulation.

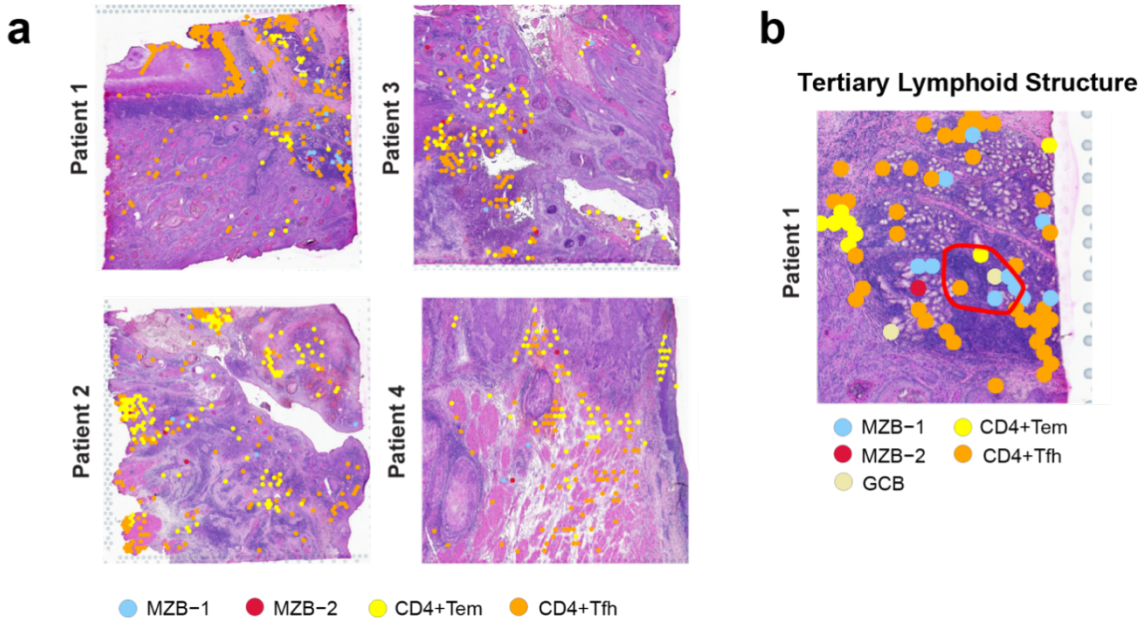

Figure 28. Spatial proximity of MZB and CD4⁺ T cell subsets in HNSCC.

(a) Spatial mapping of MZB-1/MZB-2 clusters and CD4⁺ Tfh/Tem cells shows frequent co-localization in tumor regions.

(b) TLS structure identified in Patient 1 (red circle) showing co-enrichment of GCB, MZB-1, and CD4⁺ Tfh cells.

Reprinted as an author from J.Bao 2025 [12], CC BY 4.0, https://creativecommons.org/licenses/by/4.0/.

Abbreviations: MZB, marginal zone B cell; HNSCC, head and neck squamous cell carcinoma; Tfh, follicular helper T cell; Tem, effector memory T cell; GCB, germinal center B cell; TLS, tertiary lymphoid structure.

3.7 Immunoregulatory properties and prognostic relevance of MZB subsets in HNSCC

We identified two transcriptionally distinct MZB subsets in HNSCC, each exhibiting different maturation states and MHC-mediated antigen presentation. Given previous studies that MZB populations exhibit Breg phenotypes marked by the increased expression of *NR4A1-3*, *CD83*, *ENTPD1* (CD39), and *NT5E* (CD73), we explored whether the tumor-associated MZB-1 and MZB-2 subsets also possessed these immunosuppressive markers [43, 44].

At the transcriptomic level, *NR4A1-3* and *CD83* were broadly expressed across multiple B cell subsets, particularly within AcB clusters 1–3, limiting their specificity for identifying Bregs. *ENTPD1* and *NT5E* were more enriched in the MZB-2 cluster compared to MZB-1, although these genes were also detected in other effector B cell populations, including AcB clusters (**Fig. 29**). Attempts to delineate a discrete Breg population through unsupervised clustering did not yield distinct Breg clusters.

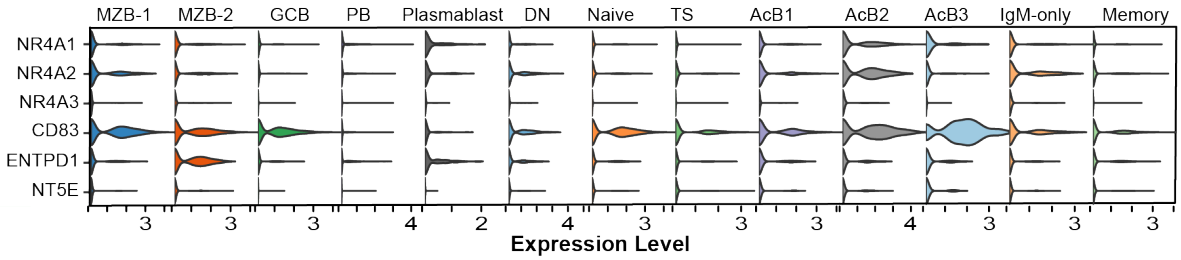

Figure 29. Immunoregulatory gene expression across B cell subsets in HNSCC.

Expression levels of Breg-associated genes derived from reference MZB bulk RNA-seq datasets, visualized across defined B cell clusters in the HNSCC scRNA-seq cohort.

Reprinted as an author from J.Bao 2025 [12], CC BY 4.0, https://creativecommons.org/licenses/by/4.0/.

Abbreviations: HNSCC, head and neck squamous cell carcinoma; Breg, regulatory B cell; MZB, marginal zone B cell; scRNA-seq, single-cell RNA sequencing.

To assess the clinical significance of MZB subsets, we leveraged bulk RNA-seq data from the TCGA HNSC cohort and applied CIBERSORTx deconvolution using our scRNA-seq-derived gene expression signatures. This allowed us to estimate the relative abundance of MZB-1, MZB-2, and GCB cells across HPV^+ and HPV^- tumor samples. MZB-2 proportions

were significantly elevated in HPV^+ tumors (**Fig. 30a**), consistent with our single-cell observations.

Next, we performed survival analysis stratified by MZB subset abundance. Kaplan–Meier analysis showed no significant difference in overall survival between high and low MZB-1 groups, irrespective of clinical stage (**Fig. 30b**). However, elevated MZB-2 levels were significantly associated with improved prognosis in early-stage (Stage I–II) HNSCC patients (**Fig. 30c**). Optimal thresholds for prognostic grouping were determined using the maxstat algorithm (MZB1: lower cutpoint/ upper cutpoint = 1.474/1.854; MZB2: lower cutpoint/ upper cutpoint = 0.469/2.298).

Our findings suggest that MZB-2 exhibits unique immunomodulatory properties — potentially balancing antigen presentation, cytokine signaling, and immune suppression. The favorable prognostic impact of MZB-2 in early-stage disease suggests its potential beneficial role for modulating immune responses in early tumor progression.

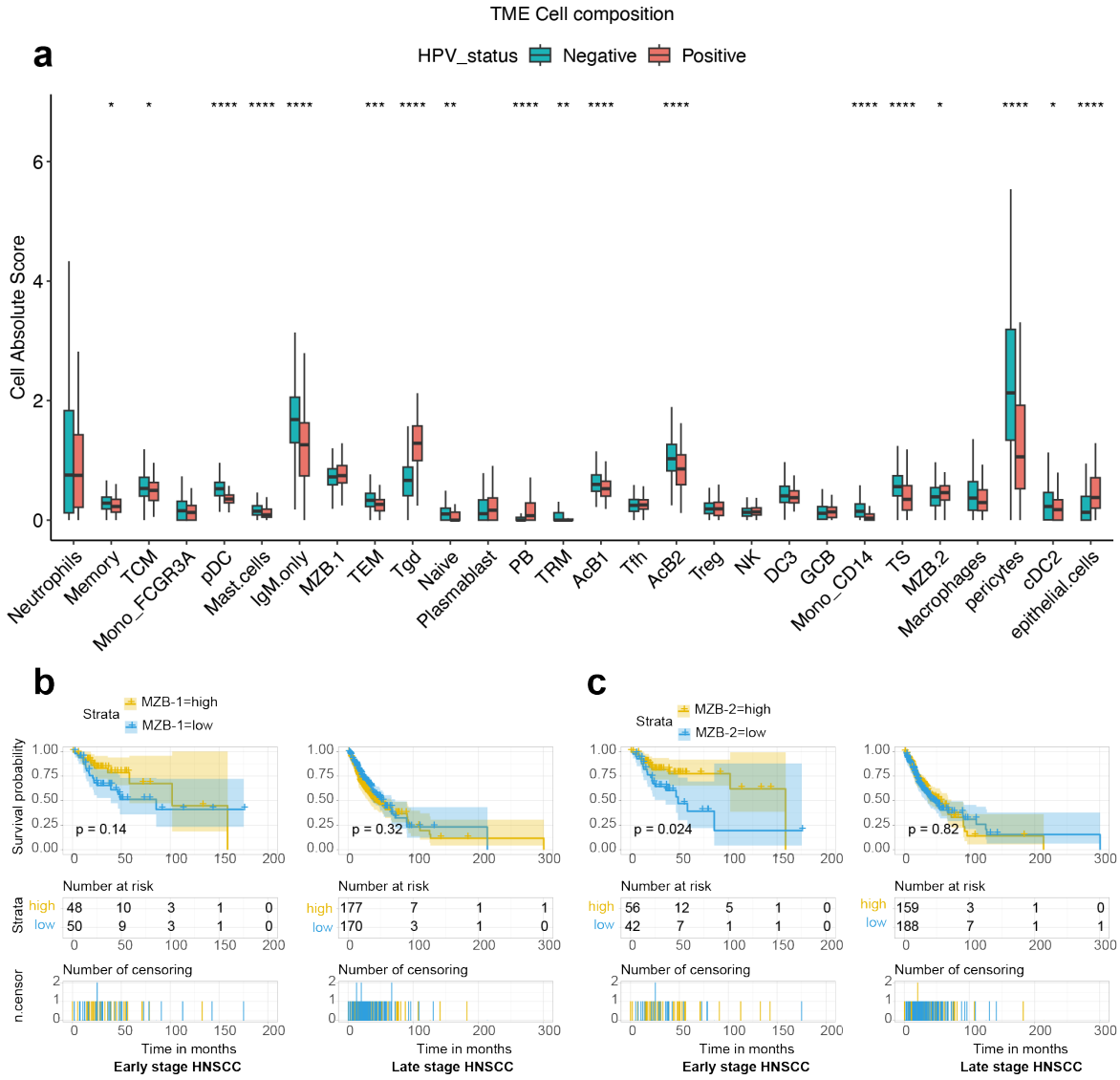

Figure 30. Prognostic significance of MZB subsets in early-stage HNSCC.

(a) CIBERSORTx deconvolution of scRNA-seq data to bulk RNA-seq TCGA HNSC data for constructing an immune infiltration matrix, showing TIL cell proportion of tumor tissues from HPV^+ HNSCC patients (n = 75) compared to HPV^- counterparts (n = 494).

(b-c) Survival analysis of MZB-1 (b) and MZB-2 (c) with TCGA HNSC bulk-RNA seq data, stratified by AJCC clinical stages.

Modified as an author from J.Bao 2025 [12], CC BY 4.0, https://creativecommons.org/licenses/by/4.0/.

Abbreviations: HNSCC, head and neck squamous cell carcinoma; MZB, marginal zone B cell; HPV, human papillomavirus; TIL, tumor-infiltrating lymphocyte; scRNA-seq, single-cell RNA sequencing; TCGA, The Cancer Genome Atlas; HNSC, head and neck squamous cell carcinoma cohort; AJCC, American Joint Committee on Cancer.

4 Discussion

This study is the first to identify and characterize MZBs both in peripheral blood and as TILs in patients with HNSCC. Given the dual immunomodulatory potential of MZBs—previously reported to exert both pro- and anti-immunogenic functions [144]—we sought to define their roles within the TIME across the continuum of HNSCC development, progression, and clinical outcome. Building on recent studies that identified two transcriptionally distinct MZB subsets (MZB-1 and MZB-2) in HDs via mass cytometry and scRNA-seq [84], we confirmed the presence of analogous subsets within the TIME of HNSCC patients using integrated scRNA-seq and ST analyses. The MZBs identified in HNSCC preserved core phenotypic and functional characteristics observed in HDs, while exhibiting signatures indicative of a conserved lineage undergoing tumor-specific transcriptional reprogramming.

4.1 Clinicopathological relevance of MZB, MZP, and GCB subsets in HNSCC

To contextualize the biological significance of B cell subpopulations in HNSCC, we examined the abundance of MZB-1, MZB-2, and GCB in relation to HPV infection status and tumor stage. Both flow cytometry and scRNA-seq analyses revealed a consistent enrichment of MZB and GCB subsets in HPV^+ tumors compared to HPV^- cases. These findings are concordant with earlier studies, including that by Ruffin et al., which demonstrated increased TLS formation and GCB infiltration in HPV^+ HNSCC, hallmarks of a highly inflamed (“hot”) TIME [161]. Indeed, HPV^+ tumors are generally characterized by higher immune cell infiltration, T cell activation, and immunoregulatory signaling compared to the immunologically “cold” microenvironments of HPV^- tumors [57].

However, some discrepancies emerged between the two methodologies. Flow cytometry suggested a progressive increase in MZB abundance with advancing tumor T stage. In contrast, scRNA-seq data indicated that MZB and GCB frequencies peaked in early T-stage tumors (T1–T2) and declined in more advanced stages (T3–T4). This divergence may reflect differences in sample pairing, data completeness, and the relative sensitivity of transcriptomic versus surface protein detection. Additionally, scRNA-seq captures transcriptional profiles, whereas flow cytometry quantifies surface markers, which may vary independently under dynamic immunological conditions.

Notably, MZB-2—identified as transcriptionally distinct and functionally more mature than MZB-1—was particularly enriched in early-stage HNSCC and correlated with improved patient prognosis. This association diminished in advanced tumors, where MZB-2 frequency and prognostic value were both reduced. These observations suggest a potential stage-specific role for MZB-2 in tumor immunosurveillance and control. Furthermore, a decline in MZB-2 abundance with increasing nodal (N stage) involvement reinforces its relevance in early immune containment and highlights its possible utility as a prognostic biomarker for early disease stages.

4.2 Comparative landscape of B cell composition and functions in HNSCC versus HDs

Across all primary tumor sites, HNSCC patients exhibited a pronounced expansion of PBs within tumor tissues compared with PB frequencies in HD tonsils, indicative of antigen-driven B cell activation. This was supported by the upregulation of immunoglobulin V(D)J genes (*IGKV1-5, IGKV3-15, IGLV3-1)* in tumor-associated PBs. In contrast, GCBs and naïve B cells were enriched in HD tonsils but underrepresented in HNSCC tumors, reflecting their differentiation into effector B cell subsets within the tumor milieu.

Comparative profiling of B cell marker genes between HNSCC and HD tonsils revealed that intratumoral B cells were enriched for metabolic programs, including ATP synthesis, oxidative phosphorylation and mitochondrial depolarization. These pathways are hallmarks of cellular stress and hypoxia, consistent with metabolic adaptations observed across diverse cancers [61, 151]. In addition, viral-response pathways were significantly upregulated in HNSCC compared with HD tonsils, reflecting the etiological contribution of HPV^+ oropharyngeal carcinoma. Indeed, ReactomePA enrichment analysis distinguished HPV^+ from HPV^- tumors, highlighting distinct molecular pathways related to viral activity in several B cell populations derived from HPV+ HNSCC compared with their HPV- counterparts.

At the level of cell–cell communication, we observed an enrichment of immunosuppressive signaling pathways, including PD-L1 and IFN-γ, in HNSCC tumors compared with HD tonsils, highlighting a tumor-adaptive shift of B cells toward regulatory functions. A

particularly notable alteration was detected in MZB-2–$CD4^+$ Tem interactions: in HDs, these were predominantly mediated by the CD86–CD28 costimulatory axis, whereas in HNSCC they were redirected toward the CD86–CTLA-4 coinhibitory axis, reflecting tumor-specific reprogramming of B cell–T cell crosstalk.

4.3 Distinctive features and functional divergence of MZB-1 and MZB-2

The transcriptional differences between MZB-1 and MZB-2 clusters suggest distinct roles in immune regulation within the HNSCC TIME. MZB-1 appears to represent a more quiescent or resting state, whereas MZB-2 is transcriptionally primed for active participation in immune responses, including antigen presentation and T cell modulation.

When comparing our HNSCC-derived MZB clusters to those reported in HDs by Siu et al. [84], we observed substantial overlap in their transcriptional signatures, indicating a conserved MZB identity across physiological and tumor contexts. However, several distinct features were apparent in the tumor-associated MZBs. Specifically, apoptosis-associated genes (*MTRNR2L8, MTRNR2L12*) and immunoglobulin gene segments (*IGKV1-5, IGKV3-15, IGLV3-1*), were markedly upregulated, reflecting tumor-induced transcriptional reprogramming likely driven by hypoxic stress and chronic antigenic stimulation within the TIME.

In terms of developmental origins, our findings do not fully support the model proposed by Siu et al., which suggested that MZB-1 originates from IgM-only precursors, whereas MZB-2 arises from a NOTCH2-dependent lineage [84]. In contrast, our analyses in HNSCC revealed substantial gene set overlap among MZB-1, IgM-only, and TS B cells, but no significant upregulation of NOTCH2 or enrichment of NOTCH signaling pathway activity in MZB-2. Instead, pseudo-time trajectory analysis suggested a developmental continuum between MZB-1 and MZB-2, rather than distinct lineage bifurcation.

In Siu et al.'s study, DDX21, an RNA helicase that inhibits viral polymerase assembly via PB1 binding [28, 176], served as a key discriminator between MZB-1 and MZB-2 subsets. In contrast, our analysis identified *SUB1* as significantly upregulated in MZB-2. *SUB1* encodes a transcriptional coactivator involved in maintaining genomic stability, regulating RNA polymerase II activity, and suppressing viral replication [38, 59, 98]. These differences

may indicate context-specific adaptations of MZBs in response to tumor-derived or inflammatory cues.

Notably, MZB-2 was the only B cell cluster in our dataset to robustly express *FCRL4*. This aligns with recent reports showing that FCRL4$^+$ TAABs interact with CD4$^+$ T cells within the tumor milieu [209]. The enrichment of MZB-2 in early-stage HNSCC, coupled with its positive prognostic association, supports the hypothesis that FCRL4$^+$ TAABs may initially contribute to antitumor responses. However, persistent activation may drive these cells toward dysfunction or exhaustion, thereby impairing their immunostimulatory capacity over time [76, 118].

Integrating the results from differential gene expression, pathway enrichment, and trajectory inference, our data suggest that MZB-1 and MZB-2 may represent sequential stages in memory B cell differentiation within the TIME, with MZB-2 displaying a more immunoactive and transcriptionally mature phenotype. Concurrently, MZB-2 expressed multiple transcription factors and receptors for inflammatory cytokines and chemokines and was highly enriched in pathways associated with immune regulation. Such an expression landscape suggests a high degree of functional plasticity, enabling MZB-2 to fine-tune immune responses and, under conditions of chronic activation or persistent inflammation, potentially transition toward an immunosuppressive state. To validate this model, longitudinal studies in HNSCC-bearing mice—coupled with functional characterization of MZB-1 and MZB-2—will be essential to elucidate their ontogeny, plasticity, and immunological roles within the tumor microenvironment.

4.4 Antigen-presentation potential of MZB in the tumor microenvironment

Under physiological conditions, MZBs express complement receptor 2 (CR2), enabling the acquisition of C3-modified peptide–MHC class II (pMHC-II) complexes from DCs via trogocytosis. This process allows MZBs to function as noncanonical APCs by delivering processed antigen to CD4$^+$ T cells [168].

In the tumor setting, our study is the first to demonstrate that MZB-2 exhibits robust potential for antigen presentation, particularly through interactions with T cells and professional APCs within the HNSCC tumor microenvironment. These interactions primarily occurred through

MHC-II-dependent mechanisms, as revealed by L-R analyses of MZB-2 with $CD4^+$ T cells and cDCs.

One notable mechanism is cross-presentation, in which APCs present exogenous antigens on MHC molecules not synthesized internally. This mechanism is especially relevant in tumors of non-hematopoietic origin or viral infections where direct APC priming is limited [67, 205]. The interaction of MZB clusters with $CD8^+$ T cells via MHC-I pathways likely reflects cross-presentation. Unlike conventional pathways, cross-presentation can operate independently of the BCR, thus extending the antigen-presenting capacity of MZBs beyond their clonal specificity.

In our dataset, MHC-I pathway activity was markedly elevated in HNSCC tumors compared with HD tonsils, underscoring its potential importance in shaping tumor immunity. However, whether this enhanced MHC-I signaling uniformly promotes antitumor responses, or whether it can be hijacked by tumor cells to evade immune recognition and dampen immunotherapeutic efficacy, remains an open question [205].

Together, these findings suggest that MZB-2 as an active immunological intermediary within the TIME—bridging innate and adaptive immunity through antigen presentation, cross-presentation, and T cell modulation, thereby contributing to the dynamic immune crosstalk that defines tumor-immune equilibrium in HNSCC.

4.5 Additional immunoregulatory communication pathways involving MZB-2

In addition to classical MHC-I and II pathways, our analysis revealed several additional L-R interactions through which MZB-2 may engage in immunomodulatory communication within the HNSCC TIME.

One such interaction is the *CD99–CD99* bidirectional signaling axis, which has been implicated in T cell activation and the induction of pro-inflammatory cytokines such as IL-6 and TNF-α [140, 182]. While CD99 has traditionally been described as a membrane protein expressed primarily on monocytes and DCs [183], our results indicate that MZB-2 also expresses CD99, suggesting its potential to participate in direct T cell modulation.

Furthermore, MZB-2 interacts with multiple T cell subsets—including $CD4^+$ Tem, Tregs, and γδ T cells—via the *CD86–CTLA-4* axis. CTLA-4 is a key immune checkpoint receptor that exerts suppressive effects on T cell responses. CTLA-4-expressing Tregs downregulate

the co-stimulatory molecules CD80 and CD86 on APCs through CTLA-4-mediated trogocytosis [185]. This downregulation not only reduces the ability to activate naïve T cells but also increases the availability of PD-L1, thereby enhancing PD-1–mediated suppression of effector T cells.

A third notable axis involves *LGALS9* (galectin-9) and its interactions with CD44, CD45, and HAVCR2 (also known as TIM-3). MZB-2 was found to engage with T cells, monocytes, and DCs through this L-R network. Galectin-9, encoded by *LGALS9*, is a β-galactoside-binding lectin involved in diverse processes such as immune escape, cell adhesion, angiogenesis, and tumor metastasis [74]. Multiple members of the galectin family have been associated with cancer progression and unfavorable prognosis across various malignancies [93, 110, 126, 143]. In hepatocellular carcinoma, for instance, galectin-9 mediates immunosuppressive interactions between tumor cells and macrophages through *SLC1A5* and is associated with poor outcomes [119].

HAVCR2, a receptor primarily expressed on Th1 cells, contributes to the regulation of macrophage activation and promotes immune tolerance by suppressing Th1-driven responses [134, 163]. The involvement of MZB-2 in this axis suggests a possible role in modulating T cell exhaustion and tolerance within the TIME.

Collectively, these additional L-R interactions position MZB-2 as an active immunoregulatory hub, capable of shaping both adaptive and innate immune responses. Its interaction with multiple immune subsets through checkpoint and lectin pathways highlights its multifaceted role in immune modulation, which may have significant implications for immunotherapy and tumor progression in HNSCC.

4.6 Conclusion

This study provides the first evidence for the presence of MZBs in both tumor tissue and peripheral blood of patients with HNSCC. Through integrative analyses combining flow cytometry, scRNA-seq, spatial transcriptomics, and bulk RNA-seq deconvolution, we elucidated the presence, heterogeneity, spatial localization, and immunological function of MZB subsets within the TIME.

MZBs were more abundant in HPV^+ tumors and demonstrated distinct gene expression signatures shaped by the TIME, including hallmarks of hypoxia and viral responses. Among

the subsets, MZB-2 emerged as the more immunoactive phenotype, presented advanced maturation markers and broad participation in immune response pathways, exhibited elevated antigen presentation capacity and robust interactions with $CD4^+$ Tfh cells and professional APCs. Importantly, MZB-2 displayed a dual immunoregulatory potential. In HDs, it exhibited antigen presentation capacity in conjunction with CD80–CD28 co-stimulation, supporting effective T cell activation. By contrast, in HNSCC patients, MZB-2 engaged $CD4^+$ T cells through both MHC-II and CD80–CTLA-4 interactions, suggesting a role in modulating, rather than sustaining, T cell responses. MZB-2 was associated with improved prognosis in early-stage HNSCC patients. Transcriptomic profiling of MZB-2 revealed its elevated transcription factors, cytokine and chemokine receptors, and enrichment of immune regulatory pathways, which underscores its functional plasticity and implies a potential shift toward immunosuppression state under certain conditions. ST analyses confirmed the co-localization of MZB-2 with GCBs and Tfh cells within the tumor, supporting the existence of a functional MZB–Tfh–GCB axis.

What limits in our study is the lack of protein-level validation and functional experiments. The precise mechanisms of MHC-I/II-mediated antigen presentation by MZBs and their role in modulating T cell responses remain to be validated at the protein level. Future work should employ proteomic techniques, such as MHC-peptidome profiling of MZBs, to identify tumor-derived neoantigens presented by these cells. Additionally, while our analysis revealed L-R interactions through the CellChat framework, the downstream functional consequences of MZB–T cell crosstalk remain to be experimentally defined. To this end, we are currently establishing genetically engineered mouse models for the selective depletion of MZBs to facilitate in vivo functional studies.

Additionally, due to the lack of a validated transcriptomic profile for MZPs, their identification in scRNA-seq data was not possible. Multimodal approaches such as CITE-seq or BCR-seq combined with protein markers may be necessary to resolve this population.

In summary, this work positions MZB-2 as a prognostically favorable biomarker in early-stage HNSCC and a potential modulator of immune responses within the TIME. Future prospective studies, particularly in ICB cohorts, will be essential for us to understand the extent to which MZBs influence patients' prognosis and immunotherapy outcomes.

5 Summary

Emerging evidence underscores the critical role of B lymphocytes in shaping tumor progression. Among these, marginal zone B cells (MZBs)—typically localized outside the marginal sinus of the spleen—are distinguished by their capacity to recognize ectopic antigens and secrete immunomodulatory cytokines. Our previous work identified tumor-associated MZBs in a murine model of head and neck squamous cell carcinoma (HNSCC). The present study aimed to validate the presence of MZBs in human HNSCC and investigate their phenotypic characteristics, functional roles, and prognostic implications.

Flow cytometry was employed to detect MZBs in tumor tissues and peripheral blood from HNSCC patients. An integrated single-cell RNA sequencing (scRNA-seq) dataset comprising 118 HNSCC patients at various clinical stages and 6 healthy donors (HDs) was assembled. Comparative transcriptomic profiling of B cell populations between HNSCC and HDs was performed. Downstream analyses, including pathway enrichment, cell communication inference, spatial transcriptomics (ST), and survival correlation, were applied.

Two transcriptionally distinct MZB subsets were identified in both peripheral blood and tumor tissues of HNSCC patients and HDs. Tumor-associated MZBs displayed a unique molecular signature enriched in hypoxia and viral response pathways, distinguishing them from their physiological counterparts. Both MZBs and germinal center B cells (GCBs) were more abundant in human papillomavirus–positive (HPV^+) HNSCC tumors compared to HPV-negative (HPV^-) cases. Notably, the MZB-2 subset, characterized by elevated expression of activation markers and immunoregulatory genes, demonstrated close interactions with $CD4^+$ T follicular helper (Tfh) cells and antigen-presenting cells. These interactions were supported by costimulatory signals in HDs but were absent in HNSCC patients. ST analysis revealed co-localization of MZB-2, GCBs, and $CD4^+$ Tfh cells within the tumor microenvironment. Clinically, MZB-2 abundance correlated with favorable prognosis in early-stage HNSCC, but not in advanced disease. Immunosuppressive gene expression was not exclusive to MZBs, indicating that they do not constitute a purely regulatory B cell phenotype.

Summary

This study provides the first evidence of tumor-associated MZB subsets in human HNSCC, revealing their putative role in immune modulation—balancing antigen presentation, cytokine signaling, and immune suppression. The spatial and functional convergence of MZB-2, Tfh, and GCB cells suggests the presence of an MZB–Tfh–GCB axis that may enhance local immune responses. The association of MZB-2 with improved prognosis in early-stage HNSCC highlights its potential as a beneficial regulator of antitumor immunity during early tumor progression.

6 References

1. Akdis M, Aab A, Altunbulakli C, Azkur K, Costa RA, Crameri R, Duan S, Eiwegger T, Eljaszewicz A, Ferstl R, Frei R, Garbani M, Globinska A, Hess L, Huitema C, Kubo T, Komlosi Z, Konieczna P, Kovacs N, Kucuksezer UC, Meyer N, Morita H, Olzhausen J, O'Mahony L, Pezer M, Prati M, Rebane A, Rhyner C, Rinaldi A, Sokolowska M, Stanic B, Sugita K, Treis A, van de Veen W, Wanke K, Wawrzyniak M, Wawrzyniak P, Wirz OF, Zakzuk JS, Akdis CA (2016) Interleukins (from IL-1 to IL-38), interferons, transforming growth factor β, and TNF-α: Receptors, functions, and roles in diseases. Journal of Allergy and Clinical Immunology 138:984–1010.

2. Alfouzan AF (2021) Radiation therapy in head and neck cancer. Saudi Med Journal 42:247–254

3. Allen E, Jabouille A, Rivera LB, Lodewijckx I, Missiaen R, Steri V, Feyen K, Tawney J, Hanahan D, Michael IP, Bergers G (2017) Combined antiangiogenic and anti–PD-L1 therapy stimulates tumor immunity through HEV formation. Sci Transl Med 9:eaak9679.

4. Allman D, Pillai S (2008) Peripheral B cell subsets. Current Opinion in Immunology 20:149–157.

5. Amatore F, Gorvel L, Olive D (2018) Inducible Co-Stimulator (ICOS) as a potential therapeutic target for anti-cancer therapy. Expert Opinion on Therapeutic Targets 22:343–351.

6. Ang KK, Harris J, Wheeler R, Weber R, Rosenthal DI, Nguyen-Tân PF, Westra WH, Chung CH, Jordan RC, Lu C, Kim H, Axelrod R, Silverman CC, Redmond KP, Gillison ML (2010) Human Papillomavirus and Survival of Patients with Oropharyngeal Cancer. N Engl J Med 363:24–35.

7. Aran D, Looney AP, Liu L, Wu E, Fong V, Hsu A, Chak S, Naikawadi RP, Wolters PJ, Abate AR, Butte AJ, Bhattacharya M (2019) Reference-based analysis of lung single-

cell sequencing reveals a transitional profibrotic macrophage. Nat Immunol 20:163–172.

8. Atanackovic D, Blum I, Cao Y, Wenzel S, Bartels K, Faltz C, Hossfeld DK, Hegewisch-Becker S, Bokemeyer C, Leuwer R (2006) Expression of cancer-testis antigens as possible targets for antigen-specific immunotherapy in head and neck squamous cell carcinoma. Cancer Biology & Therapy 5:1218–1225.

9. Athar M, Back JH, Kopelovich L, Bickers DR, Kim AL (2009) Multiple molecular targets of resveratrol: Anti-carcinogenic mechanisms. Archives of Biochemistry and Biophysics 486:95–102.

10. Attanavanich K, Kearney JF (2004) Marginal zone, but not follicular B cells, are potent activators of naive CD4 T cells. J Immunol 172:803–811.

11. Bao J, Betzler AC, Hess J, Brunner C (2023) Exploring the dual role of B cells in solid tumors: implications for head and neck squamous cell carcinoma. Front Immunol 14:1233085.

12. Bao J, Hess J, Betzler AC, Zhang Z, Tsesmelis M, Schmid S, Berry G, Schuler PJ, Greve J, Laban S, Hoffmann TK, Mulaw M, Brunner C (2025) Identification of marginal zone B cells in head and neck cancer with immunomodulatory characteristics. Journal of Advanced Research S209012322500966X.

13. Bill R, Wirapati P, Messemaker M, Roh W, Zitti B, Duval F, Kiss M, Park JC, Saal TM, Hoelzl J, Tarussio D, Benedetti F, Tissot S, Kandalaft L, Varrone M, Ciriello G, McKee TA, Monnier Y, Mermod M, Blaum EM, Gushterova I, Gonye ALK, Hacohen N, Getz G, Mempel TR, Klein AM, Weissleder R, Faquin WC, Sadow PM, Lin D, Pai SI, Sade-Feldman M, Pittet MJ (2023) CXCL9:SPP1 macrophage polarity identifies a network of cellular programs that control human cancers. Science 381:515–524.

14. Bodogai M, Lee Chang C, Wejksza K, Lai J, Merino M, Wersto RP, Gress RE, Chan AC, Hesdorffer C, Biragyn A (2013) Anti-CD20 Antibody Promotes Cancer Escape

via Enrichment of Tumor-Evoked Regulatory B Cells Expressing Low Levels of CD20 and CD137L. Cancer Res 73:2127–2138.

15. Bolotin DA, Poslavsky S, Davydov AN, Frenkel FE, Fanchi L, Zolotareva OI, Hemmers S, Putintseva EV, Obraztsova AS, Shugay M, Ataullakhanov RI, Rudensky AY, Schumacher TN, Chudakov DM (2017) Antigen receptor repertoire profiling from RNA-seq data. Nat Biotechnol 35:908–911.

16. Bonner JA, Harari PM, Giralt J, Azarnia N, Shin DM, Cohen RB, Jones CU, Sur R, Raben D, Jassem J, Ove R, Kies MS, Baselga J, Youssoufian H, Amellal N, Rowinsky EK, Ang KK (2006) Radiotherapy plus cetuximab for squamous-cell carcinoma of the head and neck. N Engl J Med 354:567–578

17. Broglie MA, Jochum W, Michel A, Waterboer T, Foerbs D, Schoenegg R, Stoeckli SJ, Pawlita M, Holzinger D (2017) Evaluation of type-specific antibodies to high risk-human papillomavirus (HPV) proteins in patients with oropharyngeal cancer. Oral Oncology 70:43–50.

18. Bruno TC, Ebner PJ, Moore BL, Squalls OG, Waugh KA, Eruslanov EB, Singhal S, Mitchell JD, Franklin WA, Merrick DT, McCarter MD, Palmer BE, Kern JA, Slansky JE (2017) Antigen-Presenting Intratumoral B Cells Affect CD4+ TIL Phenotypes in Non–Small Cell Lung Cancer Patients. Cancer Immunology Research 5:898–907.

19. Bubie A, Zoulim F, Testoni B, Miles B, Posner M, Villanueva A, Losic B (2021) Landscape of oncoviral genotype and co-infection via human papilloma and hepatitis B viral tumor in situ profiling. iScience 24:102368.

20. Buckley CD, Barone F, Nayar S, Bénézech C, Caamaño J (2015) Stromal Cells in Chronic Inflammation and Tertiary Lymphoid Organ Formation. Annu Rev Immunol 33:715–745.

21. Burtness B, Harrington KJ, Greil R, Soulières D, Tahara M, de Castro G, Psyrri A, Basté N, Neupane P, Bratland Å, Fuereder T, Hughes BGM, Mesía R, Ngamphaiboon N, Rordorf T, Wan Ishak WZ, Hong R-L, González Mendoza R, Roy A, Zhang Y,

Gumuscu B, Cheng JD, Jin F, Rischin D (2019) Pembrolizumab alone or with chemotherapy versus cetuximab with chemotherapy for recurrent or metastatic squamous cell carcinoma of the head and neck (KEYNOTE-048): a randomised, open-label, phase 3 study. Lancet 394:1915–1928.

22. Butz H, Rácz K, Hunyady L, Patócs A (2012) Crosstalk between TGF-β signaling and the microRNA machinery. Trends in Pharmacological Sciences 33:382–393.

23. Cabrita R, Lauss M, Sanna A, Donia M, Skaarup Larsen M, Mitra S, Johansson I, Phung B, Harbst K, Vallon-Christersson J, van Schoiack A, Lövgren K, Warren S, Jirström K, Olsson H, Pietras K, Ingvar C, Isaksson K, Schadendorf D, Schmidt H, Bastholt L, Carneiro A, Wargo JA, Svane IM, Jönsson G (2020) Tertiary lymphoid structures improve immunotherapy and survival in melanoma. Nature 577:561–565.

24. Caro-Maldonado A, Wang R, Nichols AG, Kuraoka M, Milasta S, Sun LD, Gavin AL, Abel ED, Kelsoe G, Green DR, Rathmell JC (2014) Metabolic Reprogramming Is Required for Antibody Production That Is Suppressed in Anergic but Exaggerated in Chronically BAFF-Exposed B Cells. JI 192:3626–3636.

25. Castino GF (2016) Spatial distribution of B cells predicts prognosis in human pancreatic adenocarcinoma. OncoImmunology 5:e1085147

26. Catalán D, Mansilla MA, Ferrier A, Soto L, Oleinika K, Aguillón JC, Aravena O (2021) Immunosuppressive Mechanisms of Regulatory B Cells. Front Immunol 12:611795.

27. Chagnon-Choquet J, Fontaine J, Poudrier J, Roger M, for the Montreal Primary HIV Infection and Slow Progressor Study Groups (2014) IL-10 and Lymphotoxin-α Expression Profiles within Marginal Zone-Like B-Cell Populations Are Associated with Control of HIV-1 Disease Progression. PLoS ONE 9:e101949.

28. Chen G, Liu C-H, Zhou L, Krug RM (2014) Cellular DDX21 RNA helicase inhibits influenza A virus replication but is counteracted by the viral NS1 protein. Cell Host Microbe 15:484–493.

29. Chen L, Taylor JL, Sabins NC, Lowe DB, Qu Y, You Z, Storkus WJ (2013) Extranodal induction of therapeutic immunity in the tumor microenvironment after intratumoral delivery of Tbet gene-modified dendritic cells. Cancer Gene Ther 20:469–477.

30. Chen W, Jiang M, Yu W, Xu Z, Liu X, Jia Q, Guan X, Zhang W (2021) CpG-Based Nanovaccines for Cancer Immunotherapy. Int J Nanomedicine 16:5281–5299.

31. Choi J-H, Lee B-S, Jang JY, Lee YS, Kim HJ, Roh J, Shin YS, Woo HG, Kim C-H (2023) Single-cell transcriptome profiling of the stepwise progression of head and neck cancer. Nat Commun 14:1055.

32. Choi JK, Egwuagu CE (2021) Interleukin 35 Regulatory B Cells. Journal of Molecular Biology 433:166607.

33. Choudhary S, Satija R (2022) Comparison and evaluation of statistical error models for scRNA-seq. Genome Biology 23:27.

34. Cillo AR, Kürten CHL, Tabib T, Qi Z, Onkar S, Wang T, Liu A, Duvvuri U, Kim S, Soose RJ, Oesterreich S, Chen W, Lafyatis R, Bruno TC, Ferris RL, Vignali DAA (2020) Immune Landscape of Viral- and Carcinogen-Driven Head and Neck Cancer. Immunity 52:183-199.e9.

35. Cinamon G, Zachariah MA, Lam OM, Foss FW, Cyster JG (2008) Follicular shuttling of marginal zone B cells facilitates antigen transport. Nat Immunol 9:54–62.

36. Colbeck EJ, Ager A, Gallimore A, Jones GW (2017) Tertiary Lymphoid Structures in Cancer: Drivers of Antitumor Immunity, Immunosuppression, or Bystander Sentinels in Disease? Front Immunol 8:1830.

37. Coppola D, Nebozhyn M, Khalil F, Dai H, Yeatman T, Loboda A, Mulé JJ (2011) Unique Ectopic Lymph Node-Like Structures Present in Human Primary Colorectal Carcinoma Are Identified by Immune Gene Array Profiling. The American Journal of Pathology 179:37–45.

38. Currie RA (1998) Biochemical characterization of the NF-Y transcription factor complex during B lymphocyte development. J Biol Chem 273:18220–18229.

39. Dambuza IM, He C, Choi JK, Yu C-R, Wang R, Mattapallil MJ, Wingfield PT, Caspi RR, Egwuagu CE (2017) IL-12p35 induces expansion of IL-10 and IL-35-expressing regulatory B cells and ameliorates autoimmune disease. Nat Commun 8:719.

40. Das S, Bar-Sagi D (2019) BTK signaling drives CD1dhiCD5+ regulatory B-cell differentiation to promote pancreatic carcinogenesis. Oncogene 38:3316–3324.

41. Delgoffe GM, Woo S-R, Turnis ME, Gravano DM, Guy C, Overacre AE, Bettini ML, Vogel P, Finkelstein D, Bonnevier J, Workman CJ, Vignali DAA (2013) Stability and function of regulatory T cells is maintained by a neuropilin-1–semaphorin-4a axis. Nature 501:252–256.

42. Dieu-Nosjean M-C, Giraldo NA, Kaplon H, Germain C, Fridman WH, Sautès-Fridman C (2016) Tertiary lymphoid structures, drivers of the anti-tumor responses in human cancers. Immunol Rev 271:260–275.

43. Doyon-Laliberté K, Aranguren M, Poudrier J, Roger M (2022) Marginal Zone B-Cell Populations and Their Regulatory Potential in the Context of HIV and Other Chronic Inflammatory Conditions. IJMS 23:3372.

44. Doyon-Laliberté K, Chagnon-Choquet J, Byrns M, Aranguren M, Memmi M, Chrobak P, Stagg J, Poudrier J, Roger M (2019) NR4A Expression by Human Marginal Zone B-Cells. Antibodies 8:50.

45. Dubois F, Limou S, Chesneau M, Degauque N, Brouard S, Danger R (2020) Transcriptional meta-analysis of regulatory B cells. Eur J Immunol 50:1757–1769.

46. Economopoulou P, Kotsantis I, Psyrri A (2016) The promise of immunotherapy in head and neck squamous cell carcinoma: combinatorial immunotherapy approaches. ESMO Open 1:e000122.

47. Egwuagu CE, Yu C-R, Sun L, Wang R (2015) Interleukin 35: Critical regulator of immunity and lymphocyte-mediated diseases. Cytokine & Growth Factor Reviews 26:587–593.

48. Evans JG, Chavez-Rueda KA, Eddaoudi A, Meyer-Bahlburg A, Rawlings DJ, Ehrenstein MR, Mauri C (2007) Novel Suppressive Function of Transitional 2 B Cells in Experimental Arthritis. The Journal of Immunology 178:7868–7878.

49. Ferguson AR, Youd ME, Corley RB (2004) Marginal zone B cells transport and deposit IgM-containing immune complexes onto follicular dendritic cells. Int Immunol 16:1411–1422.

50. Ferris RL, Blumenschein G, Fayette J, Guigay J, Colevas AD, Licitra L, Harrington K, Kasper S, Vokes EE, Even C, Worden F, Saba NF, Iglesias Docampo LC, Haddad R, Rordorf T, Kiyota N, Tahara M, Monga M, Lynch M, Geese WJ, Kopit J, Shaw JW, Gillison ML (2016) Nivolumab for Recurrent Squamous-Cell Carcinoma of the Head and Neck. N Engl J Med 375:1856–1867.

51. Fillatreau S, Sweenie CH, McGeachy MJ, Gray D, Anderton SM (2002) B cells regulate autoimmunity by provision of IL-10. Nat Immunol 3:944–950.

52. Fleige H, Ravens S, Moschovakis GL, Bölter J, Willenzon S, Sutter G, Häussler S, Kalinke U, Prinz I, Förster R (2014) IL-17–induced CXCL12 recruits B cells and induces follicle formation in BALT in the absence of differentiated FDCs. Journal of Experimental Medicine 211:643–651.

53. for the SPARC Consortium, Wood O, Woo J, Seumois G, Savelyeva N, McCann KJ, Singh D, Jones T, Peel L, Breen MS, Ward M, Garrido Martin E, Sanchez-Elsner T, Thomas G, Vijayanand P, Woelk CH, King E, Ottensmeier C (2016) Gene expression analysis of TIL rich HPV-driven head and neck tumors reveals a distinct B-cell signature when compared to HPV independent tumors. Oncotarget 7:56781–56797.

54. Forastiere A, Koch W, Trotti A, Sidransky D (2001) Head and neck cancer. The New England journal of medicine 345:1890–900

55. Forastiere AA, Ismaila N, Lewin JS, Nathan CA, Adelstein DJ, Eisbruch A, Fass G, Fisher SG, Laurie SA, Le Q-T, O'Malley B, Mendenhall WM, Patel S, Pfister DG, Provenzano AF, Weber R, Weinstein GS, Wolf GT (2017) Use of Larynx-Preservation Strategies in the Treatment of Laryngeal Cancer: American Society of Clinical Oncology Clinical Practice Guideline Update. J Clin Oncol 36:1143–1169.

56. Furtado GC, Marinkovic T, Martin AP, Garin A, Hoch B, Hubner W, Chen BK, Genden E, Skobe M, Lira SA (2007) Lymphotoxin β receptor signaling is required for inflammatory lymphangiogenesis in the thyroid. PNAS 104:6

57. Gameiro SF, Evans AM, Mymryk JS (2022) The tumor immune microenvironments of HPV(+) and HPV(-) head and neck cancers. WIREs Mech Dis 14:e1539.

58. Ganti SN, Albershardt TC, Iritani BM, Ruddell A (2015) Regulatory B cells preferentially accumulate in tumor-draining lymph nodes and promote tumor growth. Sci Rep 5:12255.

59. Garavís M, Calvo O (2017) Sub1/PC4, a multifaceted factor: from transcription to genome stability. Curr Genet 63:1023–1035.

60. Gatto D, Brink R (2010) The germinal center reaction. Journal of Allergy and Clinical Immunology 126:898–907.

61. Gavish A, Tyler M, Greenwald AC, Hoefflin R, Simkin D, Tschernichovsky R, Galili Darnell N, Somech E, Barbolin C, Antman T, Kovarsky D, Barrett T, Gonzalez Castro LN, Halder D, Chanoch-Myers R, Laffy J, Mints M, Wider A, Tal R, Spitzer A, Hara T, Raitses-Gurevich M, Stossel C, Golan T, Tirosh A, Suvà ML, Puram SV, Tirosh I (2023) Hallmarks of transcriptional intratumour heterogeneity across a thousand tumours. Nature 618:598–606.

62. Germain C, Gnjatic S, Tamzalit F, Knockaert S, Remark R, Goc J, Lepelley A, Becht E, Katsahian S, Bizouard G, Validire P, Damotte D, Alifano M, Magdeleinat P, Cremer I, Teillaud J-L, Fridman W-H, Sautès-Fridman C, Dieu-Nosjean M-C (2014) Presence

of B Cells in Tertiary Lymphoid Structures Is Associated with a Protective Immunity in Patients with Lung Cancer. Am J Respir Crit Care Med 189:832–844.

63. Gillison ML, Chaturvedi AK, Anderson WF, Fakhry C (2015) Epidemiology of Human Papillomavirus-Positive Head and Neck Squamous Cell Carcinoma. J Clin Oncol 33:3235–3242.

64. Gu Z, Eils R, Schlesner M (2016) Complex heatmaps reveal patterns and correlations in multidimensional genomic data. Bioinformatics 32:2847–2849.

65. Gu Z, Gu L, Eils R, Schlesner M, Brors B (2014) circlize implements and enhances circular visualization in R. Bioinformatics 30:2811–2812.

66. Guan H, Lan Y, Wan Y, Wang Q, Wang C, Xu L, Chen Y, Liu W, Zhang X, Li Y, Gu Y, Wang Z, Xie F (2016) PD-L1 mediated the differentiation of tumor-infiltrating CD19 $^{+}$ B lymphocytes and T cells in Invasive breast cancer. OncoImmunology 5:e1075112.

67. Gutiérrez-Martínez E, Planès R, Anselmi G, Reynolds M, Menezes S, Adiko AC, Saveanu L, Guermonprez P (2015) Cross-Presentation of Cell-Associated Antigens by MHC Class I in Dendritic Cell Subsets. Front Immunol 6:363.

68. Gu-Trantien C, Migliori E, Buisseret L, de Wind A, Brohée S, Garaud S, Noël G, C.V. LD, Lodewyckx J-N, Naveaux C, Duvillier H, Goriely S, Larsimont D, Willard-Gallo K (2017) CXCL13-producing TFH cells link immune suppression and adaptive memory in human breast cancer. JCI Insight 2:e91487.

69. Hafemeister C, Satija R (2019) Normalization and variance stabilization of single-cell RNA-seq data using regularized negative binomial regression. Genome Biol 20:296.

70. Hanna GJ, Lizotte P, Cavanaugh M, Kuo FC, Shivdasani P, Frieden A, Chau NG, Schoenfeld JD, Lorch JH, Uppaluri R, MacConaill LE, Haddad RI (2018) Frameshift events predict anti–PD-1/L1 response in head and neck cancer. JCI Insight 3:e98811.

71. Hänzelmann S, Castelo R, Guinney J (2013) GSVA: gene set variation analysis for microarray and RNA-seq data. BMC Bioinformatics 14:7.

72. Hao Y, Hao S, Andersen-Nissen E, Mauck WM, Zheng S, Butler A, Lee MJ, Wilk AJ, Darby C, Zager M, Hoffman P, Stoeckius M, Papalexi E, Mimitou EP, Jain J, Srivastava A, Stuart T, Fleming LM, Yeung B, Rogers AJ, McElrath JM, Blish CA, Gottardo R, Smibert P, Satija R (2021) Integrated analysis of multimodal single-cell data. Cell 184:3573-3587.e29.

73. Helmink BA, Reddy SM, Gao J, Zhang S, Basar R, Thakur R, Yizhak K, Sade-Feldman M, Blando J, Han G, Gopalakrishnan V, Xi Y, Zhao H, Amaria RN, Tawbi HA, Cogdill AP, Liu W, LeBleu VS, Kugeratski FG, Patel S, Davies MA, Hwu P, Lee JE, Gershenwald JE, Lucci A, Arora R, Woodman S, Keung EZ, Gaudreau P-O, Reuben A, Spencer CN, Burton EM, Haydu LE, Lazar AJ, Zapassodi R, Hudgens CW, Ledesma DA, Ong S, Bailey M, Warren S, Rao D, Krijgsman O, Rozeman EA, Peeper D, Blank CU, Schumacher TN, Butterfield LH, Zelazowska MA, McBride KM, Kalluri R, Allison J, Petitprez F, Fridman WH, Sautès-Fridman C, Hacohen N, Rezvani K, Sharma P, Tetzlaff MT, Wang L, Wargo JA (2020) B cells and tertiary lymphoid structures promote immunotherapy response. Nature 577:549–555.

74. Heusschen R, Griffioen AW, Thijssen VL (2013) Galectin-9 in tumor biology: A jack of multiple trades. Biochimica et Biophysica Acta (BBA) - Reviews on Cancer 1836:177–185.

75. Hladíková K, Koucký V, Bouček J, Laco J, Grega M, Hodek M, Zábrodský M, Vošmik M, Rozkošová K, Vošmiková H, Čelakovský P, Chrobok V, Ryška A, Špíšek R, Fialová A (2019) Tumor-infiltrating B cells affect the progression of oropharyngeal squamous cell carcinoma via cell-to-cell interactions with CD8+ T cells. j immunotherapy cancer 7:261.

76. Hollern D (2024) Memory B cell fitness and anergy has significant links to cancer lethality. Cell 187:4551–4553.

77. Hollern DP, Xu N, Thennavan A, Glodowski C, Garcia-Recio S, Mott KR, He X, Garay JP, Carey-Ewend K, Marron D, Ford J, Liu S, Vick SC, Martin M, Parker JS, Vincent BG, Serody JS, Perou CM (2019) B Cells and T Follicular Helper Cells Mediate

Response to Checkpoint Inhibitors in High Mutation Burden Mouse Models of Breast Cancer. Cell 179:1191-1206.e21.

78. Horikawa M, Minard-Colin V, Matsushita T, Tedder TF (2011) Regulatory B cell production of IL-10 inhibits lymphoma depletion during CD20 immunotherapy in mice. J Clin Invest 121:4268–4280.

79. Hu Q, Hong Y, Qi P, Lu G, Mai X, Xu S, He X, Guo Y, Gao L, Jing Z, Wang J, Cai T, Zhang Y (2021) Atlas of breast cancer infiltrated B-lymphocytes revealed by paired single-cell RNA-sequencing and antigen receptor profiling. Nat Commun 12:2186.

80. Huang SH, O'Sullivan B (2017) Overview of the 8th Edition TNM Classification for Head and Neck Cancer. Curr Treat Options in Oncol 18:40.

81. Huber K, Sármay G, Kövesdi D (2016) MZ B cells migrate in a T-bet dependent manner and might contribute to the remission of collagen-induced arthritis by the secretion of IL-10. Eur J Immunol 46:2239–2246.

82. Inoue S, Leitner WW, Golding B, Scott D (2006) Inhibitory Effects of B Cells on Antitumor Immunity. Cancer Res 66:7741–7747.

83. Iwata Y, Matsushita T, Horikawa M, DiLillo DJ, Yanaba K, Venturi GM, Szabolcs PM, Bernstein SH, Magro CM, Williams AD, Hall RP, St Clair EW, Tedder TF (2011) Characterization of a rare IL-10–competent B-cell subset in humans that parallels mouse regulatory B10 cells. Blood 117:530–541.

84. Jacqueline H.Y. Siu, Michael J. Pitcher, Thomas J. Tull, Rebekah L. Velounias, William Guesdon, Lucia Montorsi, Krishnaa T. Mahbubani, Richard Ellis, Mats Bemark, Gavin J. Pettigrew, Jo Spencer (2022) Two subsets of human marginal zone B cells resolved by global analysis of lymphoid tissues and blood. Science Immunology 7:eabm9060.

85. Jeske SS, Brand M, Ziebart A, Laban S, Doescher J, Greve J, Jackson EK, Hoffmann TK, Brunner C, Schuler PJ (2020) Adenosine-producing regulatory B cells in head and neck cancer. Cancer Immunol Immunother 69:1205–1216.

86. Jin S, Guerrero-Juarez CF, Zhang L, Chang I, Ramos R, Kuan C-H, Myung P, Plikus MV, Nie Q (2021) Inference and analysis of cell-cell communication using CellChat. Nat Commun 12:1088.

87. Johansson-Percival A, He B, Li Z-J, Kjellén A, Russell K, Li J, Larma I, Ganss R (2017) De novo induction of intratumoral lymphoid structures and vessel normalization enhances immunotherapy in resistant tumors. Nat Immunol 18:1207–1217.

88. Kessel A, Haj T, Peri R, Snir A, Melamed D, Sabo E, Toubi E (2012) Human CD19+CD25high B regulatory cells suppress proliferation of CD4+ T cells and enhance Foxp3 and CTLA-4 expression in T-regulatory cells. Autoimmunity Reviews 11:670–677.

89. Kevin Blighe, Sharmila Rana, Myles Lewis (2018) EnhancedVolcano: Publication-ready volcano plots with enhanced colouring and labeling. https://github.com/kevinblighe/EnhancedVolcano.

90. Khan AR, Hams E, Floudas A, Sparwasser T, Weaver CT, Fallon PG (2015) PD-L1hi B cells are critical regulators of humoral immunity. Nat Commun 6:5997.

91. Kim SS, Shen S, Miyauchi S, Sanders PD, Franiak-Pietryga I, Mell L, Gutkind JS, Cohen EEW, Califano JA, Sharabi AB (2020) B Cells Improve Overall Survival in HPV-Associated Squamous Cell Carcinomas and Are Activated by Radiation and PD-1 Blockade. Clin Cancer Res 26:3345–3359.

92. Kim SS, Sumner WA, Miyauchi S, Cohen EEW, Califano JA, Sharabi AB (2021) Role of B Cells in Responses to Checkpoint Blockade Immunotherapy and Overall Survival of Cancer Patients. Clin Cancer Res 27:6075–6082.

93. Kindt N, Journe F, Ghanem GE, Saussez S (2017) Galectins and Carcinogenesis: Their Role in Head and Neck Carcinomas and Thyroid Carcinomas. International Journal of Molecular Sciences 18:2745.

94. Kinker GS, Vitiello GAF, Ferreira WAS, Chaves AS, Cordeiro de Lima VC, Medina T da S (2021) B Cell Orchestration of Anti-tumor Immune Responses: A Matter of Cell Localization and Communication. Front Cell Dev Biol 9:678127.

95. Kobayashi K, Hisamatsu K, Suzui N, Hara A, Tomita H, Miyazaki T (2018) A Review of HPV-Related Head and Neck Cancer. JCM 7:241.

96. Koneva LA, Zhang Y, Virani S, Hall PB, McHugh JB, Chepeha DB, Wolf GT, Carey TE, Rozek LS, Sartor MA (2018) HPV Integration in HNSCC Correlates with Survival Outcomes, Immune Response Signatures, and Candidate Drivers. Mol Cancer Res 16:90–102.

97. Korsunsky I, Fan J, Slowikowski K, Zhang F, Wei K, Baglaenko Y, Brenner M, Loh P-R, Raychaudhuri S (2019) Fast, sensitive, and accurate integration of single cell data with Harmony. Nature Methods 16:1289–1296.

98. Kretzschmar M, Kaiser K, Lottspeich F, Meisterernst M (1994) A novel mediator of class II gene transcription with homology to viral immediate-early transcriptional regulators. Cell 78:525–534.

99. Kroeger DR, Milne K, Nelson BH (2016) Tumor-Infiltrating Plasma Cells Are Associated with Tertiary Lymphoid Structures, Cytolytic T-Cell Responses, and Superior Prognosis in Ovarian Cancer. Clin Cancer Res 22:3005–3015.

100. Kürten CHL, Kulkarni A, Cillo AR, Santos PM, Roble AK, Onkar S, Reeder C, Lang S, Chen X, Duvvuri U, Kim S, Liu A, Tabib T, Lafyatis R, Feng J, Gao S-J, Bruno TC, Vignali DAA, Lu X, Bao R, Vujanovic L, Ferris RL (2021) Investigating immune and non-immune cell interactions in head and neck tumors by single-cell RNA sequencing. Nat Commun 12:7338.

101. LeBien TW, Tedder TF (2008) B lymphocytes: how they develop and function. Blood 112:1570–1580.

102. Lechner A, Schlößer HA, Thelen M, Wennhold K, Rothschild SI, Gilles R, Quaas A, Siefer OG, Huebbers CU, Cukuroglu E, Göke J, Hillmer A, Gathof B, Meyer MF, Klussmann JP, Shimabukuro-Vornhagen A, Theurich S, Beutner D, von Bergwelt-Baildon M (2019) Tumor-associated B cells and humoral immune response in head and neck squamous cell carcinoma. OncoImmunology 8:1535293.

103. Lechner M, Engleitner T, Babushku T, Schmidt-Supprian M, Rad R, Strobl LJ, Zimber-Strobl U (2021) Notch2-mediated plasticity between marginal zone and follicular B cells. Nat Commun 12:1111.

104. Lechner M, Liu J, Masterson L, Fenton TR (2022) HPV-associated oropharyngeal cancer: epidemiology, molecular biology and clinical management. Nat Rev Clin Oncol 19:306–327.

105. Lee JM, Lee M-H, Garon E, Goldman JW, Salehi-Rad R, Baratelli FE, Schaue D, Wang G, Rosen F, Yanagawa J, Walser TC, Lin Y, Park SJ, Adams S, Marincola FM, Tumeh PC, Abtin F, Suh R, Reckamp KL, Lee G, Wallace WD, Lee S, Zeng G, Elashoff DA, Sharma S, Dubinett SM (2017) Phase I Trial of Intratumoral Injection of CCL21 Gene–Modified Dendritic Cells in Lung Cancer Elicits Tumor-Specific Immune Responses and CD8+ T-cell Infiltration. Clinical Cancer Research 23:4556–4568.

106. Lee S, Ko Y, Lee HW, Oh WJ, Hong HG, Ariyaratne D, Im SJ, Kim TJ (2024) Two distinct subpopulations of marginal zone B cells exhibit differential antibody-producing capacities and radioresistance. Cell Mol Immunol 21:393–408.

107. Lee-Chang C, Bodogai M, Martin-Montalvo A, Wejksza K, Sanghvi M, Moaddel R, de Cabo R, Biragyn A (2013) Inhibition of Breast Cancer Metastasis by Resveratrol-Mediated Inactivation of Tumor-Evoked Regulatory B Cells. JI 191:4141–4151.

108. Leemans CR, Snijders PJF, Brakenhoff RH (2018) The molecular landscape of head and neck cancer. Nature Reviews 18:269–282.

109. Li K, Guo Q, Zhang X, Dong X, Liu W, Zhang A, Li Y, Yan J, Jia G, Zheng Z, Tang W, Pan L, An M, Zhang B, Liu S, Fu B (2020) Oral cancer-associated tertiary lymphoid structures: gene expression profile and prognostic value. Clinical and Experimental Immunology 199:172–181.

110. Liao W-C, Huang B-S, Yu Y-H, Yang H-H, Chen P-R, Huang C-C, Huang H-Y, Wu M-S, Chow L-P (2019) Galectin-3 and S100A9: Novel Diabetogenic Factors Mediating Pancreatic Cancer–Associated Diabetes. Dia Care 42:1752–1759.

111. Lindner S, Dahlke K, Sontheimer K, Hagn M, Kaltenmeier C, Barth TFE, Beyer T, Reister F, Fabricius D, Lotfi R, Lunov O, Nienhaus GU, Simmet T, Kreienberg R, Möller P, Schrezenmeier H, Jahrsdörfer B (2013) Interleukin 21–Induced Granzyme B–Expressing B Cells Infiltrate Tumors and Regulate T Cells. Cancer Res 73:2468–2479.

112. Liu D, Xu H, Shih C, Wan Z, Ma X, Ma W, Luo D, Qi H (2015) T–B-cell entanglement and ICOSL-driven feed-forward regulation of germinal centre reaction. Nature 517:214–218.

113. Liu J-Q, Hu A, Zhu J, Yu J, Talebian F, Bai X-F (2020) CD200-CD200R Pathway in the Regulation of Tumor Immune Microenvironment and Immunotherapy. Adv Exp Med Biol 1223:155–165.

114. Lu N (2018) Human Semaphorin-4A drives Th2 responses by binding to receptor ILT-4. Nature Communications 9:742.

115. Luther SA, Bidgol A, Hargreaves DC, Schmidt A, Xu Y, Paniyadi J, Matloubian M, Cyster JG (2002) Differing Activities of Homeostatic Chemokines CCL19, CCL21, and CXCL12 in Lymphocyte and Dendritic Cell Recruitment and Lymphoid Neogenesis. J Immunol 169:424–433.

116. Lutz ER, Wu AA, Bigelow E, Sharma R, Mo G, Soares K, Solt S, Dorman A, Wamwea A, Yager A, Laheru D, Wolfgang CL, Wang J, Hruban RH, Anders RA, Jaffee EM,

Zheng L (2014) Immunotherapy Converts Nonimmunogenic Pancreatic Tumors into Immunogenic Foci of Immune Regulation. Cancer Immunol Res 2:616–631.

117. Lydiatt WM, Patel SG, O'Sullivan B, Brandwein MS, Ridge JA, Migliacci JC, Loomis AM, Shah JP (2017) Head and Neck cancers-major changes in the American Joint Committee on cancer eighth edition cancer staging manual. CA Cancer J Clin 67:122–137.

118. Ma J, Wu Y, Ma L, Yang X, Zhang T, Song G, Li T, Gao K, Shen X, Lin J, Chen Y, Liu X, Fu Y, Gu X, Chen Z, Jiang S, Rao D, Pan J, Zhang S, Zhou J, Huang C, Shi S, Fan J, Guo G, Zhang X, Gao Q (2024) A blueprint for tumor-infiltrating B cells across human cancers. Science 384:eadj4857.

119. Ma L, Heinrich S, Wang L, Keggenhoff FL, Khatib S, Forgues M, Kelly M, Hewitt SM, Saif A, Hernandez JM, Mabry D, Kloeckner R, Greten TF, Chaisaingmongkol J, Ruchirawat M, Marquardt JU, Wang XW (2022) Multiregional single-cell dissection of tumor and immune cells reveals stable lock-and-key features in liver cancer. Nat Commun 13:7533.

120. Machiels J-P, René Leemans C, Golusinski W, Grau C, Licitra L, Gregoire V (2020) Squamous cell carcinoma of the oral cavity, larynx, oropharynx and hypopharynx: EHNS-ESMO-ESTRO Clinical Practice Guidelines for diagnosis, treatment and follow-up. Ann Oncol 31:1462–1475.

121. Madan R, Demircik F, Surianarayanan S, Allen JL, Divanovic S, Trompette A, Yogev N, Gu Y, Khodoun M, Hildeman D, Boespflug N, Fogolin MB, Gröbe L, Greweling M, Finkelman FD, Cardin R, Mohrs M, Müller W, Waisman A, Roers A, Karp CL (2009) Nonredundant Roles for B Cell-Derived IL-10 in Immune Counter-Regulation. J Immunol 183:2312–2320.

122. Mahadevan D, Lanasa MC, Farber C, Pandey M, Whelden M, Faas SJ, Ulery T, Kukreja A, Li L, Bedrosian CL, Zhang X, Heffner LT (2019) Phase I study of samalizumab in chronic lymphocytic leukemia and multiple myeloma: blockade of the immune checkpoint CD200. J Immunother Cancer 7:227.

123. Maldonado L, Teague JE, Morrow MP, Jotova I, Wu TC, Wang C, Desmarais C, Boyer JD, Tycko B, Robins HS, Clark RA, Trimble CL (2014) Intramuscular Therapeutic Vaccination Targeting HPV16 Induces T Cell Responses That Localize in Mucosal Lesions. Sci Transl Med 6.

124. Marinkovic D, Marinkovic T (2020) Putative role of marginal zone B cells in pathophysiological processes. Scand J Immunol 92:e12920.

125. Martinet L, Garrido I, Filleron T, Le Guellec S, Bellard E, Fournie J-J, Rochaix P, Girard J-P (2011) Human Solid Tumors Contain High Endothelial Venules: Association with T- and B-Lymphocyte Infiltration and Favorable Prognosis in Breast Cancer. Cancer Res 71:5678–5687.

126. Martinez-Bosch N, Barranco LE, Orozco CA, Moreno M, Visa L, Iglesias M, Oldfield L, Neoptolemos JP, Greenhalf W, Earl J, Carrato A, Costello E, Navarro P (2018) Increased plasma levels of galectin-1 in pancreatic cancer: potential use as biomarker. Oncotarget 9:32984–32996.

127. Matsumoto M, Fujii Y, Baba A, Hikida M, Kurosaki T, Baba Y (2011) The Calcium Sensors STIM1 and STIM2 Control B Cell Regulatory Function through Interleukin-10 Production. Immunity 34:703–714.

128. Meng X, Grötsch B, Luo Y, Knaup KX, Wiesener MS, Chen X-X, Jantsch J, Fillatreau S, Schett G, Bozec A (2018) Hypoxia-inducible factor-1α is a critical transcription factor for IL-10-producing B cells in autoimmune disease. Nat Commun 9:251.

129. Menon M, Blair PA, Isenberg DA, Mauri C (2016) A Regulatory Feedback between Plasmacytoid Dendritic Cells and Regulatory B Cells Is Aberrant in Systemic Lupus Erythematosus. Immunity 44:683–697.

130. Messina JL, Fenstermacher DA, Eschrich S, Qu X, Berglund AE, Lloyd MC, Schell MJ, Sondak VK, Weber JS, Mulé JJ (2012) 12-Chemokine Gene Signature Identifies Lymph Node-like Structures in Melanoma: Potential for Patient Selection for Immunotherapy? Sci Rep 2:765.

131. Meylan M, Petitprez F, Becht E, Bougoüin A, Pupier G, Calvez A, Giglioli I, Verkarre V, Lacroix G, Verneau J, Sun C-M, Laurent-Puig P, Vano Y-A, Elaïdi R, Méjean A, Sanchez-Salas R, Barret E, Cathelineau X, Oudard S, Reynaud C-A, de Reyniès A, Sautès-Fridman C, Fridman WH (2022) Tertiary lymphoid structures generate and propagate anti-tumor antibody-producing plasma cells in renal cell cancer. Immunity 55:527-541.e5.

132. Mirlekar B, Michaud D, Lee SJ, Kren NP, Harris C, Greene K, Goldman EC, Gupta GP, Fields RC, Hawkins WG, DeNardo DG, Rashid NU, Yeh JJ, McRee AJ, Vincent BG, Vignali DAA, Pylayeva-Gupta Y (2020) B cell–Derived IL35 Drives STAT3-Dependent CD8 + T-cell Exclusion in Pancreatic Cancer. Cancer Immunol Res 8:292–308.

133. Mirlekar B, Wang Y, Li S, Zhou M, Entwistle S, De Buysscher T, Morrison A, Herrera G, Harris C, Vincent BG, Ting JP-Y, Rashid N, Kim WY, Yeh JJ, Pylayeva-Gupta Y (2022) Balance between immunoregulatory B cells and plasma cells drives pancreatic tumor immunity. Cell Reports Medicine 3:100744.

134. Monney L, Sabatos CA, Gaglia JL, Ryu A, Waldner H, Chernova T, Manning S, Greenfield EA, Coyle AJ, Sobel RA, Freeman GJ, Kuchroo VK (2002) Th1-specific cell surface protein Tim-3 regulates macrophage activation and severity of an autoimmune disease. Nature 415:536–541.

135. Morgan D, Tergaonkar V (2022) Unraveling B cell trajectories at single cell resolution. Trends in Immunology 43:210–229.

136. Motz GT, Santoro SP, Wang L-P, Garrabrant T, Lastra RR, Hagemann IS, Lal P, Feldman MD, Benencia F, Coukos G (2014) Tumor endothelium FasL establishes a selective immune barrier promoting tolerance in tumors. Nat Med 20:607–615.

137. Newman AM, Steen CB, Liu CL, Gentles AJ, Chaudhuri AA, Scherer F, Khodadoust MS, Esfahani MS, Luca BA, Steiner D, Diehn M, Alizadeh AA (2019) Determining cell type abundance and expression from bulk tissues with digital cytometry. Nat Biotechnol 37:773–782.

138. Nielsen JS, Sahota RA, Milne K, Kost SE, Nesslinger NJ, Watson PH, Nelson BH (2012) CD20+tumor-infiltrating lymphocytes have an atypical CD27− memory phenotype and together with CD8+T cells promote favorable prognosis in ovarian cancer. Clin Cancer Res 18:3281–3292.

139. Ock C-Y, Hwang J-E, Keam B, Kim S-B, Shim J-J, Jang H-J, Park S, Sohn BH, Cha M, Ajani JA, Kopetz S, Lee K-W, Kim TM, Heo DS, Lee J-S (2017) Genomic landscape associated with potential response to anti-CTLA-4 treatment in cancers. Nat Commun 8:1050.

140. Oh KI, Kim BK, Ban YL, Choi EY, Jung KC, Lee I-S, Park SH (2007) CD99 activates T cells via a costimulatory function that promotes raft association of TCR complex and tyrosine phosphorylation of TCR ζ. Experimental & Molecular Medicine 39:176–184

141. Oleinika K, Mauri C, Salama AD (2019) Effector and regulatory B cells in immune-mediated kidney disease. Nature Reviews Nephrology 15:11–26.

142. Olkhanud PB, Damdinsuren B, Bodogai M, Gress RE, Sen R, Wejksza K, Malchinkhuu E, Wersto RP, Biragyn A (2011) Tumor-Evoked Regulatory B Cells Promote Breast Cancer Metastasis by Converting Resting CD4 + T Cells to T-Regulatory Cells. Cancer Res 71:3505–3515.

143. Orozco CA, Martinez-Bosch N, Guerrero PE, Vinaixa J, Dalotto-Moreno T, Iglesias M, Moreno M, Djurec M, Poirier F, Gabius H-J, Fernandez-Zapico ME, Hwang RF, Guerra C, Rabinovich GA, Navarro P (2018) Targeting galectin-1 inhibits pancreatic cancer progression by modulating tumor–stroma crosstalk. Proc Natl Acad Sci USA 115:E3769–E3778.

144. Palm A-KE, Kleinau S (2021) Marginal zone B cells: From housekeeping function to autoimmunity? Journal of Autoimmunity 119:102627.

145. Petitprez F, de Reyniès A, Keung EZ, Chen TW-W, Sun C-M, Calderaro J, Jeng Y-M, Hsiao L-P, Lacroix L, Bougoüin A, Moreira M, Lacroix G, Natario I, Adam J,

Lucchesi C, Laizet Y, Toulmonde M, Burgess MA, Bolejack V, Reinke D, Wani KM, Wang W-L, Lazar AJ, Roland CL, Wargo JA, Italiano A, Sautès-Fridman C, Tawbi HA, Fridman WH (2020) B cells are associated with survival and immunotherapy response in sarcoma. Nature 577:556–560.

146. Phuengkham H, Ren L, Shin IW, Lim YT (2019) Nanoengineered Immune Niches for Reprogramming the Immunosuppressive Tumor Microenvironment and Enhancing Cancer Immunotherapy. Adv Mater 31:1803322.

147. Pimenta EM, De S, Weiss R, Feng D, Hall K, Kilic S, Bhanot G, Ganesan S, Ran S, Barnes BJ (2015) IRF5 is a novel regulator of CXCL13 expression in breast cancer that regulates CXCR5 $^{+}$ B- and T-cell trafficking to tumor-conditioned media. Immunol Cell Biol 93:486–499.

148. Pitzalis C, Jones GW, Bombardieri M, Jones SA (2014) Ectopic lymphoid-like structures in infection, cancer and autoimmunity. Nat Rev Immunol 14:447–462.

149. Podolsky MA, Bailey JT, Gunderson AJ, Oakes CJ, Breech K, Glick AB (2017) Differentiated State of Initiating Tumor Cells Is Key to Distinctive Immune Responses Seen in H-RasG12V–Induced Squamous Tumors. Cancer Immunol Res 5:198–210.

150. Prabhakaran S, Rizk VT, Ma Z, Cheng C-H, Berglund AE, Coppola D, Khalil F, Mulé JJ, Soliman HH (2017) Evaluation of invasive breast cancer samples using a 12-chemokine gene expression score: correlation with clinical outcomes. Breast Cancer Res 19:71.

151. Puram SV, Mints M, Pal A, Qi Z, Reeb A, Gelev K, Barrett TF, Gerndt S, Liu P, Parikh AS, Ramadan S, Law T, Mroz EA, Rocco JW, Adkins D, Thorstad WL, Gay HA, Ding L, Paniello RC, Pipkorn P, Jackson RS, Wang X, Mazul A, Chernock R, Zevallos JP, Silva-Fisher J, Tirosh I (2023) Cellular states are coupled to genomic and viral heterogeneity in HPV-related oropharyngeal carcinoma. Nat Genet 55:640–650.

152. Pylayeva-Gupta Y, Das S, Handler JS, Hajdu CH, Coffre M, Koralov SB, Bar-Sagi D (2016) IL35-Producing B Cells Promote the Development of Pancreatic Neoplasia. Cancer Discov 6:247–255.

153. Ran Z, Yue-Bei L, Qiu-Ming Z, Huan Y (2020) Regulatory B Cells and Its Role in Central Nervous System Inflammatory Demyelinating Diseases. Front Immunol 11:1884.

154. Rebecca J G, Gordon J F, Arlene H S (2005) The B7 family revisited. Annu Rev Immunol 23:515-548.

155. Ricciardi M, Zanotto M, Malpeli G, Bassi G, Perbellini O, Chilosi M, Bifari F, Krampera M (2015) Epithelial-to-mesenchymal transition (EMT) induced by inflammatory priming elicits mesenchymal stromal cell-like immune-modulatory properties in cancer cells. Br J Cancer 112:1067–1075.

156. Rischin D, Groenland SL, Lim AML, Martin-Liberal J, Moreno V, Trigo Perez JM, Le Tourneau C, Mathew M, Cho DC, Hansen AR, Vincente-Baz D, Maio M, Italiano A, Bauman JR, Chisamore M, Zhou H, Ellis C, Ballas M, Hoos A, Angevin E (2019) Inducible T cell costimulatory (ICOS) receptor agonist, GSK3359609 (GSK609) alone and in combination with pembrolizumab (pembro): Preliminary results from INDUCE-1 expansion cohorts (EC) in head and neck squamous cell carcinoma (HNSCC). Annals of Oncology 30:v454–v455.

157. Roe K (2022) NK-cell exhaustion, B-cell exhaustion and T-cell exhaustion—the differences and similarities. Immunology 166:155–168.

158. Rooney MS, Shukla SA, Wu CJ, Getz G, Hacohen N (2015) Molecular and Genetic Properties of Tumors Associated with Local Immune Cytolytic Activity. Cell 160:48–61.

159. Rosser EC, Mauri C (2015) Regulatory B Cells: Origin, Phenotype, and Function. Immunity 42:607–612.

160. Rosser EC, Oleinika K, Tonon S, Doyle R, Bosma A, Carter NA, Harris KA, Jones SA, Klein N, Mauri C (2014) Regulatory B cells are induced by gut microbiota–driven interleukin-1β and interleukin-6 production. Nature Medicine 20:1334–1339.

161. Ruffin AT, Cillo AR, Tabib T, Liu A, Onkar S, Kunning SR, Lampenfeld C, Atiya HI, Abecassis I, Kürten CHL, Qi Z, Soose R, Duvvuri U, Kim S, Oesterrich S, Lafyatis R, Coffman LG, Ferris RL, Vignali DAA, Bruno TC (2021) B cell signatures and tertiary lymphoid structures contribute to outcome in head and neck squamous cell carcinoma. Nat Commun 12:3349.

162. Saito T, Chiba S, Ichikawa M, Kunisato A, Asai T, Shimizu K, Yamaguchi T, Yamamoto G, Seo S, Kumano K, Nakagami-Yamaguchi E, Hamada Y, Aizawa S, Hirai H (2003) Notch2 Is Preferentially Expressed in Mature B Cells and Indispensable for Marginal Zone B Lineage Development. Immunity 18:675–685.

163. Sánchez-Fueyo A, Tian J, Picarella D, Domenig C, Zheng XX, Sabatos CA, Manlongat N, Bender O, Kamradt T, Kuchroo VK, Gutiérrez-Ramos J-C, Coyle AJ, Strom TB (2003) Tim-3 inhibits T helper type 1-mediated auto- and alloimmune responses and promotes immunological tolerance. Nat Immunol 4:1093–1101.

164. Sautès-Fridman C, Lawand M, Giraldo NA, Kaplon H, Germain C, Fridman WH, Dieu-Nosjean M-C (2016) Tertiary Lymphoid Structures in Cancers: Prognostic Value, Regulation, and Manipulation for Therapeutic Intervention. Front Immunol 7.

165. Sautès-Fridman C, Petitprez F, Calderaro J, Fridman WH (2019) Tertiary lymphoid structures in the era of cancer immunotherapy. Nat Rev Cancer 19:307–325.

166. Saze Z, Schuler PJ, Hong C-S, Cheng D, Jackson EK, Whiteside TL (2013) Adenosine production by human B cells and B cell–mediated suppression of activated T cells. Blood 122:9–18.

167. Schlößer HA, Thelen M, Lechner A, Wennhold K, Garcia-Marquez MA, Rothschild SI, Staib E, Zander T, Beutner D, Gathof B, Gilles R, Cukuroglu E, Göke J, Shimabukuro-Vornhagen A, Drebber U, Quaas A, Bruns CJ, Hölscher AH, Von Bergwelt-Baildon

MS (2019) B cells in esophago-gastric adenocarcinoma are highly differentiated, organize in tertiary lymphoid structures and produce tumor-specific antibodies. OncoImmunology 8:e1512458.

168. Schriek P, Ching AC, Moily NS, Moffat J, Beattie L, Steiner TM, Hosking LM, Thurman JM, Holers VM, Ishido S, Lahoud MH, Caminschi I, Heath WR, Mintern JD, Villadangos JA (2022) Marginal zone B cells acquire dendritic cell functions by trogocytosis. Science 375:eabf7470.

169. Shao A, Owens DM (2023) The immunoregulatory protein CD200 as a potentially lucrative yet elusive target for cancer therapy. Oncotarget 14:96–103.

170. Shen M, Wang J, Yu W, Zhang C, Liu M, Wang K, Yang L, Wei F, Wang SE, Sun Q, Ren X (2018) A novel MDSC-induced PD-1−PD-L1+ B-cell subset in breast tumor microenvironment possesses immuno-suppressive properties.

171. Shi J-Y, Gao Q, Wang Z-C, Zhou J, Wang X-Y, Min Z-H, Shi Y-H, Shi G-M, Ding Z-B, Ke A-W, Dai Z, Qiu S-J, Song K, Fan J (2013) Margin-infiltrating CD20(+) B cells display an atypical memory phenotype and correlate with favorable prognosis in hepatocellular carcinoma. Clin Cancer Res 19:5994–6005.

172. Shin DH, Lin H, Zheng H, Kim KS, Kim JY, Chun YS, Park JW, Nam JH, Kim WK, Zhang YH, Kim SJ (2014) HIF-1α–Mediated Upregulation of TASK-2 K^+ Channels Augments Ca^{2+} Signaling in Mouse B Cells under Hypoxia. JI 193:4924–4933.

173. Simoni Y, Becht E, Fehlings M, Loh CY, Koo S-L, Teng KWW, Yeong JPS, Nahar R, Zhang T, Kared H, Duan K, Ang N, Poidinger M, Lee YY, Larbi A, Khng AJ, Tan E, Fu C, Mathew R, Teo M, Lim WT, Toh CK, Ong B-H, Koh T, Hillmer AM, Takano A, Lim TKH, Tan EH, Zhai W, Tan DSW, Tan IB, Newell EW (2018) Bystander CD8+ T cells are abundant and phenotypically distinct in human tumour infiltrates. Nature 557:575–579.

174. Somasundaram R, Zhang G, Fukunaga-Kalabis M, Perego M, Krepler C, Xu X, Wagner C, Hristova D, Zhang J, Tian T, Wei Z, Liu Q, Garg K, Griss J, Hards R, Maurer M,

Hafner C, Mayerhöfer M, Karanikas G, Jalili A, Bauer-Pohl V, Weihsengruber F, Rappersberger K, Koller J, Lang R, Hudgens C, Chen G, Tetzlaff M, Wu L, Frederick DT, Scolyer RA, Long GV, Damle M, Ellingsworth C, Grinman L, Choi H, Gavin BJ, Dunagin M, Raj A, Scholler N, Gross L, Beqiri M, Bennett K, Watson I, Schaider H, Davies MA, Wargo J, Czerniecki BJ, Schuchter L, Herlyn D, Flaherty K, Herlyn M, Wagner SN (2017) Tumor-associated B-cells induce tumor heterogeneity and therapy resistance. Nat Commun 8:607.

175. Sonntag M, Stanojevic S, Laban S, Schuler PJ, Hoffmann TK, Brunner C (2024) Identification of B Cell Subpopulations with Pro- and Anti-Tumorigenic Properties in an Immunocompetent Mouse Model of Head and Neck Squamous Cell Carcinoma. Cells 14:20.

176. Squeglia F, Romano M, Ruggiero A, Maga G, Berisio R (2020) Host DDX Helicases as Possible SARS-CoV-2 Proviral Factors: A Structural Overview of Their Hijacking Through Multiple Viral Proteins. Front Chem 8:602162.

177. Srivastava B, Quinn WJ, Hazard K, Erikson J, Allman D (2005) Characterization of marginal zone B cell precursors. Journal of Experimental Medicine 202:1225–1234.

178. Stuart T, Butler A, Hoffman P, Hafemeister C, Papalexi E, Mauck WM, Hao Y, Stoeckius M, Smibert P, Satija R (2019) Comprehensive Integration of Single-Cell Data. Cell 177:1888-1902.e21.

179. Su GH, Ip HS, Cobb BS, Lu MM, Chen HM, Simon MC (1996) The Ets protein Spi-B is expressed exclusively in B cells and T cells during development. Journal of Experimental Medicine 184:203–214.

180. Sung H, Ferlay J, Siegel RL, Laversanne M, Soerjomataram I, Jemal A, Bray F (2021) Global Cancer Statistics 2020: GLOBOCAN Estimates of Incidence and Mortality Worldwide for 36 Cancers in 185 Countries. CA A Cancer J Clin 71:209–249.

181. Takahashi R, Macchini M, Sunagawa M, Jiang Z, Tanaka T, Valenti G, Renz BW, White RA, Hayakawa Y, Westphalen CB, Tailor Y, Iuga AC, Gonda TA, Genkinger J, Olive

KP, Wang TC (2020) Interleukin-1β-induced pancreatitis promotes pancreatic ductal adenocarcinoma via B lymphocyte–mediated immune suppression. Gut gutjnl-2019-319912.

182. Takheaw N, Earwong P, Laopajon W, Pata S, Kasinrerk W (2019) Interaction of CD99 and its ligand upregulates IL-6 and TNF-α upon T cell activation. PLOS ONE 14:e0217393.

183. Takheaw N, Pata S, Laopajon W, Roytrakul S, Kasinrerk W (2020) The presence of membrane bound CD99 ligands on leukocyte surface. BMC Research Notes 13:496.

184. Tao H, Lu L, Xia Y, Dai F, Wang Y, Bao Y, Lundy SK, Ito F, Pan Q, Zhang X, Zheng F, Shu G, Fang B, Jiang J, Xia J, Huang S, Li Q, Chang AE (2015) Antitumor effector B cells directly kill tumor cells via the Fas/FasL pathway and are regulated by IL-10: Cellular immune response. Eur J Immunol 45:999–1009.

185. Tekguc M, Wing JB, Osaki M, Long J, Sakaguchi S (2021) Treg-expressed CTLA-4 depletes CD80/CD86 by trogocytosis, releasing free PD-L1 on antigen-presenting cells. Proc Natl Acad Sci U S A 118:e2023739118.

186. Thommen DS, Koelzer VH, Herzig P, Roller A, Trefny M, Dimeloe S, Kiialainen A, Hanhart J, Schill C, Hess C, Savic Prince S, Wiese M, Lardinois D, Ho P-C, Klein C, Karanikas V, Mertz KD, Schumacher TN, Zippelius A (2018) A transcriptionally and functionally distinct PD-1+ CD8+ T cell pool with predictive potential in non-small-cell lung cancer treated with PD-1 blockade. Nat Med 24:994–1004.

187. Tull TJ, Pitcher MJ, Guesdon W, Siu JHY, Lebrero-Fernández C, Zhao Y, Petrov N, Heck S, Ellis R, Dhami P, Kadolsky UD, Kleeman M, Kamra Y, Fear DJ, John S, Jassem W, Groves RW, Sanderson JD, Robson MD, D'Cruz DP, Bemark M, Spencer J (2021) Human marginal zone B cell development from early T2 progenitors. Journal of Experimental Medicine 218:e20202001.

188. Van Der Zwaag B, Hellemons AJCGM, Leenders WPJ, Burbach JPH, Brunner HG, Padberg GW, Van Bokhoven H (2002) PLEXIN-D1, a novel plexin family member,

is expressed in vascular endothelium and the central nervous system during mouse embryogenesis. Dev Dyn 225:336–343.

189. Wang R-X, Yu C-R, Dambuza IM, Mahdi RM, Dolinska MB, Sergeev YV, Wingfield PT, Kim S-H, Egwuagu CE (2014) Interleukin-35 induces regulatory B cells that suppress autoimmune disease. Nature Medicine 20:633–641.

190. Wang T-W, Johmura Y, Suzuki N, Omori S, Migita T, Yamaguchi K, Hatakeyama S, Yamazaki S, Shimizu E, Imoto S, Furukawa Y, Yoshimura A, Nakanishi M (2022) Blocking PD-L1–PD-1 improves senescence surveillance and ageing phenotypes. Nature 611:358–364.

191. Wang W, Yuan X, Chen H, Xie G, Ma Y, Zheng Y, Zhou Y, Shen L (2015) CD19+CD24hiCD38hiBregs involved in downregulate helper T cells and upregulate regulatory T cells in gastric cancer. Oncotarget 6:33486–33499.

192. Wang Z, Cheng Q, Tang K, Sun Y, Zhang K, Zhang Y, Luo S, Zhang H, Ye D, Huang B (2015) Lipid mediator lipoxin A4 inhibits tumor growth by targeting IL-10-producing regulatory B (Breg) cells. Cancer Letters 364:118–124.

193. Weger S, Wendland M, Kleinschmidt JA, Heilbronn R (1999) The adeno-associated virus type 2 regulatory proteins rep78 and rep68 interact with the transcriptional coactivator PC4. J Virol 73:260–269.

194. Weiden J, Tel J, Figdor CG (2018) Synthetic immune niches for cancer immunotherapy. Nat Rev Immunol 18:212–219.

195. Weinstein AM, Chen L, Brzana EA, Patil PR, Taylor JL, Fabian KL, Wallace CT, Jones SD, Watkins SC, Lu B, Stroncek DF, Denning TL, Fu Y-X, Cohen PA, Storkus WJ (2017) Tbet and IL-36γ cooperate in therapeutic DC-mediated promotion of ectopic lymphoid organogenesis in the tumor microenvironment. OncoImmunology 6:e1322238.

196. Weinstein AM, Giraldo NA, Petitprez F, Julie C, Lacroix L, Peschaud F, Emile J-F, Marisa L, Fridman WH, Storkus WJ, Sautès-Fridman C (2019) Association of IL-36γ with tertiary lymphoid structures and inflammatory immune infiltrates in human colorectal cancer. Cancer Immunol Immunother 68:109–120.

197. Wejksza K, Lee-Chang C, Bodogai M, Bonzo J, Gonzalez FJ, Lehrmann E, Becker K, Biragyn A (2013) Cancer-Produced Metabolites of 5-Lipoxygenase Induce Tumor-Evoked Regulatory B Cells via Peroxisome Proliferator–Activated Receptor α. JI 190:2575–2584.

198. Wen L, Brill-Dashoff J, Shinton SA, Asano M, Hardy RR, Hayakawa K (2005) Evidence of marginal-zone B cell-positive selection in spleen. Immunity 23:297–308.

199. Wennhold K, Thelen M, Lehmann J, Schran S, Preugszat E, Garcia-Marquez M, Lechner A, Shimabukuro-Vornhagen A, Ercanoglu MS, Klein F, Thangarajah F, Eidt S, Löser H, Bruns C, Quaas A, Von Bergwelt-Baildon M, Schlößer HA (2021) CD86+ Antigen-Presenting B Cells Are Increased in Cancer, Localize in Tertiary Lymphoid Structures, and Induce Specific T-cell Responses. Cancer Immunology Research 9:1098–1108.

200. Wherry EJ, Kurachi M (2015) Molecular and cellular insights into T cell exhaustion. Nat Rev Immunol 15:486–499.

201. Wouters MCA, Nelson BH (2018) Prognostic Significance of Tumor-Infiltrating B Cells and Plasma Cells in Human Cancer. Clin Cancer Res 24:6125–6135.

202. Wu H, Xia L, Jia D, Zou H, Jin G, Qian W, Xu H, Li T (2020) PD-L1+ regulatory B cells act as a T cell suppressor in a PD-L1-dependent manner in melanoma patients with bone metastasis. Molecular Immunology 119:83–91.

203. Wu T, Hu E, Xu S, Chen M, Guo P, Dai Z, Feng T, Zhou L, Tang W, Zhan L, Fu X, Liu S, Bo X, Yu G (2021) clusterProfiler 4.0: A universal enrichment tool for interpreting omics data. The Innovation 2:100141.

204. Wu X, Gu Z, Chen Y, Chen B, Chen W, Weng L, Liu X (2019) Application of PD-1 Blockade in Cancer Immunotherapy. Computational and Structural Biotechnology Journal 17:661–674.

205. Wu X, Li T, Jiang R, Yang X, Guo H, Yang R (2023) Targeting MHC-I molecules for cancer: function, mechanism, and therapeutic prospects. Mol Cancer 22:194.

206. Xiao X, Lao X-M, Chen M-M, Liu R-X, Wei Y, Ouyang F-Z, Chen D-P, Zhao X-Y, Zhao Q, Li X-F, Liu C-L, Zheng L, Kuang D-M (2016) PD-1hi Identifies a Novel Regulatory B-cell Population in Human Hepatoma That Promotes Disease Progression. Cancer Discov 6:546–559.

207. Yagawa Y, Robertson-Tessi M, Zhou SL, Anderson ARA, Mulé JJ, Mailloux AW (2017) Systematic Screening of Chemokines to Identify Candidates to Model and Create Ectopic Lymph Node Structures for Cancer Immunotherapy. Sci Rep 7:15996.

208. Yamakoshi Y, Tanaka H, Sakimura C, Deguchi S, Mori T, Tamura T, Toyokawa T, Muguruma K, Hirakawa K, Ohira M (2020) Immunological potential of tertiary lymphoid structures surrounding the primary tumor in gastric cancer. Int J Oncol 57:171–182.

209. Yang Y, Chen X, Pan J, Ning H, Zhang Y, Bo Y, Ren X, Li J, Qin S, Wang D, Chen M-M, Zhang Z (2024) Pan-cancer single-cell dissection reveals phenotypically distinct B cell subtypes. Cell S0092867424007128.

210. Yarchoan M, Mohan AA, Dennison L, Vithayathil T, Ruggieri A, Lesinski GB, Armstrong TD, Azad NS, Jaffee EM (2019) MEK inhibition suppresses B regulatory cells and augments anti-tumor immunity. PLoS ONE 14:e0224600.

211. Ye L, Zhang Q, Cheng Y, Chen X, Wang G, Shi M, Zhang T, Cao Y, Pan H, Zhang L, Wang G, Deng Y, Yang Y, Chen G (2018) Tumor-derived exosomal HMGB1 fosters hepatocellular carcinoma immune evasion by promoting TIM-1+ regulatory B cell expansion. j immunotherapy cancer 6:145.

212. Yoshizaki A, Miyagaki T, DiLillo DJ, Matsushita T, Horikawa M, Kountikov EI, Spolski R, Poe JC, Leonard WJ, Tedder TF (2012) Regulatory B cells control T-cell autoimmunity through IL-21-dependent cognate interactions. Nature 491:264–268.

213. Yu G, Wang LG, Han Y, He QY (2012) clusterProfiler: an R package for comparing biological themes among gene clusters. Omics-a Journal of Integrative Biology 16:284–287

214. Zamunér FT, Karia BTR, de Oliveira CZ, Santos CR dos, Carvalho AL, Vettore AL (2015) A Comprehensive Expression Analysis of Cancer Testis Antigens in Head and Neck Squamous Cell Carcinoma Revels MAGEA3/6 as a Marker for Recurrence. Mol Cancer Ther 14:828–834.

215. Zhang L, Tai Y-T, Ho M, Xing L, Chauhan D, Gang A, Qiu L, Anderson KC (2017) Regulatory B cell-myeloma cell interaction confers immunosuppression and promotes their survival in the bone marrow milieu. Blood Cancer Journal 7:e547–e547.

216. Zheng L, Ding D, Edil BH, Judkins C, Durham JN, Thomas DL, Bever KM, Mo G, Solt SE, Hoare JA, Bhattacharya R, Zhu Q, Osipov A, Onner B, Purtell KA, Cai H, Parkinson R, Hacker-Prietz A, Herman JM, Le DT, Azad NS, De Jesus-Acosta AMC, Blair AB, Kim V, Soares KC, Manos L, Cameron JL, Makary MA, Weiss MJ, Schulick RD, He J, Wolfgang CL, Thompson ED, Anders RA, Sugar E, Jaffee EM, Laheru DA (2021) Vaccine-Induced Intratumoral Lymphoid Aggregates Correlate with Survival Following Treatment with a Neoadjuvant and Adjuvant Vaccine in Patients with Resectable Pancreatic Adenocarcinoma. Clinical Cancer Research 27:1278–1286.

217. Zhi Y, Wang Q, Zi M, Zhang S, Ge J, Liu K, Lu L, Fan C, Yan Q, Shi L, Chen P, Fan S, Liao Q, Guo C, Wang F, Gong Z, Xiong W, Zeng Z (2024) Spatial Transcriptomic and Metabolomic Landscapes of Oral Submucous Fibrosis-Derived Oral Squamous Cell Carcinoma and its Tumor Microenvironment. Advanced Science 11:2306515.

218. Zhou X, Su Y-X, Lao X-M, Liang Y-J, Liao G-Q (2016) CD19+IL-10+ regulatory B cells affect survival of tongue squamous cell carcinoma patients and induce resting CD4+ T cells to CD4+Foxp3+ regulatory T cells. Oral Oncology 53:27–35.

219. Zhu G, Falahat R, Wang K, Mailloux A, Artzi N, Mulé JJ (2017) Tumor-Associated Tertiary Lymphoid Structures: Gene-Expression Profiling and Their Bioengineering. Front Immunol 8:767.

220. Zhu G, Nemoto S, Mailloux AW, Perez-Villarroel P, Nakagawa R, Falahat R, Berglund AE, Mulé JJ (2018) Induction of Tertiary Lymphoid Structures With Antitumor Function by a Lymph Node-Derived Stromal Cell Line. Front Immunol 9:1609.

221. Zhu W, Germain C, Liu Z, Sebastian Y, Devi P, Knockaert S, Brohawn P, Lehmann K, Damotte D, Validire P, Yao Y, Valge-Archer V, Hammond SA, Dieu-Nosjean M-C, Higgs BW (2015) A high density of tertiary lymphoid structure B cells in lung tumors is associated with increased CD4C T cell receptor repertoire clonality. OncoImmunology 4:e1051922.

222. Clough E, Barrett T, Wilhite SE, Ledoux P, Evangelista C, Kim IF, Tomashevsky M, Marshall KA, Phillippy KH, Sherman PM, Lee H, Zhang N, Serova N, Wagner L, Zalunin V, Kochergin A, Soboleva A. NCBI GEO: archive for gene expression and epigenomics data sets: 23-year update. Nucleic Acid Res. 2023 Nov 2;52(D1):D138–D144.

223. Heath AP, Ferretti V, Agrawal S, An M, Angelakos JC, Arya R, Bajari R, Baqar B, Barnowski JHB, Burt J, Catton A, Chan BF, Chu F, Cullion K, Davidsen T, Do P-M, Dompierre C, Ferguson ML, Fitzsimons MS, Ford M, Fukuma M, Gaheen S, Ganji GL, Garcia TI, George SS, Gerhard DS, Gerthoffert F, Gomez F, Han K, Hernandez KM, Issac B, Jackson R, Jensen MA, Joshi S, Kadam A, Khurana A, Kim KMJ, Kraft VE, Li S, Lichtenberg TM, Lodato J, Lolla L, Martinov P, Mazzone JA, Miller DP, Miller I, Miller JS, Miyauchi K, Murphy MW, Nullet T, Ogwara RO, Ortuño FM, Pedrosa J, Pham PL, Popov MY, Porter JJ, Powell R, Rademacher K, Reid CP, Rich S, Rogel B, Sahni H, Savage JH, Schmitt KA, Simmons TJ, Sislow J, Spring J, Stein L, Sullivan S, Tang Y, Thiagarajan M, Troyer HD, Wang C, Wang Z, West BL, Wilmer A, Wilson S, Wu K, Wysocki WP, Xiang L, Yamada JT, Yang L, Yu C, Yung CK, Zenklusen JC, Zhang J, Zhang Z, Zhao Y, Zubair A, Staudt LM, Grossman RL (2021) The NCI Genomic Data Commons. Nature Genetics 53:257–262.

7 Acknowledegments

This thesis could not have been accomplished without the generous support of many individuals and organizations. I would like to take this opportunity to express my heartfelt gratitude to all those who have guided, encouraged, and accompanied me throughout my doctoral journey.

First and foremost, I would like to thank Prof. Dr. Hoffmann and Prof. Dr. Brunner for providing me the opportunity to begin my academic career and conduct research at the Department of Otorhinolaryngology, Head and Neck Surgery, Ulm University Medical Center. I am also deeply grateful to the China Scholarship Council (CSC) for its financial support during my studies in Germany.

My sincere appreciation goes to my research mentors for their accessibility, patient guidance, and rigorous scientific supervision. Their professionalism and insightful advice have been invaluable throughout this project, from its initiation and experimentation to data analysis and manuscript preparation.

I would also like to express my deep appreciation to all colleagues from the Department of Otorhinolaryngology, Head and Neck Surgery, Ulm University Medical Center; the Department of Otorhinolaryngology, Head and Neck Surgery, Heidelberg University Hospital; and the Unit for Single-Cell Genomics, Medical Faculty of Ulm University for their valuable discussions, technical assistance, and constructive feedback during my research.

I am profoundly thankful to all my friends in Ulm for their companionship and daily encouragement, which made my time abroad both fulfilling and memorable.

Finally, my deepest gratitude goes to my parents and my brother for their unwavering love, endless support, and constant encouragement throughout the years of my doctoral study.

8 Curriculum Vitea

CV was removed for data privacy protection reasons.